The Use of Artificial Intelligence for Assessing Damage in Concrete Affected by Alkali-Silica Reaction (ASR)

Agnes Bezerra

Thesis submitted to the University of Ottawa
in partial Fulfillment of the requirements for the

MASTER OF APPLIED SCIENCE

in Civil Engineering

Department of Civil Engineering

Faculty of Engineering

University of Ottawa

Abstract

Over the last decades, numerous techniques have been proposed worldwide to assess the actual damage of critical concrete infrastructure. A method that has progressively been used in North America is a novel microscopic tool, the Damage Rating Index (DRI). This semi-quantitative petrographic tool was developed to reliably appraise both the nature and degree of damage in concrete affected by alkali-silica reaction (ASR), which may threaten the serviceability and the durability of concrete infrastructure around the world. Performing the DRI consists of counting numerous distress features (i.e. closed and open cracks in the aggregate and cement paste) encountered on the surface of polished concrete sections (lab-made specimens or cores extracted from field structures) using a stereomicroscope at 16x magnification; once recognized and counted, the distinct distress features are multiplied by weighting factors whose purpose is to balance their relative importance towards the distress mechanism under consideration (e.g., ASR). Although reliable and efficient, performing the DRI is exceptionally time-consuming, and its results are highly operator sensitive, requiring an experienced petrographer. Therefore, this study proposes using artificial intelligence (AI) through machine learning (ML) techniques to automate the DRI test protocol estimating the damage degree of concrete affected by ASR. The ML subfield known as Deep Learning (DL) was implemented to create human-like intelligence connections using a Convolutional Neural Network (CNN) algorithm, which can predict the DRI results (machine assessment) that are close to those expected (human assessment. This research is divided into two phases: 1) performing cracks recognition using sliding windows and 2) an advanced pixel recognition. In the first phase, the results displayed some inconsistencies in cracks classification; yet, for cracks identification in the cement paste, in particular, this method presented promising results. However, the advanced pixel recognition improved the drawbacks of the first phase, providing a more accurate cracks recognition and classification. The DRI number estimation was subsequently implemented into the CNN model achieving a 74.4% accuracy. Hence, the DRI automation is a revolutionary step towards a more ubiquitous use of the method since less time is required to perform the task, besides avoiding variability among petrographers and enabling non/less experienced professionals to take advantage of this powerful microscopic tool. With a more widely accessible diagnostic tool, ASR-affected critical concrete infrastructure could be more efficiently assessed, which would ultimately increase their safety.

Keywords: Alkali-aggregate reaction, Automated condition assessment; crack detection; Damage Rating Index, Machine Learning, Artificial Intelligence.

Acknowledgments

Firstly, I would like to thank my supervisor, Prof. Dr. Leandro Sanchez, who was the one that allowed me to step into this life dream, dreamt of since I was in high school. However, I had never imagined going so far and be part of the uOttawa team. Until now, this has been the biggest challenge I have ever accepted in my entire life and career, and I can say that with Professor Sanchez's guidance, the path has been less complicated and the work more efficient. Indeed, I could not say it was not rocky; otherwise, the research would lose meaning. Yet, I can say that together, we found the solution for every setback.

Secondly, I would like to express my deepest gratitude to my family, especially my mother, my sister Hadassa and Clarissa; they are my light and strength, my true North even before I was born. With them and Luan, my boyfriend, I have learned how strong we can be when we want to pursue our dreams. Since I came to Canada, Luan taught me how big are our dreams, and how persistent our heart is when it genuinely wants something. Luan: I am sure you are a God's blessing in my life. Thank you for your support, for being there discussing my results, being the other side of my consciousness. Without you, my lab sections and the long journey would not have the laughs and all the fun.

My profound thanks to all µStructure research group colleagues and friends, especially Cassandra Trottier, Gustavo Macioski, Gabriella Puente, Diego Souza, and Andisheh Zahedi, for all their support, for teaching me from the beginning how the path I chose was fascinating and sharing their knowledge with me. Because of you, since my first day, I have felt part of this great team. Another important colleague that I am very thankful is Haoye Lu for all the lessons regarding this new world on artificial intelligence.

Last but not least, I would like to recognize two essential members of uOttawa at the Faculty of Civil Engineering: the technical officers (TOs) of the Materials and Structures Laboratory, Drs. Muslim Majeed, and Gamal Elnabelsya. They were essential during my lonely journey in the microscope room.

Table of Contents

List of Figures

List of Tables

CHAPTER ONE: INTRODUCTION

1.1. Synopsis

Alkali-silica reaction (ASR) is the most frequent type of Alkali-aggregate reaction (AAR) affecting concrete structures worldwide. It is caused by a chemical reaction between the alkali hydroxides (i.e., Na^+, K^+ and OH^-) from the concrete pore solution and some unstable siliceous phases from the aggregates used to make concrete. ASR generates a secondary product that swells upon moisture uptake, leading to induced expansion, cracking, and reducing the mechanical properties of the affected concrete [1–3]. As such, ASR is reported as a significant concern in concrete durability associated with high repair and maintenance costs [4,5]. Therefore, aiming to reduce the cost of the repairs and increase the service life of ASR-affected concrete structures, guidelines were developed using different techniques to appraise the current condition (i.e., cause(s) and extent of damage - diagnosis), and the potential of further deterioration (i.e., prognosis). Consequently, understanding both the diagnosis and prognosis of ASR-affected structures is essential for better selecting rehabilitation and management strategies [4,6–8].

To assess the current condition and predict the potential for further distress of ASR-affected concrete structures, engineers and researchers have been developing new visual, non-destructive, mechanical, and microscopic tools. Moreover, quantitative image analysis techniques using fluorescent epoxy dyes have also gained some interest. Nevertheless, drawbacks were observed, such as the sample preparation is time-consuming, requiring vacuum cleaning before epoxy impregnation, and the analysis requires more specific equipment (e.g., UV lights, UV lights protection) [19–24]. On the other hand, the Damage Rating Index (DRI) is a semi-quantitative microscopic technique that has shown quite promising results, helping to identify the cause and extent of ASR damage, especially when combined with other mechanical tools [8–18]. Unlike the extensive specimen preparation of image analysis, the DRI requires cutting a specimen longitudinally in half using a masonry saw equipped with a diamond blade followed by a sequence of grinding and polishing to obtain a flat and reflective surface, respectively. Distress features (i.e. cracks) associated with ASR are counted in 1 cm by 1 cm squares on the reflective surface of the specimen using a stereomicroscope at 16x magnification. A weighting factor is then applied to those features to balance their relative importance towards the overall distress mechanism. The counts are then normalized to 100 square centimetres, which generates the DRI number.

Furthermore, the crack's location and extension (i.e. within the aggregate versus extension into the cement paste) can be determined while performing the DRI, which corresponds to a degree of damage and is expressed by a level of expansion achieved by the concrete. In addition, losses in specific mechanical properties are correlated to the expansion level, thus, location and extension of those cracks [4,9,10,25–28]. Although the DRI is an accurate and reliable technique used to assess damage in concrete, performing the DRI is very time-consuming and requires suitable expertise from the operator (i.e. petrographer). Nevertheless, in recent years, the use of image recognition through Machine Learning (ML) has had astonishing success in classifying objects in photos and videos. This technology could therefore be used to detect and forecast damage in concrete. However, very few data are available in the literature on the use of ML systems to diagnose distressed concrete, mainly affected by ASR. Some studies used Deep Learning (DL), a subset of ML, to develop crack detection models [34–43] yet, without any correlation to the damage caused and extent. Thus, the rapidly evolving advancements in artificial intelligence, in general, are a significant asset to the unprecedented incorporation of ML of a well-established microscopic technique such as the DRI to automatically detect and classify cracks produced by ASR in damaged concrete. In consequence, this powerful automated microscopic tool will reduce the time required to perform the DRI and will be more readily accessible to all researchers and engineers; reducing the number of incompletely diagnosed concrete structures and, when addressed, increasing the service life of the affected structures through the use of the appropriate mitigation and rehabilitation strategies.

1.2. Research Objectives

The goal of this project is to estimate the damage degree of concrete affected by ASR through the automation of the Damage Rating index (DRI) using Deep Learning (DL), through Convolutional Neural Networks (CNN) models and draw a comparison between the results presented by the machine versus petrographers. Firstly, concrete samples (i.e., 100 by 200 mm cylinders) were produced using a highly reactive coarse aggregate (Springhill – Greywacke), boosted with sodium hydroxide to raise the alkali content of the concrete and thus accelerate ASR development in the laboratory. Then, the manufactured concrete specimens were stored under controlled environmental conditions (i.e., 38°C and 100% RH), enabling ASR-induced development. All specimens were monitored over time, and once they achieved targeted expansion levels (i.e., 0.05%, 0.12%, 0.20% and 0.30%), they were prepared (i.e., cut and polished), and the DRI was conducted on them by experienced petrographers. Moreover, images were taken from all specimens to provide the database required to build and improve a DL algorithm (i.e., convolutional neural network – CNN) capable of recognizing and classifying numerous ASR-related distress features.

The DL/CNN algorithm was developed in two phases: first, it was built and improved using over 55,000 features, divided into three main groups based on the typical ASR petrographic features as per the DRI: closed cracks within the aggregate (CCA), closed cracks within the aggregate with and without gel (OCA+OCAG) and crack in the cement paste without and with gel (CCP+CCPG). Some of the features were manually traced to better teach the algorithm, while others remained non-traced to assess the algorithm efficiency. Once the model was deemed accurate enough for the sake of this project (i.e., 70% in proper cracks recognition), the second phase of the project started. In the second phase, the proposed DL/CNN algorithm was used not only to recognize the cracks but rather to estimate the DRI values of ASR-affected concrete. The aforementioned petrographic features were identified, counted and multiplied by corresponding weighting factors whose purpose is to balance the overall damage towards the damage mechanism under consideration (i.e., ASR in this case). Finally, comparisons between human versus machine assessments were conducted, and limitations and further research need to be highlighted.

1.3. Thesis Organization

The activities presented in this research were performed in partnership with the Faculty of Engineering and Mathematics: thesis supervisor Dr. Leandro Sanchez, and thesis co-supervisor, Dr. Maia Fraser. Both teams created the database and the procedures to organize the algorithm's architecture, data treatment and analysis (Civil Engineering department), and model development (Mathematics and Statistics department). Likewise, I attest that all main activities conducted in this research have been performed by myself. Cassandra Trottier, a Ph.D. student, also supervised by Dr. Sanchez, contributed to the project in terms of data collection and research methodology, besides reviewing the documents. This thesis is presented in a paper-based format and is divided into five chapters, as presented hereafter:

Chapter 1: Presents a synopsis on alkali-silica reaction (ASR), microscopic techniques used to assess concrete microstructure, and discusses the potential of using Artificial Intelligence (AI) techniques to determine the current expansion and deterioration of ASR-affected concrete. This chapter also displays the main goals of this research and, finally, presents the thesis organization and structure.

Chapter 2: This chapter comprises a comprehensive literature review on concrete affected by alkali-silica reaction (ASR) and discusses ASR-induced damage development (i.e., cracks generation and propagation); additionally, this chapter includes a thorough background of microscopic analysis, specifically Damage Rating Index (DRI). Likewise, Artificial Intelligence (AI) concepts and their derivatives are summarized to enlighten the minimum necessary context to understand the main goals and characteristics of the proposed AI algorithm.

Chapter 3: Consists of an "*in press*" conference paper entitled: "The Use of Artificial Intelligence for Assessing Damage in Concrete Affected by Alkali-Aggregate Reaction (AAR)," and selected for oral presentation at the International Conference on Alkali-Aggregate Reaction (ICAAR, Lisbon 2021). The document submitted comprises some of the preliminary results of cracks recognition and classification, where the AI algorithm was developed using a technique called sliding window associated with heat maps. This was our first approach, which does not represent the current state of the art of this research.

Chapter 4: Consists of a scientific paper submitted to the prestigious Cement and Concrete Research (CCR, Elsevier) journal, which is the continuation and thorough version of the conference paper displayed in Chapter 3; this work presents the state of the art of the AI/CNN algorithm developed, which recognizes and counts ASR-related cracks with much-improved performance when compared to the conference version. Furthermore, the AI/CNN proposed model is used to estimate the overall damage of ASR-affected concrete through the DRI number. This paper is entitled: The Use of Artificial Intelligence for Assessing Damage in Concrete Affected by Alkali-Silica Reaction (ASR).

Chapter 5: Finally, Chapter 5 displays the general conclusions of this research project followed by recommendations and suggestions for future research in the field.

1.4. References

[1] I. Yurtdas, D. Chen, D.W. Hu, J.F. Shao, Influence of alkali silica reaction (ASR) on mechanical properties of mortar, Constr. Build. Mater. 47 (2013) 165–174. https://doi.org/10.1016/j.conbuildmat.2013.04.046.

[2] T. Chappex, K. Scrivener, Alkali fixation of C-S-H in blended cement pastes and its relation to alkali silica reaction, Cem. Concr. Res. 42 (2012) 1049–1054. https://doi.org/10.1016/j.cemconres.2012.03.010.

[3] Y. Khajehnouri, M. Chouteau, P. Rivard, C.L. Bérubé, Non-destructive non-invasive assessment of the development of alkali-silica reaction in concrete by spectral induced polarization: Evaluation of the complex electrical properties, Constr. Build. Mater. 238 (2020) 117719. https://doi.org/10.1016/j.conbuildmat.2019.117719.

[4] R.B. Figueira, R. Sousa, L. Coelho, M. Azenha, J.M. de Almeida, P.A.S. Jorge, C.J.R. Silva, Alkali-silica reaction in concrete: Mechanisms, mitigation and test methods, Constr. Build. Mater. 222 (2019) 903–931. https://doi.org/10.1016/j.conbuildmat.2019.07.230.

[5] M.T. Benoit Fournier, Marc-André Bérubé, Kevin J. Folliard, Report on ASR Mitigation, Fed. Highw. Adm. Publ. FHWA-HRT-04-113 Techbr. FHWA-HRT-06-071. (2010).

[6] B. Fournier, M.A. Bérubé, K.J. Folliard, M. Thomas, ASR Testing and Evaluation Protocols Prepared for the Federal Highway Administration by :, (2008).

[7] AASHTO T 380, Standard Method of Test for Potential Alkali Reactivity of Aggregates and Effectiveness of ASR Mitigation Measures (Miniature Concrete Prism Test, MCPT), (2019) 1–10.

[8] A. Zahedi, C. Trottier, L.F.M. Sanchez, M. Noël, Microscopic assessment of ASR-affected concrete under confinement conditions, Cem. Concr. Res. 145 (2021). https://doi.org/10.1016/j.cemconres.2021.106456.

[9] L.F.M. Sanchez, B. Fournier, M. Jolin, M.A.B. Bedoya, J. Bastien, J. Duchesne, Use of Damage Rating Index to quantify alkali-silica reaction damage in concrete: Fine versus coarse aggregate, ACI Mater. J. 113 (2016) 395–407. https://doi.org/10.14359/51688983.

[10] C. Trottier, A. Zahedi, R. Ziapour, L. Sanchez, F. Locati, Microscopic assessment of recycled concrete aggregate (RCA) mixtures affected by alkali-silica reaction (ASR), Constr. Build. Mater. 269 (2021) 121250. https://doi.org/10.1016/j.conbuildmat.2020.121250.

[11] V. Villenneuve, B. Fournier, J. Duchesne, Determination of the damage in concrete affected by ASR – The damage rating index (DRI)., in: 14th Int. Conf. Alkali-Aggregate React. (ICAAR)., Austin, USA., 2012.

[12] L.F.M. Sanchez, B. Fournier, M. Jolin, J. Bastien, Evaluation of the Stiffness Damage Test (SDT) as a tool for assessing damage in concrete due to alkali-silica reaction (ASR): Input parameters and variability of the test responses, Constr. Build. Mater. 77 (2015) 20–32. https://doi.org/10.1016/j.conbuildmat.2014.11.071.

[13] Grattan-Bellew, E., D. Mitchell, J. Margeson, D. Min, Is alkali-carbonate reaction just a variant of alkali-silica reaction ACR = ASR?, Cem. Concr. Res. 40 (2010) 556–562. https://doi.org/10.1016/j.cemconres.2009.09.002.

[14] P. Rivard, B. Fournier, G. Ballivy, Quantitative petrographic technique for concrete damage due to ASR: Experimental and application, Cem. Concr. Aggregates. 22 (2000) 63–72. https://doi.org/10.1520/cca10465j.

[15] L.F.M. Sanchez, B. Fournier, T. Drimalas, J. Bastien, L.D. Mitchell, M. Noel, Semi-Quantitative Condition Assessment of Concrete Distress Through the Damage Rating Index, Int. Conf. Alkali Aggragete React. (2016) 10.

[16] L.F.M. Sanchez, B. Fournier, M. Jolin, D. Mitchell, J. Bastien, Overall assessment of Alkali-Aggregate Reaction (AAR) in concretes presenting different strengths and incorporating a wide range of reactive aggregate types and natures, Cem. Concr. Res. 93 (2017) 17–31. https://doi.org/10.1016/j.cemconres.2016.12.001.

[17] S. Bilodeau, A. Allard, J. Bastien, F. Pissot, B. Fournier, B. Bissonnette, Performance Evaluation of Thick Concrete Slabs Affected by Alkali-Silica Reaction (ASR) - Part II: Structural Aspects, Conf. Proc. 15th ICAAR. (2016) 1–9.

[18] P.E. Grattan-Bellew, L.D. Mitchell, Quantitative Petrographic Analysis of Concrete – The Damage Rating Index (DRI) Method , A Review, 8th CANMET/ACI Int. Conf. Recent Adv. Concr. Technol. (2006) 14.

[19] N. Castro, B.J. Wigum, Assessment of the potential alkali-reactivity of aggregates for concrete by image analysis petrography, Cem. Concr. Res. 42 (2012) 1635–1644. https://doi.org/10.1016/j.cemconres.2012.08.009.

[20] V. Jensen, S. Sujjavanich, Alkali Silica Reaction in Concrete Foundations in Thailand, 15th ICAAR - Intenational Conf. Alkali Aggreg. React. Concr. (2016).

[21] A. du Plessis, WP Boshoff, A review of X-ray computed tomography of concrete and asphalt construction materials, Constr. Build. Mater. 199 (2019) 637–651. https://doi.org/10.1016/j.conbuildmat.2018.12.049.

[22] K.J. Leśnicki, J.Y. Kim, K.E. Kurtis, L.J. Jacobs, Assessment of alkali-silica reaction damage through quantification of concrete nonlinearity, Mater. Struct. Constr. 46 (2013) 497–509. https://doi.org/10.1617/s11527-012-9942-y.

[23] R.A. Barbosa, S. Gustenhoff Hansen, K. Kielsgaard Hansen, L. Cao Hoang, B. Grelk, I. Maag, Assessment of severely ASR damaged bridges: From diagnosis to structural effects, Proc. 15th Int. Conf. Alkali-Aggregate React. Concr. (2016) 10.

[24] A. Malek, A. Scott, S. Pampanin, G. MacRae, Post-event damage assessment of concrete using the fluorescent microscopy technique, Cem. Concr. Res. 102 (2017) 203–211. https://doi.org/10.1016/j.cemconres.2017.09.015.

[25] L.F.M. Sanchez, B. Fournier, M. Jolin, J. Duchesne, Reliable quantification of AAR damage through assessment of the Damage Rating Index (DRI), Cem. Concr. Res. 67 (2015) 74–92. https://doi.org/10.1016/j.cemconres.2014.08.002.

[26] L.F.M. Sanchez, T. Drimalas, B. Fournier, D. Mitchell, J. Bastien, Comprehensive damage assessment in concrete affected by different internal swelling reaction (ISR) mechanisms, Cem. Concr. Res. 107 (2018) 284–303. https://doi.org/10.1016/j.cemconres.2018.02.017.

[27] DJ De Souza, L.F.M. Sanchez, M.T. De Grazia, Evaluation of a direct shear test setup to quantify AAR-induced expansion and damage in concrete, Constr. Build. Mater. 229 (2019) 116806. https://doi.org/10.1016/j.conbuildmat.2019.116806.

[28] N. Smaoui, B. Bissonnette, M.A. Bérubé, B. Fournier, B. Durand, Mechanical properties of ASR-affected concrete containing fine or coarse reactive aggregates, J. ASTM Int. 3 (2006) 1–16. https://doi.org/10.1520/jai12010.

[29] M.A. Hariri-Ardebili, F. Pourkamali-Anaraki, Simplified reliability analysis of multi hazard risk in gravity dams via machine learning techniques, Arch. Civ. Mech. Eng. 18 (2018) 592–610. https://doi.org/10.1016/j.acme.2017.09.003.

[30] M.A. Hariri-Ardebili, B. Sudret, Polynomial chaos expansion for uncertainty quantification of dam engineering problems, Eng. Struct. 203 (2020) 109631. https://doi.org/10.1016/j.engstruct.2019.109631.

[31] V. Ranković, N. Grujović, D. Divac, N. Milivojević, Development of support vector regression identification model for prediction of dam structural behaviour, Struct. Saf. 48 (2014) 33–39. https://doi.org/10.1016/j.strusafe.2014.02.004.

[32] C. Comi, B. Kirchmayr, R. Pignatelli, Two-phase damage modeling of concrete affected by alkali-silica reaction under variable temperature and humidity conditions, Int. J. Solids Struct. 49 (2012) 3367–3380. https://doi.org/10.1016/j.ijsolstr.2012.07.015.

[33] M. Alnaggar, G. Cusatis, G. Di Luzio, Lattice Discrete Particle Modeling (LDPM) of Alkali Silica Reaction (ASR) deterioration of concrete structures, Cem. Concr. Compos. 41 (2013) 45–59. https://doi.org/10.1016/j.cemconcomp.2013.04.015.

[34] Z. Wang, G. Xu, Y. Ding, B. Wu, G. Lu, A vision-based active learning convolutional neural network model for concrete surface crack detection, Adv. Struct. Eng. 23 (2020) 2952–2964. https://doi.org/10.1177/1369433220924792.

[35] J. Kim, S. Shim, Y. Cha, G.C. Cho, Lightweight pixel-wise segmentation for efficient concrete crack detection using hierarchical convolutional neural network, Smart Mater. Struct. 30 (2021). https://doi.org/10.1088/1361-665X/abea1e.

[36] J. Deng, Y. Lu, V.C.S. Lee, Concrete crack detection with handwriting script interferences using faster region-based convolutional neural network, Comput. Civ. Infrastruct. Eng. 35 (2020) 373–388. https://doi.org/10.1111/mice.12497.

[37] S. Li, X. Zhao, Image-Based Concrete Crack Detection Using Convolutional Neural Network and Exhaustive Search Technique, Adv. Civ. Eng. 2019 (2019). https://doi.org/10.1155/2019/6520620.

[38] N.-D. Hoang, An Artificial Intelligence Method for Asphalt Pavement Pothole Detection Using Least Squares Support Vector Machine and Neural Network with Steerable Filter-Based Feature Extraction, Adv. Civ. Eng. 2018 (2018) 1–12.

[39] H. Nhat-Duc, Q.L. Nguyen, V.D. Tran, Automatic recognition of asphalt pavement cracks using metaheuristic optimized edge detection algorithms and convolution neural network, Autom. Constr. 94 (2018) 203–213. https://doi.org/10.1016/j.autcon.2018.07.008.

[40] G.H. Beckman, D. Polyzois, Y.J. Cha, Deep learning-based automatic volumetric damage quantification using depth camera, Autom. Constr. 99 (2019) 114–124. https://doi.org/10.1016/j.autcon.2018.12.006.

[41] C.V. Dung, L.D. Anh, Autonomous concrete crack detection using deep fully convolutional neural network, Autom. Constr. 99 (2019) 52–58. https://doi.org/10.1016/j.autcon.2018.11.028.

[42] Y.J. Cha, W. Choi, O. Büyüköztürk, Deep Learning-Based Crack Damage Detection Using Convolutional Neural Networks, Comput. Civ. Infrastruct. Eng. 32 (2017) 361–378. https://doi.org/10.1111/mice.12263.

[43] W. Song, G. Jia, H. Zhu, D. Jia, L. Gao, Automated pavement crack damage detection using deep multiscale convolutional features, J. Adv. Transp. 2020 (2020). https://doi.org/10.1155/2020/6412562.

CHAPTER TWO: LITERATURE REVIEW

2.1. Alkali-Aggregate Reaction (AAR)

Alkali-aggregate reaction (AAR) is among the most harmful damage mechanisms affecting concrete infrastructure worldwide. The first time the term was mentioned in the literature was in 1940, by Stanton [1] and associated the reactants with the disorders observed in concrete structures. Since then, AAR has been recognized as one of the most detrimental distress mechanisms, which can compromise serviceability and, in some cases, the safety of the affected structure. At first, it was observed as a reaction between cement and some types of aggregate, and nowadays, the AAR is differentiated into two significant types [1,2]:

Alkali-carbonate reactions (ACR) - Being the rarest form, it is caused by the presence of carbonate rocks (i.e. limestone and/or dolomite aggregates) and is characterized by a rapid expansion and a high damage level due to the extensive crack network in the affected concrete [3–5]. A general agreement of the distress mechanism has not been reached for ACR-affected concrete; however, the process of dedolomitization where calcite and brucite are formed within the aggregate's boundaries have been reported. Nevertheless, researchers demonstrated through mechanical behaviour that ACR's distress mechanism is entirely different from the other AAR mechanism, ACR being more deleterious as per the ACI 221.2R-16 Guide to Durable Concrete - differentiating both deleterious mechanisms [3–9].

Alkali-silica reactions (ASR) - The most widespread form of AAR, ASR is caused by the reaction between the alkalis (Na^+, K^+ and OH^-) present in the concrete pore solution and some unstable siliceous phase materials found within the aggregate, forming a volumetric expansive hygroscopic reaction by-product (i.e., silica gel) in the presence of moisture, as shown in **Figure 2.1** [10–15]. The formed silica gel swells, generating tensile stresses within the concrete and undertaking the development of a microcrack network beginning within the aggregate and propagating towards and through the cement paste until it reaches its maximum tensile stress capacity and cracks the concrete.

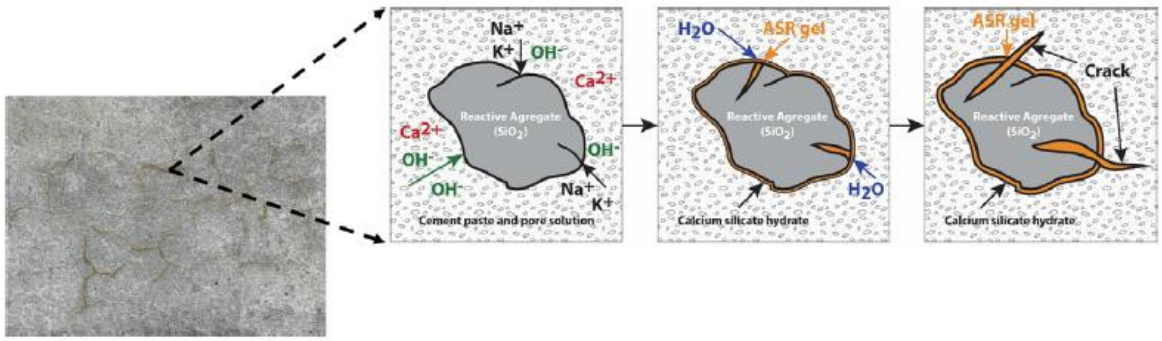

Figure 2.1: Mechanism of the ASR in concrete - Schematic illustration [15].

Macroscopically, the cracks can also appear at the concrete's surface, characterized as map cracking. However, the crack propagation can be influenced according to the restraint or reinforcement as it creates an internal confined condition, resulting in crack development perpendicular to the direction having the least reinforcement [16]. **Figure 2.2** demonstrates both types of surface cracks: a) the map-cracking commonly observed in block foundations or surfaces with a thick concrete cover, and b) directional cracks usually appearing in reinforced members such as slabs, beams and columns where the reinforcement percentage is elevated. [5,8,9,16–20].

a) map-cracking **b) directional cracks**

Figure 2.2: ASR-related signs in bridge elements [11,21].

Indeed, this damage is observed as cracks within and at the surface of the concrete and consequently, reduces its mechanical properties. Likewise, another consequence of this expansion is a loss of serviceability. For example, when experiencing high expansion levels, a dam's gates may encounter difficulty opening and operating due to the swelling of the concrete; in this case, notches are normally generated (i.e., slot cuts) to release ASR-induced pressure and improve their operation. As such, an example of this intervention in the structure is the ICOLD Chickamauga Dam, USA. The dam suffered from ASR in most of its members, and slices of concrete were removed to release the pressure obstructing the gates from opening [22]. As it is possible to notice in **Figure 2.3** the critical region affected by ASR is the corner connecting the dam and the spillway, which prevents the gates from opening.

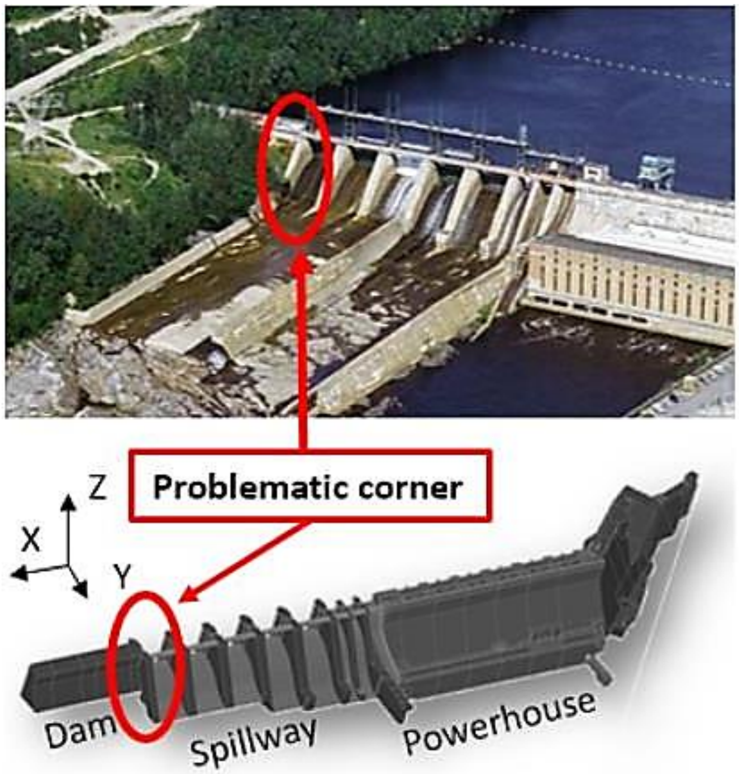

Figure 2.3: Problems caused by ASR volumetric expansion in dams [22].

Factors influencing ASR-induced development (i.e., kinetics) are the concrete's alkali content, the temperature and relative humidity as well as the aggregate type (i.e., coarse or fine aggregate) and nature (i.e., lithotype). However, a different crack generation and propagation is observed for different aggregate types. As displayed in **Figure 2.4**.**a**, a concrete made with reactive fine aggregate generates the microcracks within the fine aggregate particles (i.e., sand) which spread rapidly through the bulk cement paste and interfacial transition zone (ITZ); forming a more sparsely distributed cracking pattern. Those cracks may even propagate through the non-reactive coarse aggregate particles because of the extensive pressure. Conversely, ASR triggered by a reactive coarse aggregate presents a different cracking behaviour **(Figure2.4.b**) when compared to a fine reactive aggregate. Cracks are generated and propagated within the coarse aggregate particles before entering the ITZ and extending into the bulk cement paste; rarely propagating through the non-reactive fine aggregates.

a) fine reactive aggregate **b) reactive coarse aggregate**

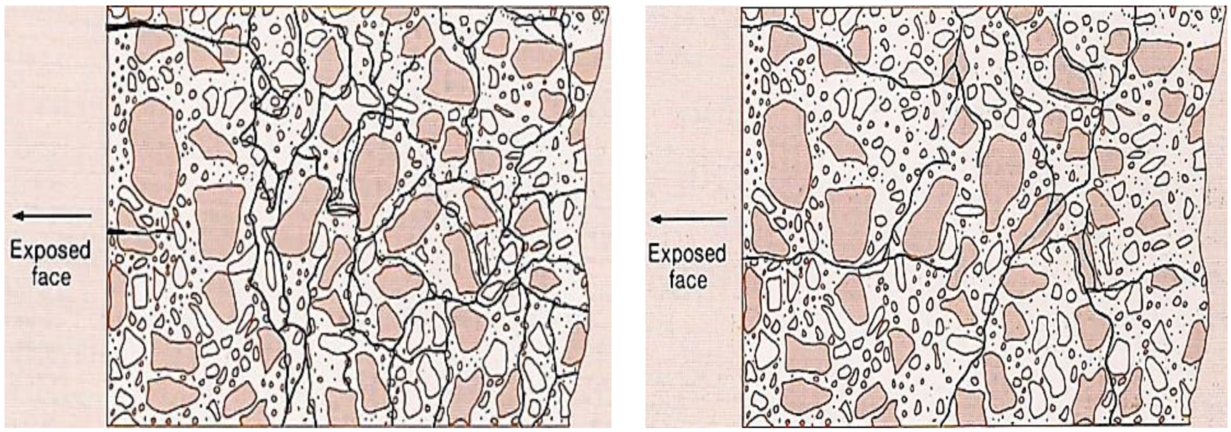

Figure 2.4: ASR crack propagation model per aggregate type [23].

Damage is defined by Sanchez et al. [8] as the reduction of stiffness (i.e. modulus of elasticity)[18,24], mechanical properties (i.e. tensile and compressive strength) [18,24], aggregate interlock resulting in a decrease in the shear capacity [25] and loss of physical integrity, directly affecting the durability of affected concrete. The damage caused by ASR in concrete is therefore expressed by the level of expansion achieved by the concrete. As the level of expansion increases, the cracks propagate (**Figure 2.5)** and the consequences of ASR-induced deterioration become more severe. For ASR, cracks are generated within the aggregate as (A) sharp type cracks or (B) onion skin type cracks formed at the periphery of the aggregate and unfold tangentially to the edges of the aggregate particle until the crack reaches the cement paste.

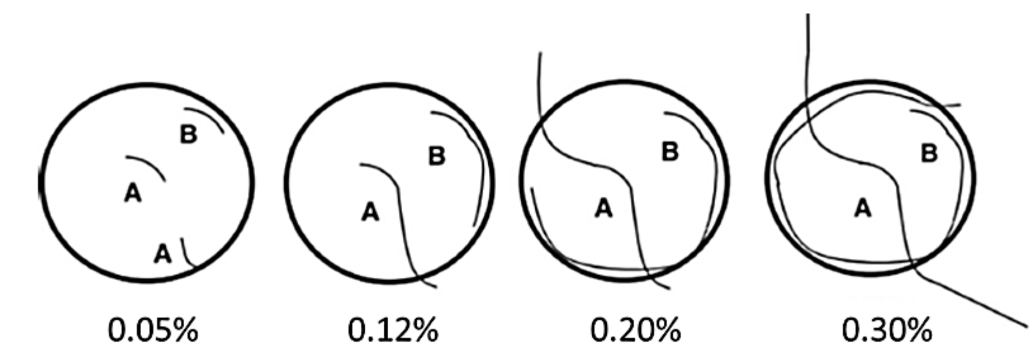

Figure 2.5: Qualitative model of ASR development through crack propagation as a function of the expansion with A) sharp cracks and B) onion skin type cracks [8].

At a low damage degree (i.e., expansion level of 0.05%), cracks are generally closed (i.e. have not been opened by the pressure of the silica gel) and only observed within the aggregate and rarely within the cement paste. Some of these closed cracks may not be ASR related but rather due to rock formation and weathering as well as aggregate processing. Nonetheless, as the ASR-induced expansion develops, some of these closed cracks may start to open gradually and extend due to ASR.

Likewise, at a moderate degree of damage (i.e. 0.12% level of expansion), the sharp cracks continue to propagate through the aggregate and may extend into the cement paste at least on one side of the aggregate while the onion skin type cracks continue to follow the aggregate's periphery. Upon reaching a high degree of damage (i.e. expansion level of 0.20%), the onion skin type crack further elongates within the aggregate whereas the sharp type cracks extend into the cement paste on both sides of the aggregate, splitting it in half and reaching the yield strain of the steel reinforcement. Correspondingly, at very high damage degrees (i.e. 0.30% expansion levels), the sharp type cracks propagate into the cement paste linking to one another thus, forming a network and connecting the aggregates to another [13] while the onion skin type cracks begins to extend into the cement paste after having cracks the entire periphery of the aggregate. Consequently, the aforementioned losses in stiffness, tensile strength and aggregate interlock are influenced by cracks within the aggregate (i.e. low to moderate damage degrees). In contrast, extension of the cracks in the cement paste is captured by the reduction in the compressive strength at higher degrees of damage. Even though there is no record of structures collapsing due to ASR, this reaction can be the accelerator of other deleterious agents, compromising or even condemning the structure. Therefore, the earlier they are identified, the greater are the chances of an effective and more economic intervention.

2.2. Methods to Assess Damage in ASR-Affected Concrete

2.2.1. Investigative protocol

ASR affects many of the critical concrete infrastructure vital to everyday use and therefore, clear and concise protocol and methodologies must be followed to appraise such important structures. As such, several guidelines were proposed to help identify the potential cause and extent of a given damaged concrete [26,27] . The protocol developed in 2010 by Fournier et al. [27] (**Figure 2.6**). consists of a global approach divided into three levels:

1) **Condition Survey –** visual signs of premature deterioration associated with those commonly observed by ASR-affected structures, identified during the routine visual inspection. At this stage, the surrounding environmental conditions such as water accumulation, wetting and drying cycles, temperature, etc. may be reported to indicate potential areas susceptible to ASR.

2) **Preliminary Studies for the Diagnosis of ASR** – this step consists of reviewing documentation to see whether the aggregates were appraised for reactivity potential or not and search for reports of

ASR-related cases in that region. Furthermore, a field inspection is initiated through the Crack Index (CI) method developed by Fournier et. al (2010) [27], giving an indication of the extent of ASR cracking of the affected concrete. The CI consists of drawing a 0.5 m by 0.5 m square with 10 equal intervals on the distressed surface, following the direction of the main reinforcements after which the number of cracks and their width crossing these intervals are recorded. The CI is therefore the average crack width per meter measured as mm/m in both directions. A CI of over 0.5 mm/m and a crack wider than 0.15 mm indicates that further investigation is required. Moreover, preliminary sampling for petrographic examination may be carried out in the laboratory.

3) **Detailed Studies for the Diagnosis/Prognosis of ASR** – the third step entails determining the damage/expansion degree attained to date and the potential for further distress (i.e. diagnosis and prognosis, respectively). Generally, it is required to determine the extent of ASR in the concrete and evaluate its structural stability. The rate of expansion is then monitored, provided that the concrete structure continues to remain in service, to forecast the decrease in its structural stability. As such, the residual expansion (i.e., in laboratory accelerated expansion) is evaluated from cores taken from the concrete structure to determine the remaining reactive potential of the concrete. Indeed, the in-situ concrete may not reach the maximum permissible expansion level to ensure the structures' serviceability and safety as many factors influence the occurrence of on-going ASR, such as moisture, temperature, etc. Therefore, these factors are to be taken into account during the prognosis stage (i.e. ASR modeling) [28]. However, considering the seasonal climatic variations in Canada and the lack of correlation between the residual expansion and real structures subjected to the environment, it is suggested that two years of in-situ concrete expansion measurements are to be performed.

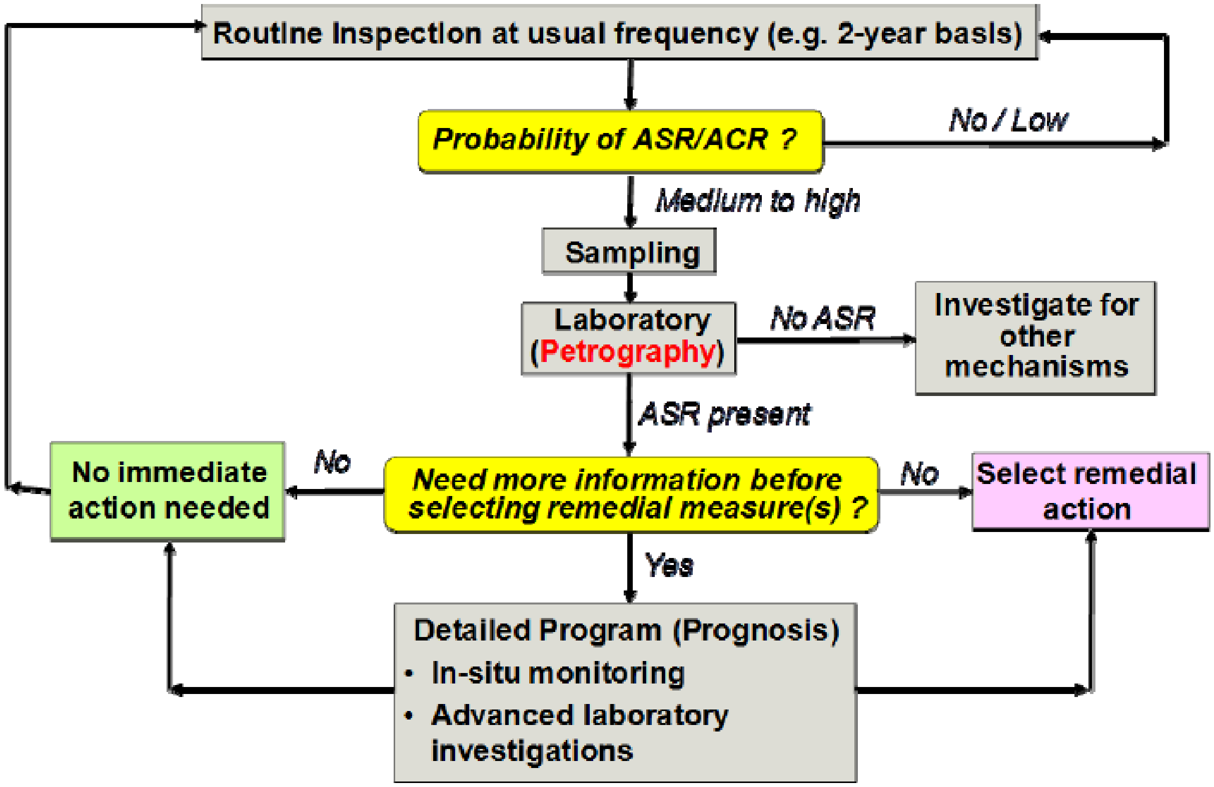

Figure 2.6: Diagnosis and Prognosis of ASR in Concrete Structures - Global Approach [26].

The methodology used to appraise concrete structures can be represented by different scales (e.g., macroscopic, mesoscopic, microscopic). **Figure 2.7a** shows the macroscopic scale, referring to visual inspection such that when a problem is identified through this assessment, further investigations are required. Generally, a concrete exhibiting signs related to substantial damage are assessed through non-destructive techniques and their compressive and tensile strength, and modulus of elasticity. Although these tools can provide the loss in these properties, they do not necessarily capture the cause and extent of the damage thus, resulting in an incomplete diagnosis of the concrete structure. Therefore, the next step in the investigation should be a mesoscale or microscopic scale assessment. At this stage, a closer investigation may reveal the cause and extent of the damage through image analysis and petrographic techniques, presenting a more reliable diagnosis.

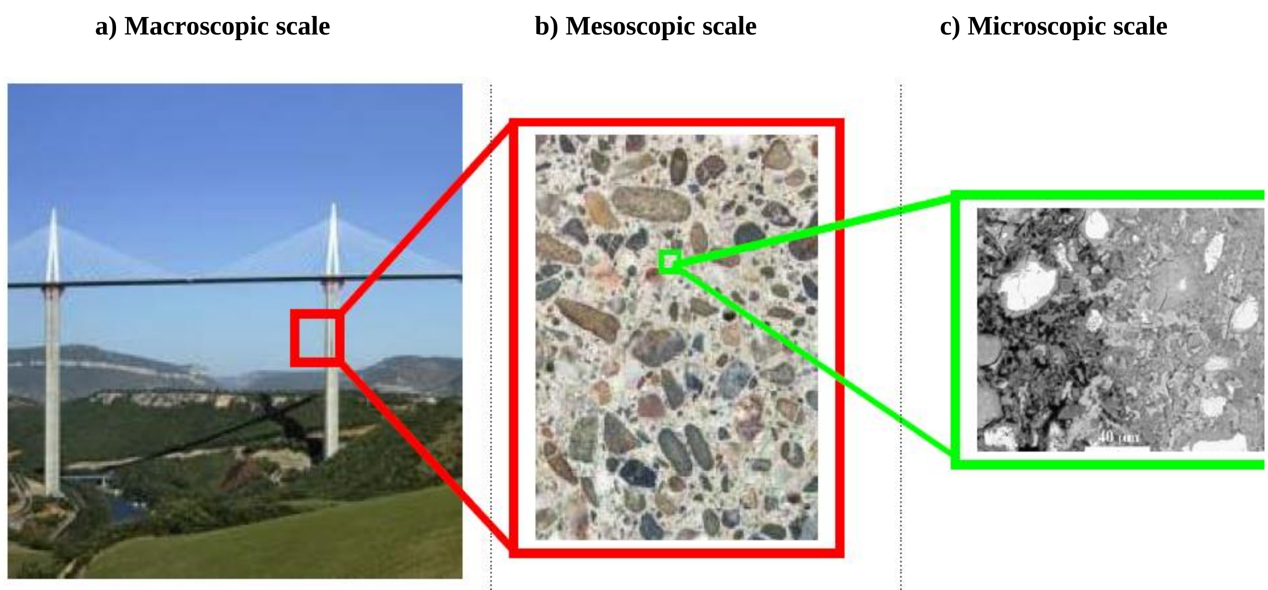

Figure2.7: Millaud viaduct, France. A view from Macroscopic to microscopic scale [2].

2.2.2. Petrographic analysis

According to the protocol mentioned above, once ASR signs are encountered in the structure, one of the methods to confirm the cause of deterioration is to perform an optical microscopy assessment, the so-called petrographic analysis using thin sections. Through the optical microscope, certain petrographic features (i.e., colour of reactive minerals) and distress features (i.e., cracks filled with reaction product) can be identified (**Figure 2.8a)**. Additionally, scanning electron microscopy (SEM) and energy-dispersive x-ray micro-analysis system (EDS) evaluations are performed, as exhibited in **Figure 2.8ab** to confirm the presence of ASR products such as silica, potassium, sodium normally found within the cracks in the aggregates. At the same time, calcium is a principal constituent of the cracks in the cement paste.

a) Micrographs of thin sections showing gel filled cracks

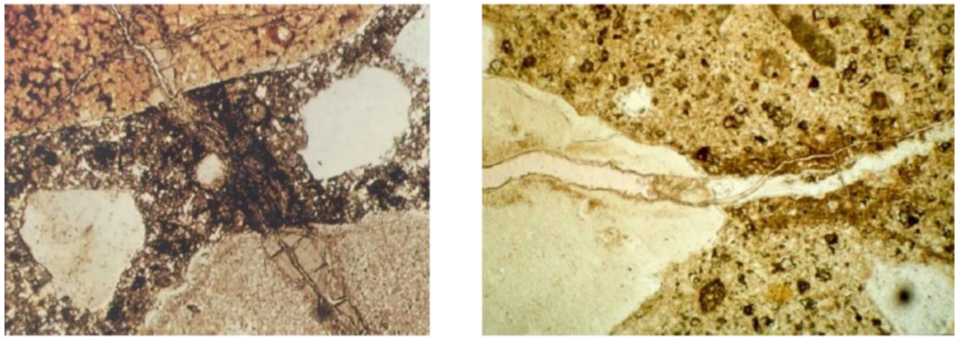

b) SEM and EDX method

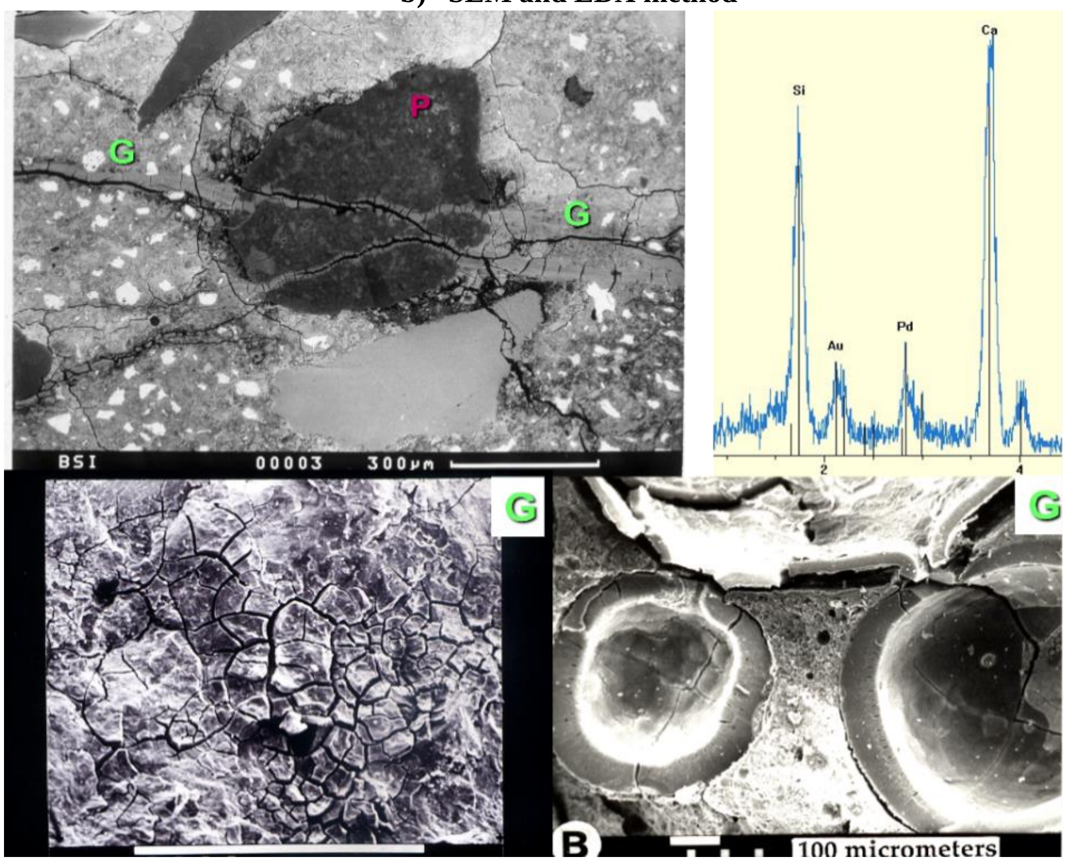

Figure 2.8: Cracks filled with reaction product and extending from reactive aggregate particles through the cement paste [27].

2.2.3. Damage Rating Index (DRI)

Among the petrographic techniques, the Damage Rating Index (DRI) has shown promising results as a tool used for diagnosing ASR-affected concrete, especially when combined with other mechanical tools [8,9,18]. Grattan-Bellew and co-workers [29,30] initially developed the DRI method to evaluate ASR damage in concrete, where the origin of the damage came from the reactive coarse aggregate particles. Sanchez et al. [31] later considered the coarser fraction of the fine aggregates when assessing ASR damage originating from reactive sand. Consequently, crack counts were obtained from particles of 20 mm down to 1 mm in size.

The sample preparation for the DRI analysis consists of cutting the concrete specimen in half longitudinally and polishing its surface prior to drawing a grid of 1cm^2 (i.e. 10 x 10 mm units) on this surface [6,8,12,18,32–35]. The technique is then performed using a stereomicroscope (15-16x magnification) to identify petrographic/distress features related to AAR by analyzing each of these 1 cm^2 squares in the grid as illustrated by **Figure 2.9.** The counts corresponding to each type of petrographic/distress feature is then multiplied by a weighting factor as presented in **Table 2.1**, whose purpose is to balance their relative importance towards the overall mechanism of distress. The factors used in this method were selected on a rational basis but somewhat arbitrarily. These weighting factors were recently modified to account for the severity of the distress features and reduce the variability between the petrographers performing the test [18,36].

A closed crack in the aggregate (CCA) receives the lowest weighting factor (0.25) since they could have been formed by weathering and/or manufacturing instead of being generated by ASR. An open crack in the aggregate without and with gel (OCA and OCAG, respectively) and disaggregated particle (DAP) are associated with a higher relevance when compared with CCA, represented with a weight of 2 since they correspond to the progression of ASR damage in concrete. The highest weighting factor of 3.0 is attributed to cracks in the cement paste without and with gel (CCP and CCPG, respectively) and de-bonded aggregates (CAD) due to their extension into the cement paste thus, higher level of damage. The value obtained from these weighted counts is normalized to a 100 cm^2 area representing the DRI number, a quantitative value. To obtain a representative DRI number of a core extracted from an actual structure, an area of at least 200 cm^2 should be analyzed.

THEREFORE, the DRI number correlates with the damage degree achieved by the concrete as it increases linearly with expansion. Moreover, it has been shown that DRI numbers are associated with induced expansion and damage caused by different types of distress mechanisms (i.e. single and combined) such as delayed ettringite formation (DEF), and freeze-thaw (FT) [8,18,37]. Nevertheless, the DRI allows the visualization of the distress mechanism, allowing the identification of crack patterns associated with literature to determine not only the cause but also extent of the damage due to the extension of the cracks.

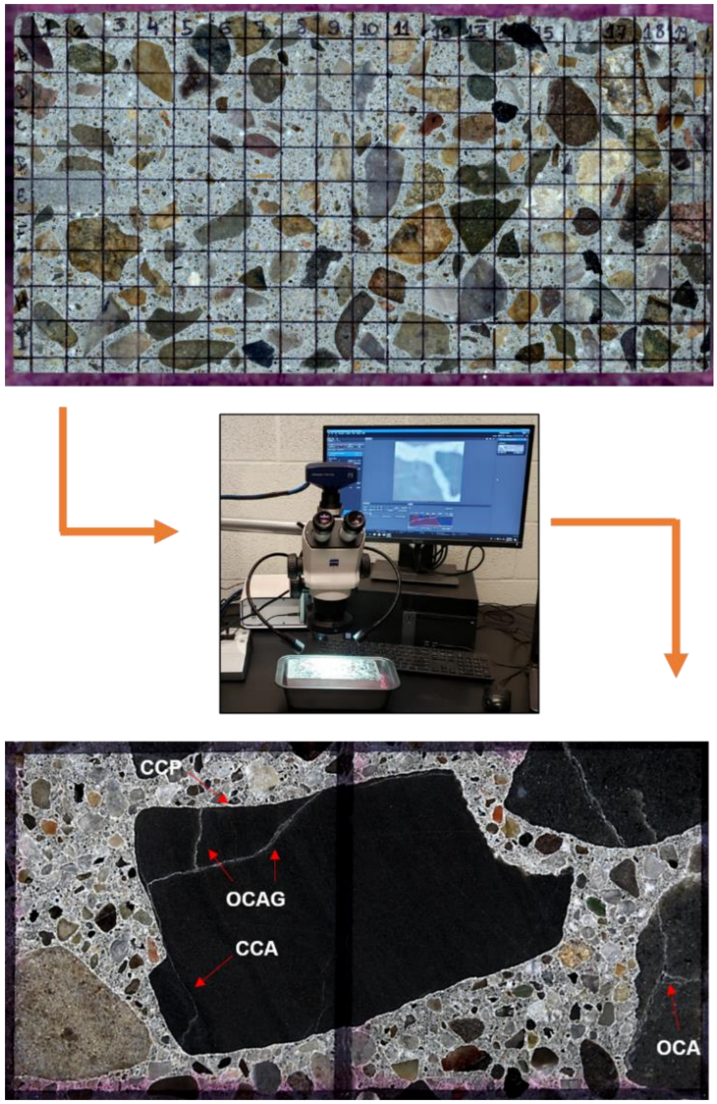

Figure2.9: DRI Setup, including petrographic features.

Table 2.1: Petrographic/distress features and respective weighting factors [8,36,38]

Petrographic/distress features	**Abbreviation**	**Weighting Factor**
Closed cracks in coarse aggregate	CCA	0.25
Opened cracks in coarse aggregate	OCA	2
Crack with reaction product in coarse aggregate	OCAG	2
Coarse aggregate de-bonded	CAD	3
Disaggregate/corroded aggregate particle	DAP	2
Crack in cement paste	CCP	3
Crack with reaction product in cement paste	CCPG	3

Additionally, based on the DRI parameters, another petrographic analysis was developed which required impregnation of the polished concrete surface with a fluorescent epoxy aiming better to highlight the cracks [39–41]. However, the sample preparation of this method is exceptionally time-consuming while also requiring UV lights and its apparatus to protect the petrographer. Despite presenting interesting results, it is less practical and more expensive than the traditional DRI regarding equipment and sample preparation.

2.3. Artificial Intelligence Techniques (AI)

Artificial intelligence (AI) is considered a machine that imitates human cognitive activities, with its functions applied to different human abilities such as learning, vision, language (communication), speech recognition (decoding), among others, as illustrated in **Figure 2.10**.

Machine Learning (ML) is the technical area of AI that develops algorithms and studies their properties, allowing systems to make predictions or take actions based on data/experience instead of following explicitly pre-programmed commands [42]. This technique is used to parse data, learn from it, and make decisions based on what was learned. Deep learning (DL) is a subfield of ML; it is used to create human-like AI by structuring in layers, creating the “artificial neural network” (ANN) or also called fully connected networks (FCN), which can learn and make intelligent decisions by themselves. However, the FCN uses fully connected layers and can be used only for small images, considering the entire image for learning the patterns, without dividing the images into small patches, resulting in heavy data being processed.

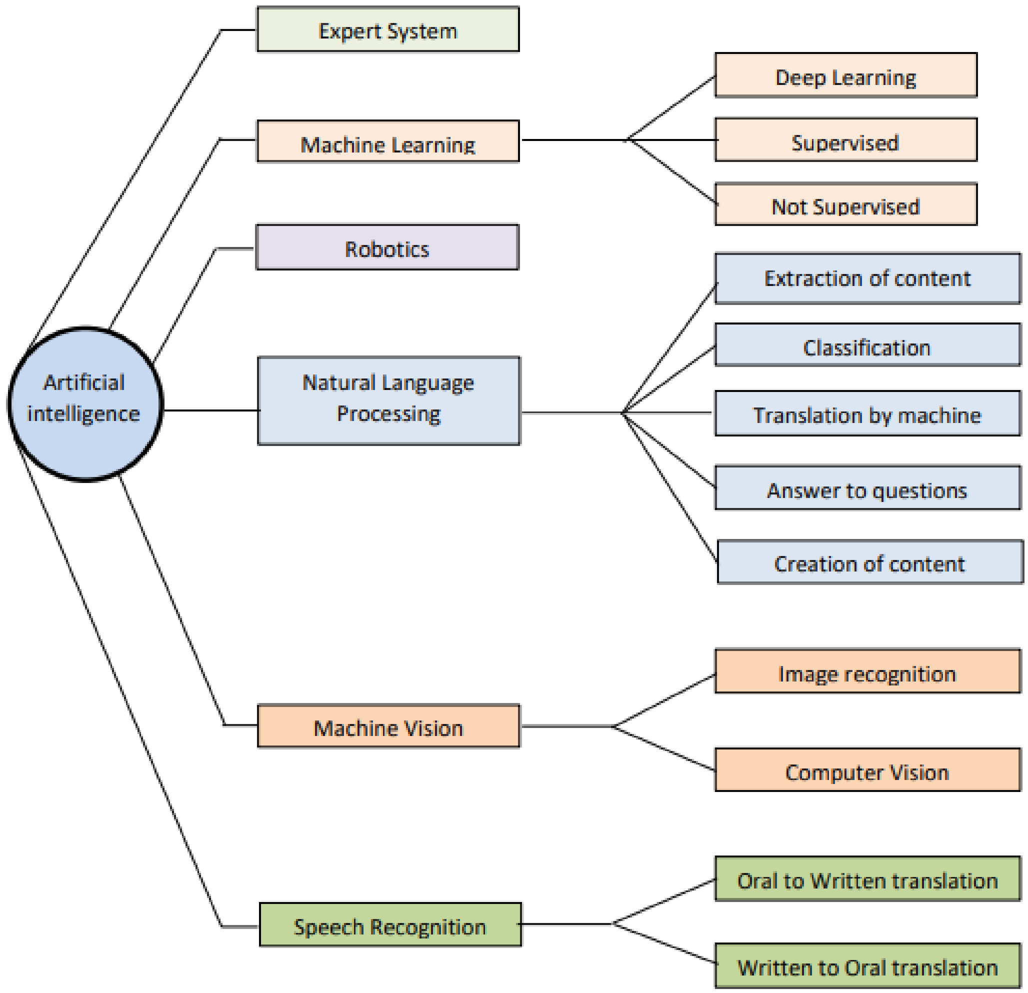

Figure 2,10: Artificial Intelligence functions and techniques.

The crack detection methods mainly use two types of ML methods: support vector machines (SVM) [43–45] and fully connected networks (FCN) [46,47]. Researchers focused on two problems at this stage: verify if an image contains cracks and classify the types of them. Due to the simplicity of models and the computation power limitations, the methods mentioned above cannot capture high-level features. It, therefore, triggers the models to make unreliable estimations when the input images have different brightness and complicated background.

Since approximately 2015, Deep Learning (DL)-based methods have become popular in crack detection problems, allowing researchers to develop very expressive detection models and have been used for crack detection in three different levels [48]: (1) verify whether the image contains cracks; (2) use bounding boxes to locate the areas containing cracks; (3) label all pixels consisting of cracks. A lot of ML-based methods have been proposed for the first task [49,50]. Meanwhile, the second task is somehow simple because the networks only need to learn limited crack features to predict their appearance. For more accurate predictions, researchers have also used a sliding window to iterate the big images. In each iteration, the image patch in the window is used for detection [51,52]. Once completed, all the prediction results are combined to generate a heatmap (**Figure 2.11**).

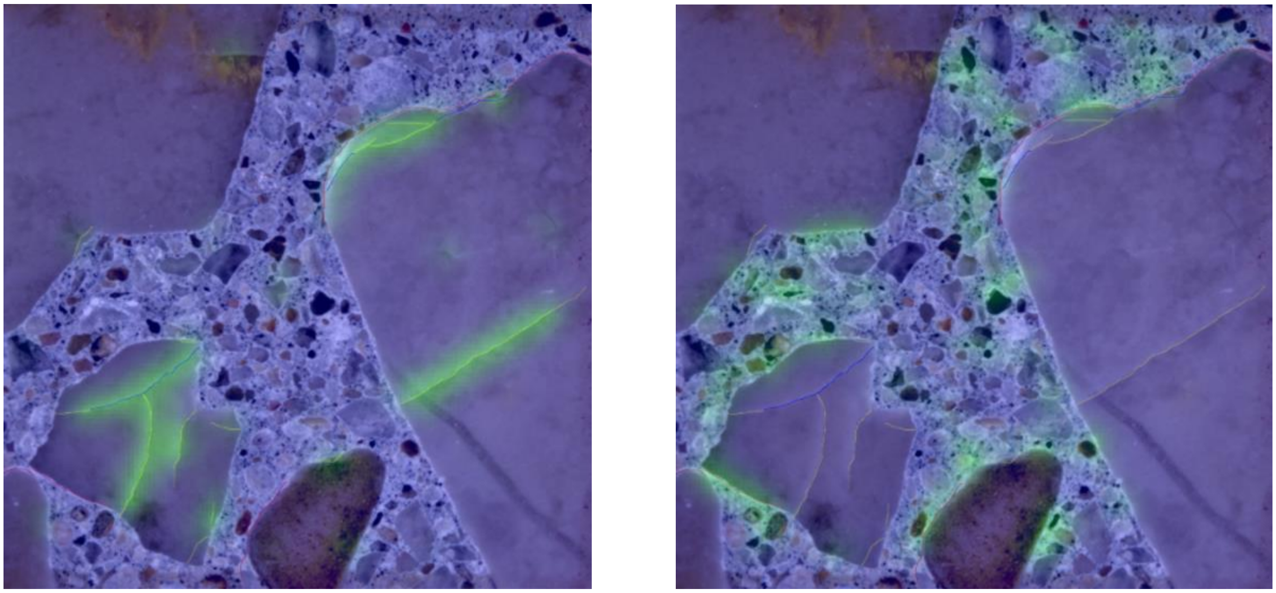

Figure 2.11: Crack Identification using heat maps

Consequently, using sliding windows allows researchers to generate results similar to those produced in the third task. However, there are two substantial problems: (1) the generated heatmap is of low resolution since the detection is performed on the patch level, and (2) if the cracks appear on the window's boundary, the detection algorithms would not be able to detect them. The first problem can be partially alleviated by choosing a smaller window size; however, the detection accuracy may also decrease since the window could be too small to contain enough crack structures. Regarding the second problem, a common technique is to move the window with a stride less than one in exchange for an increasing number of patches to predict and a smoother heatmap.

While the previous task focuses on the crack existence, bounding box techniques are used to locate them [53–55]. Conversely, the Convolutional Neural Networks (CNN) considers only the part of the image, which is in the receptive field of filter, reducing the number of parameters almost 30 times when compared to FCN, reducing the necessity of mighty machines to process the data. Likewise, the CNN can also use the spatial hierarchy of patterns, which helps identifying the patterns (or cracks) more precisely. **Figure 2.12** illustrates the sequence of procedures based on layers since the input is provided until the model takes the final decisions.

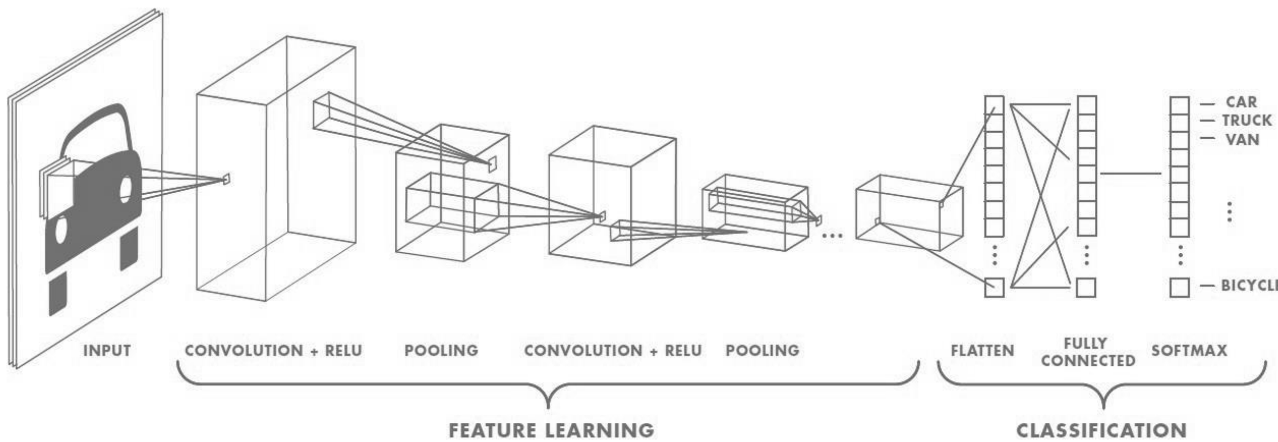

Figure 2.12: A CNN sequence to classify vehicles [56]

The leading researchers of network structures have adapted Faster-RCNN [57] and YOLO [58]. Some researchers have also designed their models using pre-trained backbones like VGG16 [59] and ResNet [60]. The overhead mentioned techniques are part of the CNN classification. Although the bounding box-based methods can provide some location information of cracks, the algorithms cannot predict their shapes, width, and directions. Such limitations motivate researchers to work on pixel-level detection problems, which are usually referred to as segmentation.

Image segmentation is a pixel-level detection problem that requires the algorithms to predict, for each pixel, whether it belongs to a crack or not. Most algorithms for this problem have an encoder-decoder-based architecture [61–63]. To achieve pixel-level prediction, the models preserve the spatial information during the inference so that a one-to-one correspondence relationship can be constructed between the pixels of the input image and the output prediction. Moreover, apart from the mainstream of the segmentation problem defined in a supervised manner, researchers have also adapted generative adversarial networks (GAN) to implement unsupervised learning. The input images and the segmentation targets in the training dataset are not necessarily matched [64].

The aforementioned technique works with this noise as a strength to compete against the factual information (cracks), and the model improves both streams in the system: the noise production and the crack detection success. The foremost disadvantage of this technique is that once it is unsupervised learning, the algorithm does not follow what was taught to perform, not obeying the pre-established layers.

In this regard, this project developed a DL/CNN algorithm, using pixel-level detection in supervised learning, to ensure that the crack identification, counting, and classification are being performed strictly according to the DRI parameter to automate the DRI estimation. Hence, using DL/CNN techniques is a breakthrough in automating the recognition/classification of cracks (i.e., damage) in concrete.

2.4. Research Gap

Although the DRI is a reliable and very efficient microscopic procedure to appraise the cause and extent of damage in concrete affected by ASR, it presents some drawbacks. Among others, the DRI is quite time-consuming and operator sensitive; thus, the DRI automation becomes an excellent opportunity to improve speed and accuracy of the method along with increasing its use worldwide. Artificial intelligence (AI) has been used to recognize cracks in concrete, namely at the material's surface, yet without addressing diagnosis aspects in the appraisal (i.e., search for the damage's cause and extent. This works aims to use DL/CNN techniques to fully automate the DRI through automated crack recognition and classification. Therefore, this novel automated microscopic tool will become more accessible to all researchers and engineers, revolutionizing the investigative microscopic protocols of ASR damaged concrete thus, increasing the safety of concrete structures by providing a more thorough and complete diagnosis.

2.5. References

[1] T.E. Stanton, Expansion of Concrete through Reaction between Cement and Aggregate, in: ASCE, 1940: pp. 1781–1811.

[2] I.C. Peyrot, Development and Validation of a 3D Computational Tool To Describe Damage and Fracture Due To Alkali Silica Reaction in Concrete, École NationaleSupérieuredesMinesdeParis, 2006.

[3] ACI 201.2R-16, 201.2R-16 Guide to Durable Concrete, 2008.

[4] T. Katayama, The so-called alkali-carbonate reaction (ACR) - Its mineralogical and geochemical details, with special reference to ASR, Cem. Concr. Res. 40 (2010) 643–675. https://doi.org/10.1016/j.cemconres.2009.09.020.

[5] Grattan-Bellew, E., D. Mitchell, J. Margeson, D. Min, Is alkali-carbonate reaction just a variant of alkali-silica reaction ACR = ASR?, Cem. Concr. Res. 40 (2010) 556–562. https://doi.org/10.1016/j.cemconres.2009.09.002.

[6] P. Fecteau, B. Fournier, G. Engineering, USE OF SCMs ON ACR-AFFECTED CONCRETE : EXPANSION AND DAMAGE EVALUATION THROUGH THE DAMAGE RATING INDEX, 15th Int. Conf. Alkali-Aggregate React. (2016).

[7] S.W. Forster, R.L. Boone, M.S. Hammer, J.F. Lamond, D.S. Lane, R.E. Miller, S.E. Parker, A. Pergalsky, J.S. Pierce, M.Q. Robert, J.W. Schmitt, R.E. Tobin, State-of-the-Art Report on Alkali-Aggregate Reactivity Reported by ACI Committee 221, 98 (1998) 1–31.

[8] L.F.M. Sanchez, B. Fournier, M. Jolin, J. Duchesne, Reliable quantification of AAR damage through assessment of the Damage Rating Index (DRI), Cem. Concr. Res. 67 (2015) 74–92. https://doi.org/10.1016/j.cemconres.2014.08.002.

[9] L.F.M. Sanchez, B. Fournier, M. Jolin, D. Mitchell, J. Bastien, Overall assessment of Alkali-Aggregate Reaction (AAR) in concretes presenting different strengths and incorporating a wide range of reactive aggregate types and natures, Cem. Concr. Res. 93 (2017) 17–31. https://doi.org/10.1016/j.cemconres.2016.12.001.

[10] B. Fournier, M.A. Bérubé, Alkali-aggregate reaction in concrete: A review of basic concepts and engineering implications, Can. J. Civ. Eng. 27 (2000) 167–191. https://doi.org/10.1139/l99-072.

[11] B. Fournier, M.A. Bérubé, K.J. Folliard, M. Thomas, ASR Testing and Evaluation Protocols Prepared for the Federal Highway Administration by :, (2008).

[12] P. Rivard, B. Fournier, G. Ballivy, Quantitative petrographic technique for concrete damage due to ASR: Experimental and application, Cem. Concr. Aggregates. 22 (2000) 63–72. https://doi.org/10.1520/cca10465j.

[13] M.T. Benoit Fournier, Marc-André Bérubé, Kevin J. Folliard, Report on ASR Mitigation, Fed. Highw. Adm. Publ. FHWA-HRT-04-113 Techbr. FHWA-HRT-06-071. (2010).

[14] T. Miura, S. Multon, Y. Kawabata, Influence of the distribution of expansive sites in aggregates on microscopic damage caused by alkali-silica reaction: Insights into the mechanical origin of expansion, Cem. Concr. Res. 142 (2021). https://doi.org/10.1016/j.cemconres.2021.106355.

[15] R.B. Figueira, R. Sousa, L. Coelho, M. Azenha, J.M. de Almeida, P.A.S. Jorge, C.J.R. Silva, Alkali-silica reaction in concrete: Mechanisms, mitigation and test methods, Constr. Build. Mater. 222 (2019) 903–931. https://doi.org/10.1016/j.conbuildmat.2019.07.230.

[16] A. Zahedi, C. Trottier, L.F.M. Sanchez, M. Noël, Microscopic assessment of ASR-affected concrete under confinement conditions, Cem. Concr. Res. 145 (2021). https://doi.org/10.1016/j.cemconres.2021.106456.

[17] L.F.M. Sanchez, B. Fournier, M. Jolin, M.A.B. Bedoya, J. Bastien, J. Duchesne, Use of Damage Rating Index to quantify alkali-silica reaction damage in concrete: Fine versus coarse aggregate, ACI Mater. J. 113 (2016) 395–407. https://doi.org/10.14359/51688983.

[18] L.F.M. Sanchez, T. Drimalas, B. Fournier, D. Mitchell, J. Bastien, Comprehensive damage assessment in concrete affected by different internal swelling reaction (ISR) mechanisms, Cem. Concr. Res. 107 (2018) 284–303. https://doi.org/10.1016/j.cemconres.2018.02.017.

[19] N. Castro, B.J. Wigum, Assessment of the potential alkali-reactivity of aggregates for concrete by image analysis petrography, Cem. Concr. Res. 42 (2012) 1635–1644. https://doi.org/10.1016/j.cemconres.2012.08.009.

[20] S. Multon, F. Toutlemonde, Effect of applied stresses on alkali-silica reaction-induced expansions, Cem. Concr. Res. 36 (2006) 912–920. https://doi.org/10.1016/j.cemconres.2005.11.012.

[21] L.F.M. Sanchez, B. Fournier, D. Mitchell, J. Bastien, Condition assessment of an ASR-affected overpass after nearly 50 years in service, Constr. Build. Mater. 236 (2020) 117554. https://doi.org/10.1016/j.conbuildmat.2019.117554.

[22] A. Sellier, É. Grimal, S. Multon, É. Bourdarot, eds., Swelling Concrete in Dams and Hydraulic Structures, Wiey, 2017. https://doi.org/10.1002/9781119437703.

[23] British Cement Association, The Diagnosis of Alkali-Silica Reaction, in: Wexham Springs, Slough, UK, 1992.

[24] N. Smaoui, B. Bissonnette, M.A. Bérubé, B. Fournier, B. Durand, Mechanical properties of ASR-affected concrete containing fine or coarse reactive aggregates, J. ASTM Int. 3 (2006) 1–16. https://doi.org/10.1520/jai12010.

[25] D.J. De Souza, L.F.M. Sanchez, M.T. De Grazia, Evaluation of a direct shear test setup to quantify AAR-induced expansion and damage in concrete, Constr. Build. Mater. 229 (2019) 116806. https://doi.org/10.1016/j.conbuildmat.2019.116806.

[26] M. D. A. Thomas, B. Fournier, K. J. Folliard, Alkali-Aggregate Reactivity (AAR) Facts Book, 2013.

[27] M.D.A. n Fournier, B., Bérubé, M.A., Folliard, K.J. and Thomas, Report on the diagnosis, prognosis and mitigation of alkali-silica reaction (ASR) in transportation structures. FHWAHIF-09-004, 2010.

[28] M.T. De Grazia, N. Goshayeshi, R. Gorga, L.F.M. Sanchez, A.C. Santos, D.J. Souza, Comprehensive semi-empirical approach to describe alkali aggregate reaction (AAR) induced expansion in the laboratory, J. Build. Eng. 40 (2021). https://doi.org/10.1016/j.jobe.2021.102298.

[29] P.A. Dunbar, P.E. Grattan-Bellew, Results of damage rating evaluation of condition of concrete from a number of structures affected by AAR, in: Proc. CANMET/ACI Int. Work. Alkali-Aggregate React. Concr., National Resources Canada, Dartmouth, 1995: pp. 257–265.

[30] P.E. Grattan-Bellew, L.D. Mitchell, Quantitative Petrographic Analysis of Concrete – The Damage Rating Index (DRI) Method , A Review, 8th CANMET/ACI Int. Conf. Recent Adv. Concr. Technol. (2006) 14.

[31] L.F.M. Sanchez, B. Fournier, M. Jolin, J. Bastien, Evaluation of the Stiffness Damage Test (SDT) as a tool for assessing damage in concrete due to alkali-silica reaction (ASR): Input parameters and variability of the test responses, Constr. Build. Mater. 77 (2015) 20–32. https://doi.org/10.1016/j.conbuildmat.2014.11.071.

[32] L.F.M. Sanchez, B. Fournier, M. Jolin, D. Mitchell, M. Noel, Thorough Characterization of Concrete Damage Caused By Aar Through the Use of a Multi-Level Approach, 15th Int. Conf. Alkali-Aggregate React. (2016).

[33] P. Rivard, B. Fournier, G. Ballivy, The damage rating index method for ASR affected concrete - A critical review of petrographic features of deterioration and evaluation criteria, Cem. Concr. Aggregates. 24 (2002) 81–91. https://doi.org/10.1520/cca10531j.

[34] L.F.M. Sanchez, B. Fournier, T. Drimalas, J. Bastien, L.D. Mitchell, M. Noel, Semi-Quantitative Condition Assessment of Concrete Distress Through the Damage Rating Index, Int. Conf. Alkali Aggragete React. (2016) 10.

[35] L.F.M. Sanchez, B. Fournier, M. Jolin, J. Bastien, D. Mitchell, M. Noel, The Use of the Damage Rating Index (DRI) for the Condition Assessment of Aging Distressed Concrete, 15th Int. Conf. Alkali-Aggregate React. (2016) 10.

[36] V. Villenneuve, B. Fournier, J. Duchesne, Determination of the damage in concrete affected by ASR – The damage rating index (DRI)., in: 14th Int. Conf. Alkali-Aggregate React. (ICAAR)., Austin, USA., 2012.

[37] S. Bilodeau, A. Allard, J. Bastien, F. Pissot, B. Fournier, B. Bissonnette, Performance Evaluation of Thick Concrete Slabs Affected by Alkali-Silica Reaction (ASR) - Part II: Structural Aspects, Conf. Proc. 15th ICAAR. (2016) 1–9.

[38] T. Sugiyama, M.A.B. Promentilla, T. Hitomi, N. Takeda, Application of synchrotron microtomography for pore structure characterization of deteriorated cementitious materials due to leaching, Cem. Concr. Res. 40 (2010) 1265–1270. https://doi.org/10.1016/j.cemconres.2009.10.009.

[39] V. Jensen, S. Sujjavanich, Alkali Silica Reaction in Concrete Foundations in Thailand, 15th ICAAR - Intenational Conf. Alkali Aggreg. React. Concr. (2016).

[40] V. Jensen, Diagnosis of Alkali Silica Reaction, 15th Int. Conf. Alkali-Aggregate React. (2016).

[41] A. Malek, A. Scott, S. Pampanin, G. MacRae, Post-event damage assessment of concrete using the fluorescent microscopy technique, Cem. Concr. Res. 102 (2017) 203–211. https://doi.org/10.1016/j.cemconres.2017.09.015.

[42] Unsupervised learning foundations of neural computation, MIT Press, Cambridge, Mass, 1999.

[43] N. Li, X. Hou, X. Yang, Y. Dong, Automation Recognition of Pavement Surface Distress Based on Support Vector Machine, in: 2009 Second Int. Conf. Intell. Networks Intell. Syst., 2009: pp. 346–349. https://doi.org/10.1109/ICINIS.2009.95.

[44] M. Gavilán, D. Balcones, O. Marcos, D. Llorca, M. Sotelo, I. Parra, M. Ocaña, P. Aliseda, A. Amírola, A. Yarza, Adaptive Road Crack Detection System by Pavement Classification, Sensors. 11 (2011) 9628–9657.

[45] S. Wang, S. Qiu, W. Wang, D. Xiao, K.C.P. Wang, Cracking classification using minimum rectangular cover-based support vector machine, J. Comput. Civ. Eng. 31 (2017).

[46] N.-D. Hoang, An Artificial Intelligence Method for Asphalt Pavement Pothole Detection Using Least Squares Support Vector Machine and Neural Network with Steerable Filter-Based Feature Extraction, Adv. Civ. Eng. 2018 (2018) 1–12.

[47] H.D. Cheng, J. Wang, Y.G. Hu, C. Glazier, X.J. Shi, X.W. Chen, Novel approach to pavement cracking detection based on neural network, Transp. Res. Rec. 1764 (2001) 119–127.

[48] Y.-A. Hsieh, Y.J. Tsai, Machine Learning for Crack Detection: Review and Model Performance Comparison, J. Comput. Civ. Eng. 34 (2020).

[49] M.H. Ke Ma, D. Samaras, Large-scale Continual Road Inspection: Visual Infrastructure Assessment in the Wild, in: Proc. Br. Mach. Vis. Conf., 2017.

[50] K. Gopalakrishnan, H. Gholami, A. Vidyadharan, A. Choudhary, A. Agrawal, CRACK Damage Detection In Unmanned Aerial Vehicle Images Of Civil Infrastructure Using Pre-Trained Deep Learning Model, Int. J. Traffic Transp. Eng. 8 (2018) 1–14.

[51] M. Eisenbach, R. Stricker, D. Seichter, K. Amende, K. Debes, M. Sesselmann, D. Ebersbach, U. Stoeckert, H. Gross, How to get pavement distress detection ready for deep learning? A systematic approach, in: 2017 Int. Jt. Conf. Neural Networks, 2017: pp. 2039–2047. https://doi.org/10.1109/IJCNN.2017.7966101.

[52] F.-C. Chen, M.R. Jahanshahi, NB-CNN: Deep Learning-Based Crack Detection Using Convolutional Neural Network and Naïve Bayes Data Fusion, IEEE Trans. Ind. Electron. 65 (2018) 4392–4400.

[53] H. Maeda, Y. Sekimoto, T. Seto, T. Kashiyama, H. Omata, Road Damage Detection and Classification Using Deep Neural Networks with Smartphone Images: Road damage detection and classification, Comput. Civ. Infrastruct. Eng. 33 (2018) 1127–1141.

[54] V. Mandal, L. Uong, Y. Adu-Gyamfi, Automated Road Crack Detection Using Deep Convolutional Neural Networks, in: 2018 IEEE Int. Conf. Big Data (Big Data), 2018: pp. 5212–5215. https://doi.org/10.1109/BigData.2018.8622327.

[55] Y. Xue, Y. Li, A Fast Detection Method via Region-Based Fully Convolutional Neural Networks for Shield Tunnel Lining Defects, Comput. Civ. Infrastruct. Eng. 33 (2018) 638–654.

[56] S. Saha, A Comprehensive Guide to Convolutional Neural Networks - the ELI5 way., (2018).

[57] S. Ren, K. He, R. Girshick, J. Sun, Faster R-CNN: Towards Real-Time Object Detection with Region Proposal Networks, IEEE Trans. Pattern Anal. Mach. Intell. 39 (2017) 1137–1149. https://doi.org/10.1109/TPAMI.2016.2577031.

[58] J. Redmon, S. Divvala, R. Girshick, A. Farhadi, You Only Look Once: Unified, Real-Time Object Detection, in: 2016 IEEE Conf. Comput. Vis. Pattern Recognit., 2016: pp. 779–788. https://doi.org/10.1109/CVPR.2016.91.

[59] K. Simonyan, A. Zisserman, Very deep convolutional networks for large-scale image recognition, ArXiv Prepr. ArXiv1409.1556. (2014).

[60] K. He, X. Zhang, S. Ren, J. Sun, Deep Residual Learning for Image Recognition, in: 2016 IEEE Conf. Comput. Vis. Pattern Recognit., 2016: pp. 770–778. https://doi.org/10.1109/CVPR.2016.90.

[61] F. Yang, L. Zhang, S. Yu, D. Prokhorov, X. Mei, H. Ling, Feature Pyramid and Hierarchical Boosting Network for Pavement Crack Detection, IEEE Trans. Intell. Transp. Syst. 21 (2020) 1525–1535. https://doi.org/10.1109/TITS.2019.2910595.

[62] Q. Zou, Y. Cao, Q. Li, Q. Mao, S. Wang, CrackTree: Automatic crack detection from pavement images, Pattern Recognit. Lett. 33 (2012) 227–238.

[63] S. Bang, S. Park, H. Kim, H. Kim, Encoder-decoder network for pixel-level road crack detection in black-box images, Comput. Civ. Infrastruct. Eng. 34 (2019) 713–727.

[64] K. Zhang, Y. Zhang, H.D. Cheng, Self-Supervised Structure Learning for Crack Detection Based on Cycle-Consistent Generative Adversarial Networks, J. Comput. Civ. Eng. 34 (2020) 4020004.

CHAPTER THREE: AUTOMATED ASSESSMENT OF AAR DAMAGE IN CONCRETE IN PROGRESS

Agnes Bezerra[1], Gabriella Andrade[1], Leandro Sanchez[1], Maia Fraser[2].

[1]Department of Civil Engineering, University of Ottawa, Ottawa, Canada.

[2]Departament of Mathematics and Statistics, University of Ottawa, Ottawa, Canada.

Abstract

Over the last decades, different techniques with the aim of assessing the actual damage of ageing concrete infrastructure have been proposed around the world. A method that has progressively been used in North America is the Damage Rating Index (DRI). This microscopic and semi-quantitative petrographic tool was developed to provide a reliable characterization of both nature and degree of damage in concrete distressed by alkali-aggregate reaction (AAR) and combined mechanisms. However, carrying out the DRI is time-consuming. Its results may vary somewhat among petrographers, and only a few professionals worldwide are appropriately trained to perform it. This study proposed using machine learning (ML) techniques to automate the DRI test protocol, particularly detecting cracks of various types as usually performed by the human professional during test protocol. This was done by training a so-called Convolutional Neural Network to predict results (machine assessment) that are close to the expected ones (human assessment). This automation of the DRI test protocol, employing ML techniques, is a revolutionary step towards more ubiquitous use of the DRI in civil engineering since it speeds up the process, avoids variability among petrographers and enables non/less experienced professionals to take advantage of this powerful microscopic tool. Further development is still required and is currently being conducted so that the automated DRI may become a reliable approach for the concrete community in the foreseeable future, after validations.

Keywords: Automated condition assessment; crack detection; Damage Rating Index, Machine Learning.

3.1. Introduction

Civil infrastructure is an essential part of social development, connecting nations' businesses, communities, and people. It directly influences the economy and life quality across generations. Usually, civil infrastructure is designed with a service life of about 50-75 years, depending on the code used and structure type (i.e., dams, bridges, tunnels, stadiums, etc.). It is widely known that several critical structures built from the 1960s to 1980s in Canada and worldwide are now achieving the end of their service lives. Thus, it is necessary to take specific actions so that these structures keep their performance without presenting risks to users over their last years of service or even to increase their remaining service life. Furthermore, many of these structures already display clear signs of distress due to severe damage mechanisms, which may reduce the structure's performance to unacceptable thresholds (**Figure 3.1**).

In this perspective, alkali-aggregate reaction (AAR) is one of the most critical Internal Swelling Reaction (ISR) mechanisms influencing the overall performance of concrete infrastructure worldwide [1]. AAR is often divided into two types:

Alkali-silica reaction (ASR): the chemical reaction between the alkali ions present in the concrete pore solution (Na^+, K^+ and OH^-) and some unstable siliceous mineral phases from the aggregates. It is by far the most widespread reaction mechanism found in concrete across the world [1,2]; and

Alkali-carbonate reaction (ACR): a chemical reaction in the presence of carbonate rocks (i.e., limestone and/or dolomite aggregates). Currently, there is no unanimity in the technical community on the real mechanisms causing ACR-induced expansion and damage. Nevertheless, the dedolomitization of dolomite seems to be one of the potential causes [2,3].

a) b)

Figure 3.1: Bibb Graves Bridge. a) north face. b) cracking on of archway supporting the fifth span. Wetumpka, Alabama. Adapted from [4].

The concrete industry currently relies on standardized techniques and methods to perform infrastructure assessment, diagnose the possible causes of existing damage and the damage extension (i.e., diagnosis), evaluate the potential of further distress over time (i.e. prognosis), structural implications and, selection of rehabilitation strategies. Assessment is currently based on tools that evaluate mechanical properties, physical integrity, and durability of deteriorated structural materials and components [4-6]. Making a correlation between the damage cause(s), current and future mechanical properties, and durability losses are critical in structure management [2,5–7].

To assess the current condition and predict the potential for further distress of AAR-affected concrete, engineers and researchers have been trying to develop new visual, non-destructive, mechanical and microscopic protocols. Special attention has been given to the Damage Rating Index (DRI), a semi-quantitative microscopic procedure, as well as to some quantitative image analysis techniques through the use of fluorescent epoxy dyes [7]. Although the DRI is an accurate method with consistent results, it is pretty time-consuming and requires suitable judgement on the part of the petrographer analyzing the sample. The results are directly linked to the experience of the petrographer performing the test, which is unscalable and somewhat variable since each petrographer may find a different result. On the other hand, several Machine Learning (ML) techniques have had dramatic success in classifying objects in photos and videos in recent years. This raises the hope to use these to detect and forecast damage in concrete. However, very little data are available in the literature on the use of ML systems for diagnosing concrete affected by AAR.

This work aims to use ML techniques to assess damage in concrete in an automated fashion. First, a set of data of AAR-affected concrete will be selected and used for training through a Convolutional Neural Network (CNN)-based ML algorithm. Then, this algorithm will be used to assess AAR damage from untrained data. The project's final goal is to fully automate the DRI test protocol to assess AAR-affected concrete and predict not just crack types and amounts but rather the actual DRI number. It is worth noting that the methodology presented in this project is explicitly focused on substantial distress caused by AAR. However, the approach used could also very likely be applied to evaluate other deterioration mechanisms (e.g., freeze-thaw damage, delayed ettringite formation, etc.). Therefore, this work provides a preliminary basis for identifying and isolating the effects of several mechanisms that may be present simultaneously in a single sample, a task that is currently very difficult to evaluate through manual methods.

Since the eventual application of the above tools will largely depend on their reliability, an essential component of this project will be validating the planned automated tools by assessing actual structures exposed to different macro-climates.

3.2. Methodology

3.2.1. Techniques for Assessing Damage in Concrete

Aiming to improve the assessment of concrete structures, Bérubé et al. [8] developed a management protocol of ageing infrastructure based on several chemicals, physical, and mechanical laboratory test procedures. Building on these, improved guidelines have been introduced [4]. Several researchers [2,5–7] proposed enhanced testing protocols and models to diagnose and better understand plentiful distress processes into concrete, such as AAR, delayed ettringite formation (DEF), and freezing and thawing cycles (FT). The conventional approach is a multi-level analysis that uses advanced microscopic examination and mechanical testing techniques. Amongst the most promising proposed techniques are microscopic methods such as the Damage Rating Index (DRI) and quantitative image analysis (IA) techniques [1,7] (**Figure 3.2**).

The DRI procedure is performed using a stereomicroscope (15x-16x magnification) to identify features usually associated with AAR. These features are analyzed in squares drawn on affected samples with a grid of $1cm^2$ (i.e., 10 x 10 mm units). Concrete samples under analysis are cut in half, and their surfaces are polished before the grid's drawing [5,9,10]. The quantity of counts corresponding to each type of petrographic feature is multiplied by weighting factors, whose purpose is to balance their relative significance towards the mechanism of distress, in this case, AAR. The factors used in the method were selected on a logical basis but relatively arbitrarily [2,11]; they were recently modified in order to reduce the variability between the petrographers performing the test [11]. For comparative targets, the final DRI value is normalized to a 100 cm² area. It has been demonstrated that DRI values are evidently associated with induced expansion and damage caused by AAR, DEF, and FT [2,9,11,12].

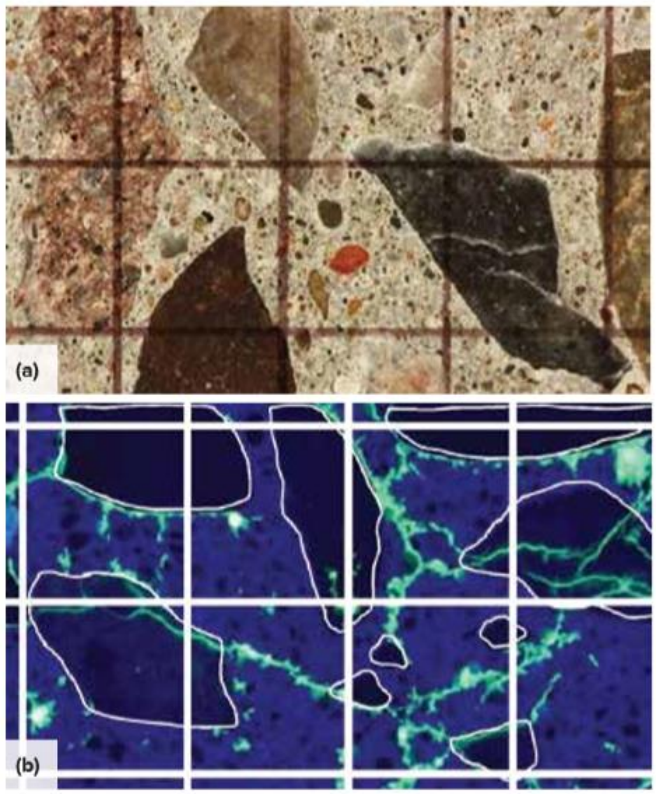

Figure 3.2: Polished concrete samples: (a) sample prepared for damage rating index (DRI) analysis by drawing 10 mm (0.4 in.) square grids on the surface; and (b) sample prepared for quantitative image analysis (IA) by impregnating with an epoxy dye that fluoresces under UV illumination [12].

The DRI has shown a remarkable correlation between expansion measurements and damage caused by AAR to concrete, presenting different compressive strengths and incorporating a broad spectrum of reactive aggregates [7]. However, the DRI is also time-consuming, which could be partially improved using automated techniques such as machine learning (ML) processes [13–16]. Moreover, DRI values depend largely on the skill and experience of the researcher/petrographer involved in the analysis, and it can be somewhat subjective. By training computers to perform automated analysis, more consistent and objective results can be expected.

Recently, Rivard et al. [7] proposed a quantitative IA technique (**Figure 3.2.b**). Crack density and total length have been associated with induced expansion, yet a proper crack quantification was found to be crucially dependent on effective sample groundwork (polishing and impregnation with epoxy). Both DRI and quantitative IA require specialists to perform time-consuming procedures on affected samples. Thus, the methods are not scalable, and they are not commonly accessible [1–11]. This means that many structures may remain with neither proper inspection nor adequate protection against a potential loss of serviceability and performance for the foreseeable future. However, machine learning (ML) techniques may provide potential solutions, enabling to lessen the subjectivity of the testy yet increasing its speed, reproducibility, and accessibility.

3.3. Automating Microscopic Procedures through Machine Learning

Machine Learning (ML) is the technical area of artificial intelligence that develops algorithms to allow systems to make predictions or act based on data/experience instead of following explicitly pre-programmed commands [13–16].

In this project, a first phase was conducted where a proof-of-concept assessment used deep learning, i.e., an ML architecture comprising many layers of artificial neurons, to recognize the seven distinct types of damage features in the DRI method (**Figure 3.3a**). More precisely, a so-called Convolutional Neural Network has trained on just over 200 square grid digital images on 24 concrete samples affected by AAR.

The samples comprised a comprehensive range of reactive aggregate sizes and mineral types; exhibited distinct mechanical properties (i.e., compressive strength of 25, 35 and 45 MPa); and expansion levels (i.e., 0.05, 0.12, 0.20 and 0.30%). All samples were prepared by slicing and polishing, and the DRI was conventionally conducted on each of them. The images were then labelled to identify the damage characteristics in each one, and these labelled images were used as training data for the ML algorithm.

CNN algorithms consist of a class of artificial neural networks applied very successfully to classify objects in photos and videos [13–16]. Depending on the depth of the network and the quantity of pixels in the incoming images, CNN's algorithms may include thousands (in some cases millions) of parameters (commonly called weights). These weights are sequentially adjusted during the training of a CNN model, in which the algorithm's feature predictions are compared with actual data (labelled images). Errors between predictions and ground truth data are successively reduced by adjusting the weights in repeated passes through the training data.

A CNN model can accurately predict the labels on new images, provided it is trained with sufficient examples. For the experience of this project, the training examples were images with 10 x 10mm grids drawn on polished concrete samples, labelled with 0 or 1 (yes or no) for each of the seven DRI damage characteristics. Several CNN architectures were analyzed, and the one that produced the best performance was selected to continue the project.

Petrographic characteristics	Abbreviation	Weighting factor
Cracks in coarse aggregate	CCA	0.25
Opened cracks in coarse aggregates	OCA	2
Crack with reaction product in coarse aggregate	OCAG	2
Coarse aggregate debonded	CAD	3
Disaggregate/corroded aggregate particle	DAP	2
Cracks in cement paste	CCP	3
Cracks with reaction product in cement paste	CCPG	3

a)

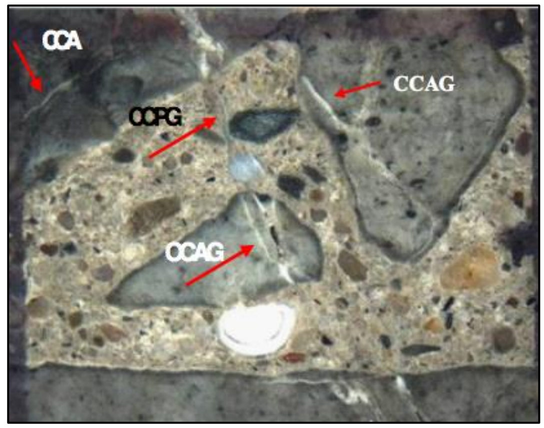

b)

Figure 3.3: Using the damage rating index (DRI) method, weighting factors are applied to damage features identified in a petrographic examination: (a) weighting factors are assigned to each feature to reflect its relative importance toward deterioration; and (b) an exemplar micrograph of a 10 mm (0.4 in.) square grid section on a specimen, with labels added to indicate damage features [12].

3.4. Results and Ongoing Developments

Once trained, the ML system adopted in the first phase could predict the seven different petrographic characteristics (or concepts) with an average accuracy of 64%. Given the tiny amount of training data (only 200 images), this is a reasonably high accuracy, as CNN models of this size are often trained with thousands of images. However, the DRI value was not computed for any of the images because the crack detectors built in this first approach were still considered to be too inaccurate.

At the moment, a second phase of the project is being conducted, using additional training data to enhance the accuracy of predictions and thus enabling DRI number’s calculations. The goal is to completely automate the DRI test protocol to evaluate AAR-affected concrete, predicting not only types, amounts and features of cracks but also the overall DRI evaluation. Finally, an additional step in the current and second phase of the project will take place, which is intended to use the sophisticated ML system to evaluate other damage mechanisms such as external and internal sulphate attack, FT damage, and steel corrosion, so that the proposed approach can become a comprehensive protocol for evaluating critical ageing infrastructure (**Figure 3.4**).

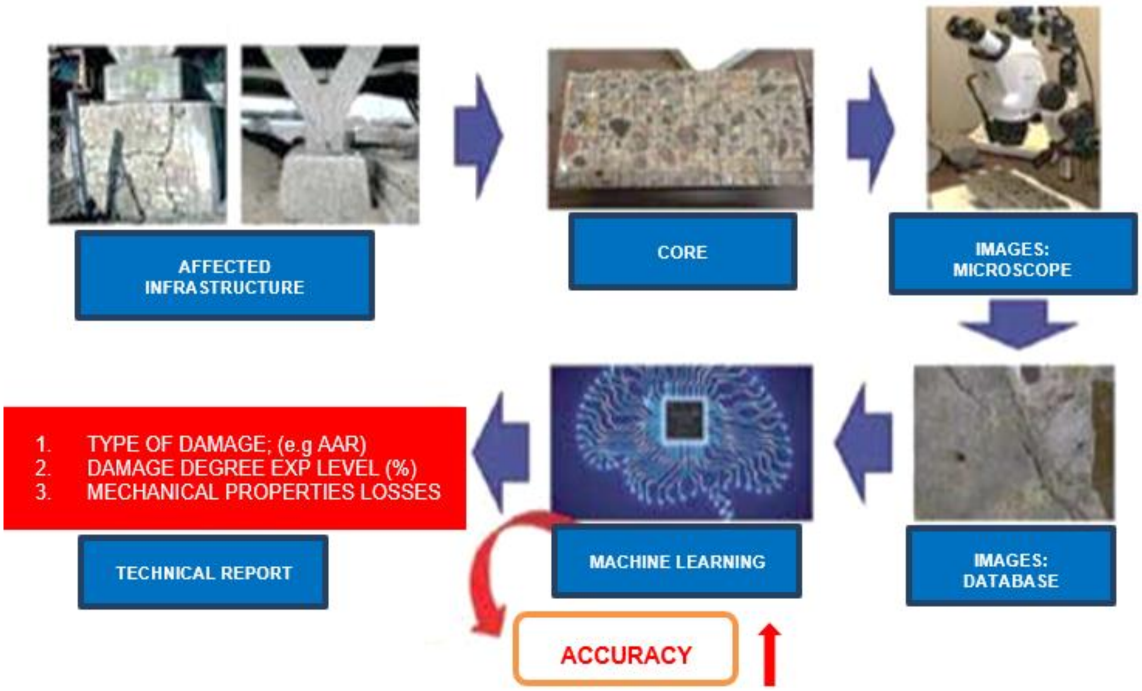

Figure 3.4: Comprehensive damage protocol for assessing damage in critical ageing infrastructure [18].

Since the end of the first phase of the project, the crack detectors have already been substantially improved and may now recognize cracks through 1 cm^2 image with about 80% accuracy. Additional enhancements are in progress to improve this furthermore. Moreover, 4000 new images are being incorporated in the research from 36 new specimens (already DRI assessed) representing distinct mixtures and expansion levels. The latter might vastly improve the results gathered so far.

3.5. Forthcoming Projects

To use deep learning in any field, achieving high accuracy in principle requires training the model with large amounts of data. Fortunately, workarounds do exist. Transfer learning, in particular, allows experience in one learning problem to help with another, and one instance of this in deep learning is the use of so-called pre-trained models. These are models which have been trained on similar data, and the idea is that only a tiny percentage of the model weights must be retrained to identify unique features such as cracks in concrete.

Another workaround is the use of feature-extraction techniques. This project, in particular, will incorporate techniques that have been highly successful in texture analysis for biomedical images (for lesion detection),

With these innovations and roughly 10,000 new, high-resolution images of DRI grid areas from AAR-affected concrete, it is expected to reach human accuracy levels of 90% or greater in the counting of cracks. To ensure interpretability, it is intended to apply the current DRI method (linking crack counts for individual damage types), evaluated in combination with the current CNN-based algorithm used. In this logic, the machine will replace only the petrographer's capability to identify and count cracks related to each damage feature.

After the new automated DRI approach is effectively employed for AAR cases, forthcoming steps will pursue its extension for a much wider variety of damage mechanisms, establishing a ground-breaking, comprehensive automated protocol for assessing damage in concrete. Finally, other innovative studies in this context are about to be started in parallel, including automation of the counting of entrained air voids in concrete, for example. Soon, it will be possible to develop applications (apps) that will automate the visual inspection of critical concrete infrastructure by providing preliminary diagnoses of the causes and extents of damage using only images captured on smartphones.

3.6. Final Remarks

All the above forthcoming steps have the purpose of raising the accuracy levels to numbers close to or above human accuracy levels of approximately 90%. This is crucial since, in terms of crossover risks in infrastructure assessment, a misclassification from an outlier input could have potentially catastrophic consequences.

Since the eventual utilization of the above tools will largely depend on their reliability, an additional, essential component of the research will require validation of the proposed automated tools by assessing actual structures exposed to distinct micro/macro-climates. This new tool brings to light a novel, reliable and scalable tool to assess structures, facilitating proper inspection, and protecting against sudden and potential structural failures.

3.7.References

[1] B. Fournier, M.A. Bérubé, Alkali-aggregate reaction in concrete: A review of basic concepts and engineering implications, Can. J. Civ. Eng. 27 (2000) 167–191. https://doi.org/10.1139/l99-072.

[2] L.F.M. Sanchez, B. Fournier, M. Jolin, J. Duchesne, Reliable quantification of AAR damage through assessment of the Damage Rating Index (DRI), Cem. Concr. Res. 67 (2015) 74–92. https://doi.org/10.1016/j.cemconres.2014.08.002.

[3] Grattan-Bellew, E., D. Mitchell, J. Margeson, D. Min, Is alkali-carbonate reaction just a variant of alkali-silica reaction ACR = ASR?, Cem. Concr. Res. 40 (2010) 556–562. https://doi.org/10.1016/j.cemconres.2009.09.002.

[4] MDA n Fournier, B., Bérubé, M.A., Folliard, K.J. and Thomas, Report on the diagnosis, prognosis and mitigation of alkali-silica reaction (ASR) in transportation structures. FHWAHIF-09-004, 2010.

[5] P.A. Dunbar, P.E. Grattan-Bellew, Results of damage rating evaluation of condition of concrete from a number of structures affected by AAR, in: Proc. CANMET/ACI Int. Work. Alkali-Aggregate React. Concr., National Resources Canada, Dartmouth, 1995: pp. 257–265.

[6] P.E. Grattan-Bellew, L.D. Mitchell, Quantitative Petrographic Analysis of Concrete – The Damage Rating Index (DRI) Method , A Review, 8th CANMET/ACI Int. Conf. Recent Adv. Concr. Technol. (2006) 14.

[7] P. Rivard, B. Fournier, G. Ballivy, Quantitative petrographic technique for concrete damage due to ASR: Experimental and application, Cem. Concr. Aggregates. 22 (2000) 63–72. https://doi.org/10.1520/cca10465j.

[8] M.-A. Bérubé, N. Smaoui, B. Fournier, B. Bissonnette, B. Durand, Evaluation of the expansion attained to date by concrete affected by ..., Can. J. Civ. Eng. 32 (2005) 463.

[9] L.F.M. Sanchez, T. Drimalas, B. Fournier, D. Mitchell, J. Bastien, Comprehensive damage assessment in concrete affected by different internal swelling reaction (ISR) mechanisms, Cem. Concr. Res. 107 (2018) 284–303. https://doi.org/10.1016/j.cemconres.2018.02.017.

[10] V. Villenneuve, B. Fournier, J. Duchesne, Determination of the damage in concrete affected by ASR – The damage rating index (DRI)., in: 14th Int. Conf. Alkali-Aggregate React. (ICAAR)., Austin, USA., 2012.

[11] L.F.M. Sanchez, B. Fournier, M. Jolin, D. Mitchell, J. Bastien, Overall assessment of Alkali-Aggregate Reaction (AAR) in concretes presenting different strengths and incorporating a wide range of reactive aggregate types and natures, Cem. Concr. Res. 93 (2017) 17–31. https://doi.org/10.1016/j.cemconres.2016.12.001.

[12] L.F.M. Sanchez, B. Fournier, M. Jolin, M.A.B. Bedoya, J. Bastien, J. Duchesne, Use of Damage Rating Index to quantify alkali-silica reaction damage in concrete: Fine versus coarse aggregate, ACI Mater. J. 113 (2016) 395–407. https://doi.org/10.14359/51688983.

[13] Y. Xue, Y. Li, A Fast Detection Method via Region-Based Fully Convolutional Neural Networks for Shield Tunnel Lining Defects, Comput. Civ. Infrastruct. Eng. 33 (2018) 638–654.

[14] N. Li, X. Hou, X. Yang, Y. Dong, Automation Recognition of Pavement Surface Distress Based on Support Vector Machine, in: 2009 Second Int. Conf. Intell. Networks Intell. Syst., 2009: pp. 346–349. https://doi.org/10.1109/ICINIS.2009.95.

[15] G.H. Beckman, D. Polyzois, Y.J. Cha, Deep learning-based automatic volumetric damage quantification using depth camera, Autom. Constr. 99 (2019) 114–124. https://doi.org/10.1016/j.autcon.2018.12.006.

[16] V. Maini, S. Sabri, (Part 2.1: Supervised Learning), in: Mach. Learn. Humans, 2017: p. 97. https://medium.com/machinelearning-for-humans/why-machine-learning-matters-6164faf1df12.

CHAPTER FOUR: THE USE OF ARTIFICIAL INTELLIGENCE FOR ASSESSING DAMAGE IN CONCRETE AFFECTED BY ALKALI-SILICA REACTION (ASR)

Agnes Bezerra1; Cassandra Trottier1; Haoye Lu2; Leandro Sanchez1; Maia Fraser2; Yongyi Mao2.

1Department of Civil Engineering, University of Ottawa, Ottawa, Canada.
2Departament of Mathematics and Statistics, University of Ottawa, Ottawa, Canada.

Abstract

Over the last decades, different techniques have been proposed worldwide to assess the actual damage of critical and ageing concrete infrastructure. A method that has gradually been used in North America is the novel Damage Rating Index (DRI). This semi-quantitative microscopic petrographic tool was developed to provide a reliable characterization of both the nature and degree of damage in concrete distressed by alkali-silica reaction (ASR), which may threaten the serviceability and durability of the affected concrete. However, performing the DRI is exceptionally time-consuming, and its results depend highly on the petrographer's experience. Therefore, this study proposes using artificial intelligence (AI) through Deep learning (DL) techniques to automate the DRI test protocol, estimating the damage degree in concrete structures affected by ASR. The automation process was accomplished by training a so-called Convolutional Neural Network (CNN) through pixel-level assessment, which can predict results (machine assessment) that are close to the expected ones (human assessment). The model presents an overall precision of 76.5%. With a more widely accessible diagnostic tool, critical concrete infrastructure affected by ASR could be more efficiently assessed which would ultimately increase their safety.

Keywords: Alkali-aggregate reaction, automated condition assessment, crack detection, Damage Rating Index, Convolution Neural Networks, Artificial Intelligence.

4.1. Introduction

Alkali-silica reaction (ASR) is one of the most harmful mechanisms affecting concrete worldwide and its repair and maintenance are associated with elevated costs [1–11]. Over the past decades, several tools have been proposed to determine the cause and extent of damage (e.g., diagnosis) and the likelihood of further deterioration (i.e., prognosis) of ASR-affected concrete. Amongst those, one of the most promising techniques is the Damage Rating Index (DRI) [1,2,4,12]. The DRI is a semi-quantitative microscopic procedure where distress features on a polished concrete surface are counted and weighted according to the importance of that feature. Literature shows that the DRI is a very reliable procedure to appraise the damage degree of concrete affected by ASR [1,2,4–6,12–17]; however, the method presents some important drawbacks, such as its time consuming and operator sensitive nature. Hence, automating the DRI is deemed a great opportunity to improve speed, reproducibility, and accuracy, while reducing the subjectivity of the method [2,4,16,18–25]. This work aims to use Machine Learning (ML) techniques, particularly Deep Learning (DL) through the use of convolutional neural networks (CNN) to automate the recognition and classification of the various distress features evaluated in the DRI method. Ultimately, the purpose of this research is to develop a machine able to estimate the DRI number of ASR-affected concrete presenting distinct deterioration degrees (i.e., low, moderate, high and very high).

4.2. Background

4.2.1. ASR-induced deterioration pattern

Alkali-silica reaction (ASR) is a distress mechanism where the alkalis in the concrete's pore solution (Na^+, K^+ and OH^-) react with certain reactive mineral phases found within the aggregate, producing a secondary reaction product (i.e., silica gel) that swells upon water intake thus, cracking the concrete. ASR presents specific damage features, which increase as a function of its induced development (i.e., expansion level). These damage features can be found in the macro and micro scales. Macroscopically, the cracks appear at the concrete's surface, very often randomly distributed, and defined as map-cracking **(Figure 4.1)**; however, this randomly distributed pattern is influenced and can become more oriented as per the restrain/confinement conditions (e.g., reinforcement, etc.) of the affected member. Whenever this deterioration condition is observed in ageing concrete structures, further evaluation is required such as microscopic investigation to detect the cause(s) of the deterioration [1,2,4,12,14,21,26,27]. Conversely, certain petrographic features (i.e., colour of reactive minerals) and distress features (i.e., cracks filled with reaction product) can be identified in thin sections through an optical microscope. Additionally, scanning electron microscopy (SEM) and energy-dispersive x-ray micro-analysis system (EDS) evaluations are performed to confirm the presence of ASR products such as silica, potassium, sodium normally found within the cracks in the aggregates while calcium is the main constituent of the cracks in the cement paste [28]. However, the preparation of such specimens is time-consuming, and their analysis requires a high level of expertise.

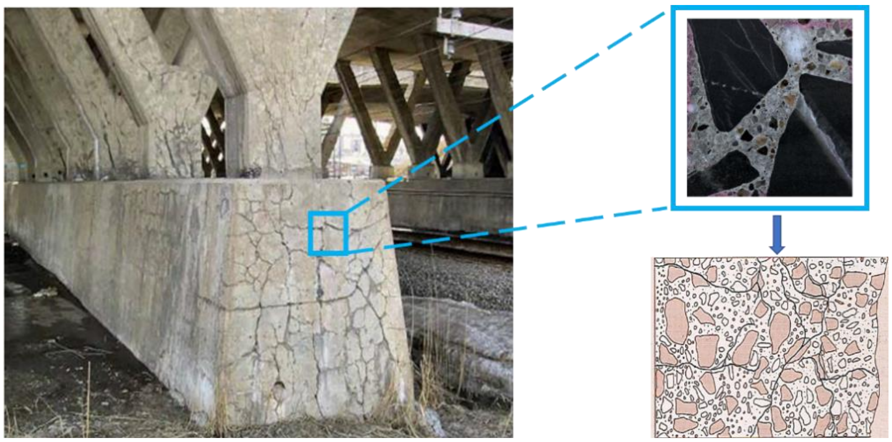

Figure 4.1: ASR-related signs in bridge elements. A view from Macroscopic to microscopic scale adapted from [16,29].

Generally, ASR cracks begin within the aggregate and propagate towards and through the cement paste as the degree of damage (i.e., expansion level) increases. According to the model proposed by Sanchez et al. [2] illustrated in **Figure 4.2**, there are two types of cracks in ASR-affected concrete: (A) sharp and (B) onion skin type. Onion skin type cracks begin near the periphery of the aggregate and unfold tangentially to the edges of the aggregate until the crack reaches the cement paste at a very high expansion level (i.e., 0.30%). Conversely, sharp cracks can initiate in any aggregate location and continue to propagate through the aggregate until reaching the cement paste. At low expansion levels (i.e., 0.05%), the cracks in the aggregate are closed and may not necessarily be due to ASR but rather rock formation and weathering or aggregate processing. Cracks in the cement paste are rarely observed at low expansion levels. Nevertheless, as the ASR-induced expansion develops, some of these cracks may begin to gradually open and lengthen, propagating into the cement paste until cracks link together and form a network of cracks [3]. Different mechanical properties are consequently reduced as the cracks propagate until the entire physical integrity of the concrete is compromised [2,4,5,7,25].

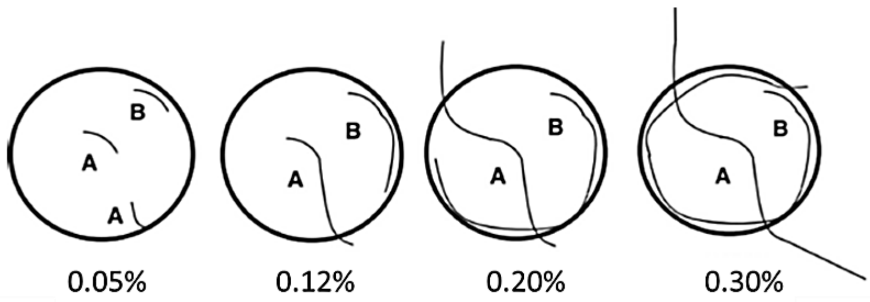

Figure 4.2: Qualitative model of ASR development through crack propagation as a function of the expansion with A) sharp cracks and B) onion skin type cracks [2].

4.2.2. Damage Rating Index (DRI)

The Damage Rating Index (DRI) was initially developed by Grattan-Bellew and co-workers [20,30] to evaluate ASR-induced damage in concrete triggered by reactive coarse aggregate particles. The procedure consists in counting the damage features and multiplying them by weighting factors, which were originally selected on a logical basis but relatively arbitrarily; they were recently modified to reduce the variability between the petrographers performing the test and accommodate the importance of the distress features [4,13]. Sanchez et al. [31] proposed to consider the coarser fraction of the fine aggregates to assess ASR damage originating from reactive sand. Consequently, crack counts were obtained from particles of 20 mm down to 1 mm in size. As opposed to the sample preparation of thin sections and SEM-EDX specimens, the sample preparation for the DRI analysis requires little experience and consists of cutting the concrete specimen in half longitudinally followed by grinding and polishing its surface to obtain a flat and reflective surface prior to drawing a grid of 1cm2 (i.e. 10 x 10 mm units) on this surface [2,4,22,23,25,32–34]. The procedure is then performed using a stereomicroscope (15-16x magnification) to identify petrographic/distress features associated with ASR by analyzing each of these 1 cm2 squares in the grid (**Figure 4.3**). It is to be remarked that cracks of 1 mm in length and larger are to be counted. The quantity of counts corresponding to each type of petrographic/distress feature is multiplied by weighting factors as presented in **Table 4.1**, whose purpose is to balance their relative importance towards the mechanism of distress.

The closed crack in the aggregate (CCA) receives the lowest weighting factor (0.25), since is not necessarily generated by ASR. An open crack (without and with gel) (OCA+OCAG) and disaggregated particle (DAP) are associated with higher relevance when compared with CCA, represented with a 2.0 of weight. The higher weighting factor (3.0) is attributed to cracks in the cement paste (without and with gel) (CCP+CCPG) and de-bonded aggregates (CAD). The value obtained from these weighted counts is normalized to a 100 cm² area which represents the DRI number, a quantitative value. To obtain a representative DRI number of a core extracted from a real structure, an area of at least 200 cm2 should be analyzed. Moreover, quantitative image analysis techniques using fluorescent epoxy dyes have also gained some interest, yet drawbacks were observed, such as the sample preparation is time-consuming, requiring vacuum cleaning prior to epoxy impregnation and the analysis require more specific apparatus (e.g., UV lights, UV lights protection) [35,36].

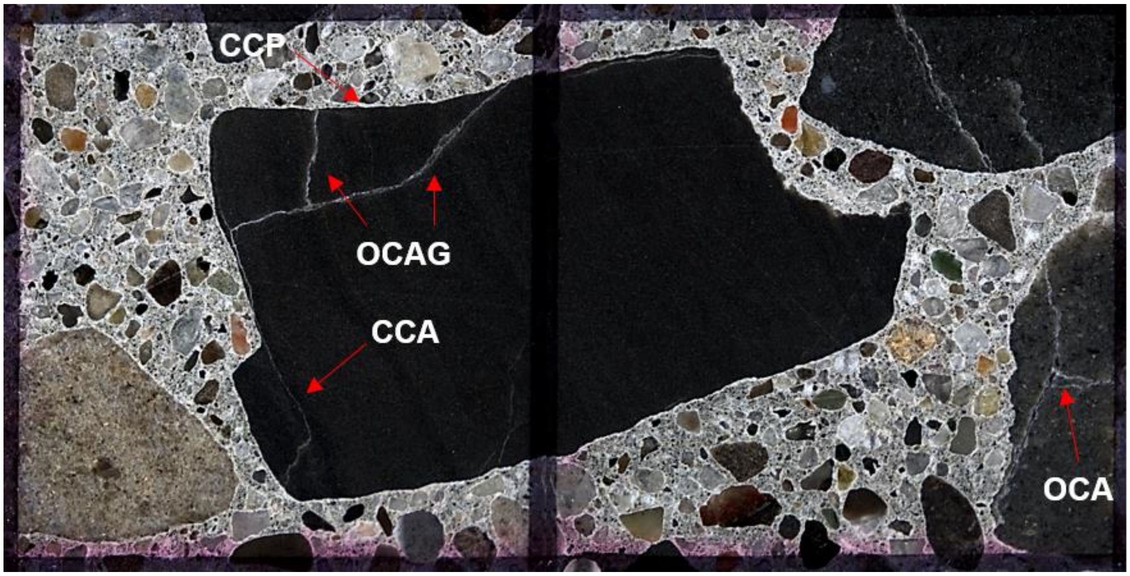

Figure 4.3: Petrographic features.

Table 4.1: Petrographic/distress features and respective weighting factors [2,13,37]

Petrographic/distress features	Abbreviation	Weighting Factor
Closed cracks in the aggregate	CCA	0.25
Opened cracks in the aggregate	OCA	2
Crack with reaction product in the aggregate	OCAG	2
Coarse aggregate de-bonded	CAD	3
Disaggregate/corroded aggregate particle	DAP	2
Crack in the cement paste	CCP	3
Crack with reaction product in the cement paste	CCPG	3

Regardless of the aggregate type, the DRI values of ASR-affected concrete increase in a linear manner as the expansion level increases. A range of DRI values was obtained for various types of aggregates by Sanchez et al. as displayed in **Figure 4.4.** Moreover, as observed by the King+Lav curve, the DRI can also capture the cause of distress mechanisms different than that of ASR. Furthermore, the progression of ASR through cracks propagating from the aggregates to the cement paste is apparent in the DRI bar charts shown in **Figure 4.5** where ASR is generally identified through an increase in open cracks in the aggregates (i.e. OCA+OCAG) and cracks in the cement paste (i.e. CCP+CCPG).

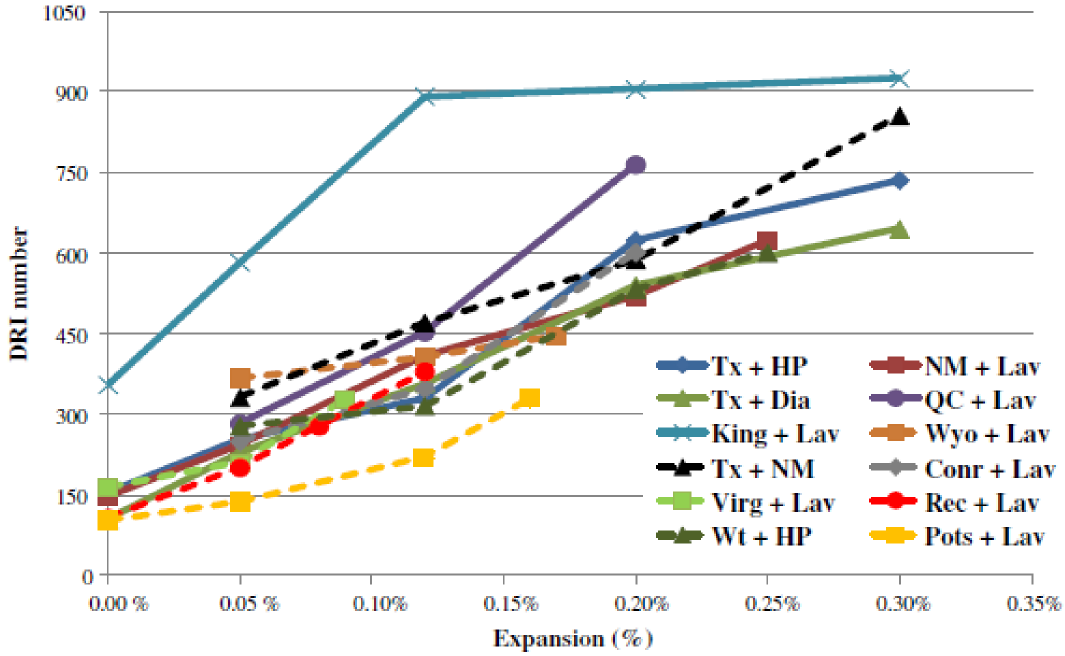

Figure 4.4: DRI number as a function of expansion of ASR affected concrete incorporating various types of aggregates [2].

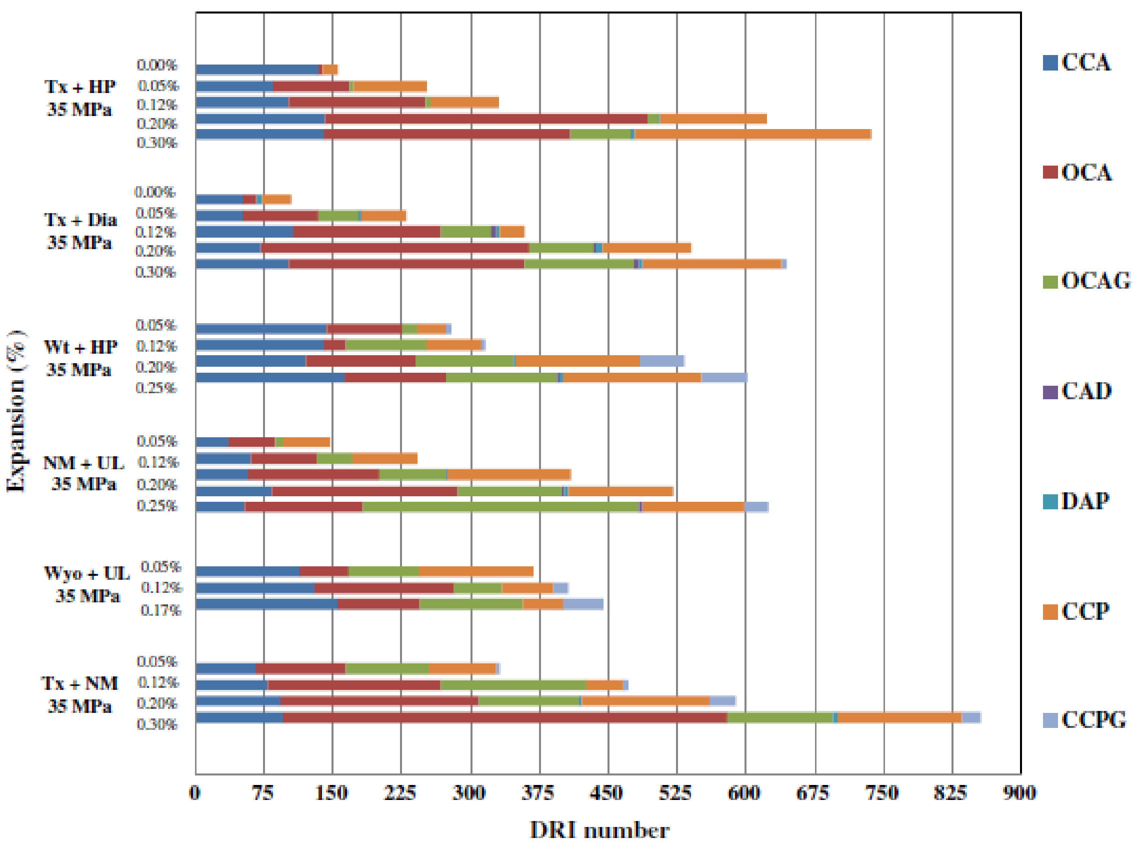

Figure 4.5: DRI bar charts of ASR-affected concrete for various aggregate types [2].

4.2.3. Artificial Intelligence (AI) and Convolutional Neural Networks (CNN)

Artificial intelligence (AI) is considered a machine that imitates human cognitive activities, with its functions applied to different human abilities such as learning, vision, language (communication), speech recognition (decoding). Machine Learning (ML) is the technical area of AI that develops algorithms and studies their properties, allowing systems to make predictions or take actions based on data/experience instead of following explicitly pre-programmed commands [38]. This technique is used to parse data, learn from it, and make decisions based on what was learned.

The crack detection methods mainly use two types of ML methods: Support Vector Machines (SVM) [39–41] and Fully Connected Networks FCN [42,43]. Researchers focused on two problems at this stage: verify if an image contains cracks and classify their types. Due to the simplicity of models and the computation power limitations, the methods mentioned above cannot capture high-level features such as cracks in concrete. It, therefore, triggers the models to make unreliable estimations when the input images have different brightness and complicated background.

Since approximately 2015, Deep Learning (DL)-based methods have become popular in crack detection problems, allowing scientists to develop very expressive recognition models and have been used for crack detection in three different levels [44]: (1) verify whether the image contains cracks; (2) use bounding boxes to locate the areas containing cracks; (3) label all pixels consisted in the cracks. Numerous ML-based methods have been proposed for the first task [45,46]. Meanwhile, the second task is somehow simple because the networks only need to learn limited crack features to predict their appearance. For more accurate predictions, researchers have also used a sliding window to iterate the big images. In each iteration, the image patch in the window is used for detection [47,48]. Once completed, all the prediction results are combined to generate a heatmap.

Consequently, using sliding windows allows researchers to generate results similar to those produced in the third task. However, there are two major problems: (1) the generated heatmap is of low resolution since the detection is performed on the patch level, and (2) if the cracks appear on the window's boundary, the detection algorithms would not be able to detect them. The first problem can be partially alleviated by choosing a smaller window size; however, the detection accuracy may also decrease since the window could be too small to contain enough crack structures. Regarding the second problem, a common technique is to move the window with a stride less than one in exchange for an increasing number of patches to predict and a smoother heatmap.

While the previous task focuses on the crack existence, bounding box techniques are used to locate them [49–54]. Likewise, the CNN can also use the spatial hierarchy of patterns, which helps identify the patterns (or cracks) more precisely. Although the bounding box-based methods can provide some location information of cracks, the algorithms cannot predict their shapes, width, and directions. Such limitations motivate researchers to work on pixel-level detection problems, which are usually referred to as segmentation.

Image segmentation is a pixel-level detection problem that requires the algorithms to predict, for each pixel, whether it belongs to a crack or not. Most algorithms for this problem have an encoder-decoder-based architecture [55–57]. To achieve pixel-level prediction, the models preserve the spatial information during the inference so that a one-to-one correspondence relationship can be constructed between the pixels of the input image and the output prediction.

Nevertheless, in recent years, the use of image recognition through ML has had astonishing success in classifying objects in photos and videos. This technology could be used to detect and forecast damage in concrete. Some studies apply ML to predict failures or proceed with the analysis of multi-risk hazards in dams, but few works consider the influence of ASR in their models; however, it is treated as a non-linear factor that may jeopardize the concrete structure integrity [58–60]. The state of the art or crack recognition a the surface of concrete, applies CNN models to assess the deteriorated concrete, but only for crack recognition, without correlating them with their causes [61–74]. Even though the studies are promising, they are not capable of diagnosing concrete affected by ASR.

4.3. Scope of the Work

As the previous sections demonstrated, the DRI, a reliable semi-quantitative microscopic test procedure, currently displays some issues such as its time-consuming and operator dependency characters; these factors limit its widespread use worldwide. However, Deep Learning (DL) and convolutional neural networks (CNN) have demonstrated the potential to recognize and classify cracks in concrete. This work aims to develop a DL-CNN algorithm, precisely an advanced pixel recognition method [55–57][75,76], to recognize and classify microscopic distress features related to ASR and ultimately estimate the DRI number of concrete specimens affected by ASR incorporating a reactive coarse aggregate. To accomplish the research goal, concrete specimens incorporating a highly reactive coarse aggregate from New Brunswick (Canada) were manufactured and stored in the laboratory under conditions enabling ASR. Four levels of expansion were selected for further analysis (i.e., 0.05%, 0.12%, 0.20%, and 0.30%). The DRI was then performed while 1cm2 images were taken from the specimens under analysis and divided into two groups: 1) the training/validation dataset, composed of more than 50 layers with core information regarding the algorithm appraisal and 2) the assessment which were implemented upon reaching an accuracy over 70% through the training phase to build the proposed CNN algorithm. The DRI estimation was then obtained and compared to human assessment.

4.4. Materials And Methods

4.4.1. Materials, mixture proportions, and fabrication of ASR-induced concrete specimens

Fifteen concrete cylinders (i.e., 100 x 200 mm in size) were manufactured in the laboratory using a concrete mixture with a design compressive strength of 35 MPa. A highly reactive coarse aggregate (Springhill - Greywacke) combined with a local non-reactive fine aggregate were selected for concrete manufacturing. **Table 4.2** provides information on the different aggregates used in this study, including the mineralogical composition of the aggregates. The coarse aggregates ranged in size from 5 to 20 mm. A conventional Portland cement (CSA Type GU, ASTM type 1) containing a high alkali content (0.88% Na2Oeq) was used in the mixture. Reagent grade sodium hydroxide pellets were used to raise the total alkali content to 1.25% Na2Oeq, by cement mass, to accelerate ASR-induced expansion. The concrete specimens were proportioned using the Concrete Prism Test (CPT) standard mixture proportion as per ASTM C 1293 [46] and displayed **Table 4.3**.

Table 4.2: Aggregates used in this study

Aggregate	Location	Rock Type	Specific Gravity	Absorption (%)
Reactive coarse (Springhill–SPR)	Fredericton, New Brunswick (Canada)	Greywacke	2.71	0.70
Non-reactive fine (Ottawa Sand-OS)	Ottawa, Ontario (Canada)	Derived from Granite	2.60	0.82

Table 4.3: Concrete mixture proportion

Components	(k/m^3)
Cement	420
Sand	823
Coarse aggregate	934
Water	189

The specimens were moist cured for 24 hours at 20ºC before being demoulded. In both ends of each specimen, small holes of 8.5 mm in diameter and 19 mm in length were drilled, and stainless-steel gauge studs were glued using a fast-setting cement paste slurry and moist cured at 20ºC for an additional 24 hours, after which the initial readings were registered. The concrete specimens were then stored in conditions enabling ASR-induced development (i.e., 38°C and 100% RH) and monitored over time. Upon reaching the targeted expansion levels (i.e., 0.05%, 0.12%, 0.20% and 0.30%), the concrete specimens were further prepared (cut and polished) for the DRI analysis [77].

4.4.2. Specimen surface and image preparation

Upon reaching the targeted expansion levels (i.e., 0.05%, 0.12%, 0.20% and 0.30%), the concrete specimens were further prepared for the DRI analysis [77]. The concrete specimens were cut longitudinally using a masonry saw equipped with a diamond blade, after which the surfaces were ground flat and polished with a mechanical polishing table and magnetic laps with grits of 30, 60, 140, 280 (80-100 microns), 600 (20-40 microns), 1200 (10-20 microns), and 3000 (4-8 microns). A 1 cm by 1 cm 3D printed grid was then placed over the polished surface, as shown in **Figure 4.6**.

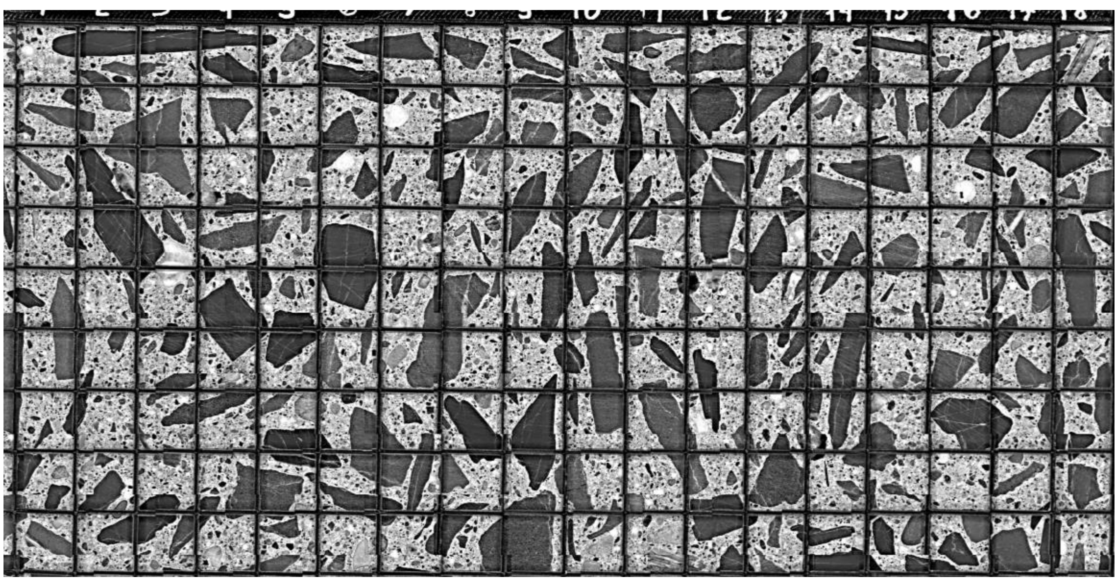

Figure 4.6: Springhill concrete sample surface prepared for DRI test.

Given that the identification of cracks in concrete through DLCNN is very recent, some simplifications were required; yet they do not impact the actual calculation of the DRI number or the damage assessment. It was, therefore, necessary to cluster the cracks in the cement paste, without and with gel (i.e., CCP+CCPG), as the CCPG is a quite rare feature at lower and moderate expansions, being more frequent in high expansion levels. Furthermore, the CAD and DAP type cracks were not considered in the crack classification because both are considerably rare phenomena in concrete affected by ASR and more often observed in concrete affected by other distress mechanisms such as delayed ettringite formation (DEF) and alkali-carbonate reaction (ACR); the latter being a rare form of AAR.

4.4.3. Crack recognition and classification through Machine Learning (ML)

The model algorithm was developed comprising an architecture model built with 50 layers of artificial neurons containing the core information regarding the different classifications to be performed. Furthermore, to achieve the pixel-level prediction using supervised learning, the model preserves the spatial information during the inference so that a one-to-one correspondence relationship can be constructed between the pixels of the input image and the output prediction. To recognize the main three distinct types of damage features in the DRI procedure, the DL/CNN was trained using 55,055 ASR related distress features from different types of aggregates, mixing natural and manufactured origins, besides fine and coarse reactive aggregates, combined with non-reactive coarse aggregate; this means that for the same mixture only one source of reactive aggregate was used at time, either coarse or fine. Mix designs with both fine and coarse together were not used in this research. The distress features differing in the depth of the network and the number of pixels in the incoming images. These weights are successively adjusted during the DL-CNN model training, in which the algorithm’s feature predictions are compared with actual data (labelled images). Errors between predictions and ground truth data are successively reduced by adjusting the weights in repeated steps through the training data. A 0 or 1 (yes or no) classification for each of the four petrographic/distress features (i.e., CCA, OCA, OCAG, and CCP+CCPG) was used throughout this study.

4.4.4. Image collection and preparation for DL/CNN

Following the surface preparation to perform the DRI, the polished specimen is assembled on an automatic stage that moves longitudinally and transversely under the stereomicroscope, using a camera with a 12-megapixel resolution connected to the stereomicroscope where the magnification is set to 16x. The working distance (i.e., the distance between the analyzed surface and objective lens) is automatically adjusted using a 3-point levelling method. The brightness and image contrasts are then adjusted using two oblique natural lights that better perceive depth in the image. Launching the image collection from one corner of the specimen, its length is scanned in the X-direction using a step range of 10 mm (the approximate field of view under the microscope at 16x magnification). The stage is thereafter automatically moved 10 mm in the Y-direction, and this process is repeated until the entire surface has been digitalized. Following the image collection, the features encountered were manually traced on these images using distinct colours (listed in **Table 4.4** and shown in **Figure 4.7**) for each type of crack/distress feature regardless of their length.

The cracks/distress features were traced for the highly damaged specimens (i.e., 0.20% and 0.30% levels of expansion) to incorporate a greater number of cracks/distress features per specimen/image. Furthermore, previously made specimens using a wider range of reactive coarse and fine aggregates were selected and used to train the model in detecting distress features in concrete having different backgrounds (i.e. aggregate size, colour, texture, etc.). Those aggregates provided to the DL/CNN model, a massive background record on natural veins in the aggregates, distinct coloration, distinct crack backdrop, also called "noise", challenging the model to increase its accuracy. However, in this study, only concrete incorporating Springhill coarse aggregate was therefore used for the automated DRI estimation, to better understand how the model behaves with a given dataset pattern and evaluate its susceptibility to create bias in the analysis.

Table 4.4: DRI Petrographic features and labelling tailored to ML categories.

Petrographic Characteristics	Abbreviation	Label	Group
Closed cracks in the aggregate	CCA	Yellow	I
Crack without and with reaction product in the aggregate	OCAG	Green	II
Crack in cement paste without and with a reaction product	CCP+CCPG	Red	III

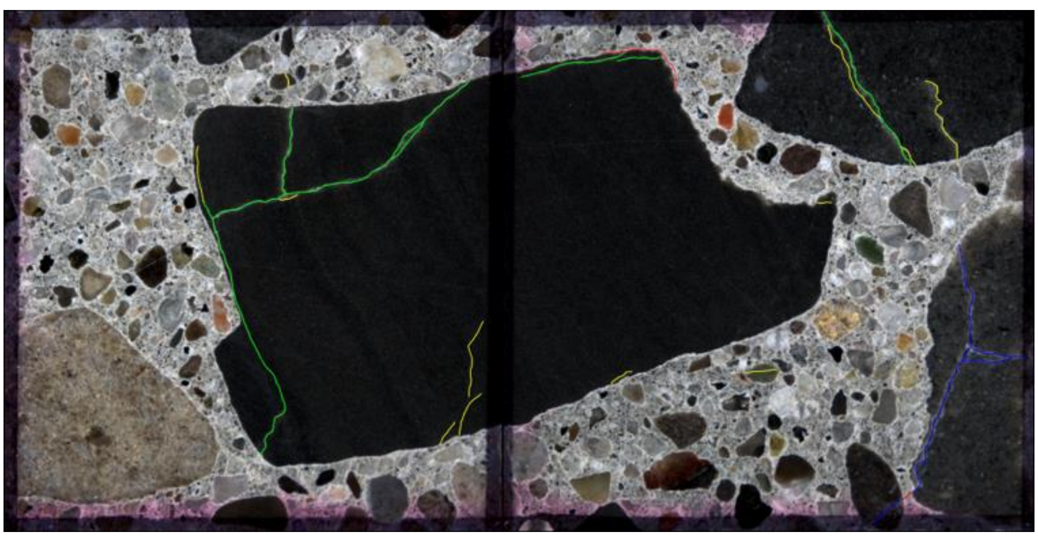

Figure 4.7: Manually traced distress features on two consecutive images of 1 cm by 1 cm from ASR-affected concrete.

4.4.5. Performing the DRI

An experienced petrographer first performed the DRI on the ASR-affected concrete specimens at different expansion levels (i.e., 0.05%, 0.12%, 0.20% and 0.30%) by counting the distress features in each 1 cm by 1 cm squares on the polished surface. A weighting factor is then applied to those features to balance their relative importance towards the overall distress mechanism, ASR. Moreover, the extended version of the DRI, developed by Sanchez [1,2] was performed to a better understanding of ASR damage generation and propagation and compare those with the automation. This version consists in appraising the distress features in a relative (%) and absolute (counts) manners, without applying the weighing factor.

To carry out the extended version of the DRI, the microscopic distress features were divided into three groups: Group I – closed cracks in the aggregate (CCA); Group II – open cracks in the aggregate with and without reaction products (OCA+OCAG) and, finally, Group III – cracks in the cement paste with and without gel (CCP+CCPG). Likewise, the crack density was used to complete the extended DRI version assessment as per [1,2], representing the summation of OCA+OCAG and CCP+CCPG per square centimetre.

The algorithm was therefore trained using the above mentioned organization, where each group of cracks was represented using a distinct color to classify the traced cracks during the "teaching" phase for example, when a crack is traced using a yellow line, it means the DL-CNN algorithm must understand that this is a CCA type crack. Upon reaching a suitable level of accuracy from the crack recognition and classification, the DRI was estimated and compared to the human assessment.

4.5. Results

4.5.1. ASR induced expansion and damage

ASR-induced expansion and kinetics for the twenty Springhill coarse aggregate specimens are displayed in **Figure 4.8**, including the data range bars. The standard deviation related to the expansion levels reached by the concrete ranges from 0.01% to 0.04%. The variability of the data is due to the variability of the reactive silica present within the aggregates. A low expansion level of 0.05% is achieved after 52 days, followed by 75 days to attain a moderate damage degree (i.e., 0.12% level of expansion) while achieving 0.20% and 0.30% of the expansion in 93 and 145 days, respectively. These two last expansion levels are classified correspondingly as high and very high ASR damage degrees, respectively, according to Sanchez et al. [4] and represent a greater number and severity of distress features.

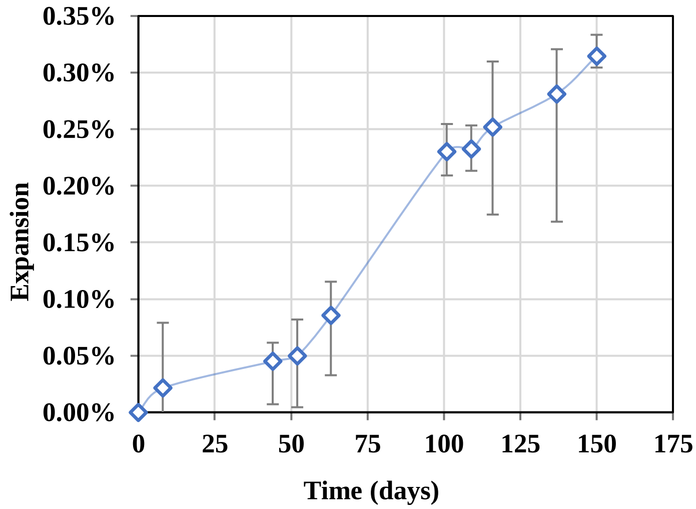

Figure 4.8: Expansion as a function of time for concrete made with Springhill coarse aggregate affected by ASR.

The DRI numbers generally increase with expansion in a linear trend, demonstrating the direct correlation between the DRI number and the expansion reached by ASR-affected concrete, as shown in **Figure 4.9**. A DRI number of 280 is obtained for an expansion level of 0.05%, followed by 472 for 0.12% of expansion, representing low and moderate damage degrees, respectively. At a high expansion level of 0.20%, a DRI number of 989 is verified, while for very high expansion of 0.30%, a DRI number of 1160 is achieved. The closed cracks in the aggregates (i.e., CCA) increase slightly from 0.12% to 0.20% of expansion whereas the increase in open cracks in the aggregates without and with gel (i.e., OCA and OCAG, respectively) show the largest increase as the expansion level increases; the latter being the more prominent distress feature overall. Very few cracks in the cement paste without and with gel (i.e., CCP and CCPG, respectively) are observed at a low expansion level of 0.05% yet, a slight increase is observed at 0.12% of expansion. At 0.20% of expansion, more CCP and CCPG cracks are observed as expected and continuing to increase in number at 0.30% of expansion. Moreover, from the 0.20% to 0.30% level of expansion, cracks in the aggregate (i.e., CCA, OCA and OCAG) do not show any increase as cracks begin to propagate within the cement paste as opposed to new cracks being formed within the aggregate.

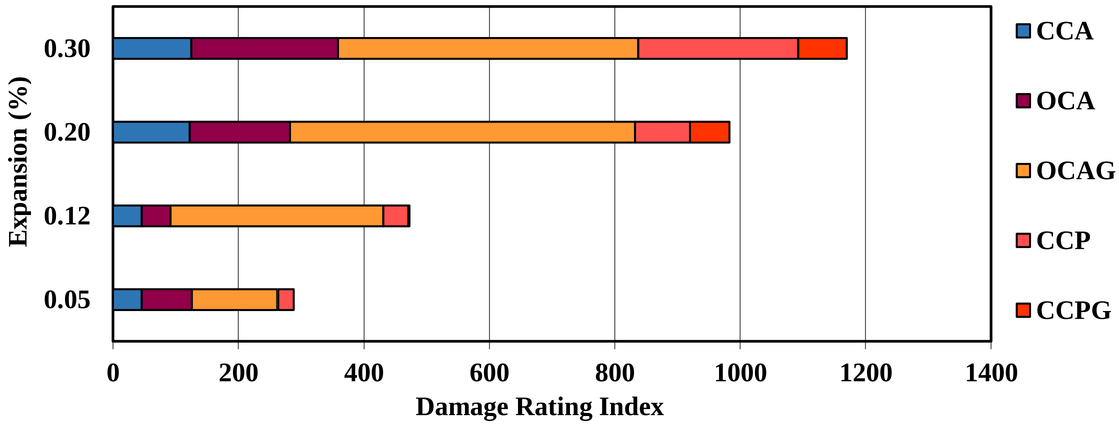

Figure 4.9: DRI number per level of expansion.

The distress features are also characterized in accordance with the extended version of the DRI [1,2] to better understand the crack distribution and proportions associated with each expansion level where features are counted in an absolute (counts per 100 square centimetres) and relative manner (percentage) without applying any weighting factors. Conversely, the counts of distress features present a different perspective to assist in the distress features entry process since the algorithm separates the distinct analyzed features, and it is of utmost importance to ensure that a minimum representative sampling of each petrographic feature type is entered to have a trustworthy output data, which is based on the model's interaction, and outcomes. There is no standardized threshold since this value relies on the number of filtering layers required for the model.

Figure 4.10a and **b** show the distress features as counts and proportions, respectively, of the Springhill coarse aggregate specimens per expansion level. Noticeably, the total number of cracks per square centimeter increases with expansion where an abrupt increase is identified from 0.12% to 0.20% of level of expansion (i.e., 391 and 906, respectively) followed by a slight increase at 0.30% of expansion (i.e., 963). Although the CCA type cracks are most likely generated through the rock formation and weathering as well as aggregate processing as opposed to being ASR generated, an increase in the counts from 185 to 501 per square centimeter is observed at 0.12% of expansion while remaining constant hereafter. On the other hand, the proportions of CCA are lower at 0.12% to 0.30% (i.e., 50% and below) compared to 0.05% of expansion (i.e., 62%); an indication that those cracks are becoming opened and creating OCA+OCAG type cracks. Nevertheless, OCA+OCAG and CCP+CCPG are the most reported distress characteristic related to ASR-affected concrete compared to others [1,2,23,24,78]. Even though the proportions of the OCA+OCAG type cracks remain similar, their counts generally increase with expansion from 105 to 356 counts per square centimeter. Likewise, an increase of CCP+CCPG type cracks from 9 to 109 counts per square centimeter is observed from 0.05% to 0.30% of expansion levels yet, representing 10% of all cracks at an expansion level of 0.30% thus, indicating that the OCA+OCAG type cracks govern the distress mechanism.

The slight increase in the total counts per square centimeter (i.e., observed at expansion levels between 0.20% to 0.30% is caused by the increase in cracks in the cement paste from 50 to 109 counts per square centimeter. Their connection among themselves may cause this limited growth in CCP+CCPG at very high expansion levels, increasing the length and not necessarily generating new cracks, as per the model presented by Sanchez et al. [2] and shown in **Figure 4.2.** Moreover, based on the minimum energy law, less energy is required to lengthen cracks than for them to be generated. Thus, the number of cracks may not necessarily increase while an increase in their lengths may be observed [1,2]. Nonetheless, this accentuated difference in the occurrence of these damage characteristics directly influences the sample selection to train the ML algorithm since it must be trained without bias. Thus, it is necessary to have a database representative of all the data trained by the model.

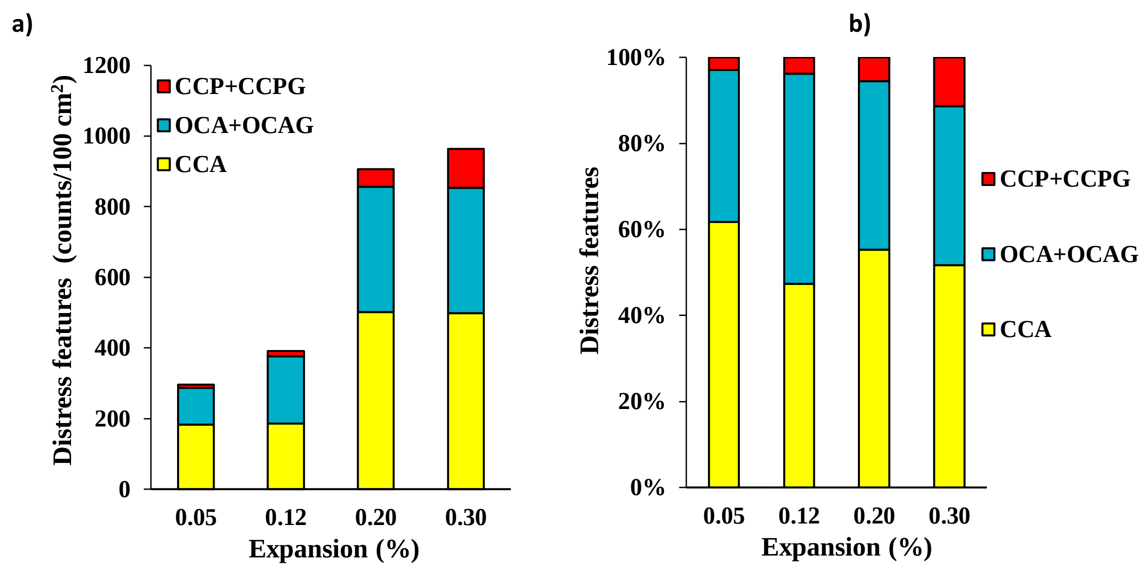

Figure 4.10: a) Counts and b) Percentage of microscopic features as a function of expansion for concrete affected by ASR**.**

4.5.2. Algorithm development and performance

The ML process is divided into two phases: 1) identifying cracks through a pixel recognition method and 2) classifying cracks based on their types as per the DRI. Therefore, the ML algorithm was trained based on the number, location, and nature of those cracks identified while performing the DRI. First, the original image (**Figure 4.11a**) is used as input, followed by a mask of the manually traced cracks without the image in the background (**Figure 4.11b**). When given the raw input image, the ML algorithm makes two predictions: 1) detect the cracks and 2) calculate the probabilities that the pixel belongs to distinct crack types for each pixel within this crack as displayed in **Figure 4.11c** and **d**, respectively.

To improve the crack prediction quality, some computer vision techniques were applied where the weak pixels were first removed to reduce the noise in the image (**Figure 4.11e**), and the strong pixels were then enhanced (**Figure 4.11f**), facilitating the model's work. Since the crack detection is pixel-based, the algorithm connects all of the pixels belonging to a crack, regardless of the type, and generates a bounding box traced in red (**Figure 4.11g**) to enable the crack length measurement using the diagonal of the box through the pixel size as all of the image acquisition properties were kept constant (i.e. 1 cm length is equivalent to 3 000 pixels). As previously mentioned, all cracks shorter than 1mm (i.e., 300 pixels) are not considered in the DRI procedure. Thus, a filter is applied to remove all features smaller than this length, (**Figure 4.11h)**.

The next task performed by the ML algorithm is to classify the cracks based on their type as per the DRI (i.e., CCA – yellow, OCA+OCAG – green and CCP+CCPG – red). As aforementioned, the pixels belonging to a crack, regardless of its type, are connected to form the crack and are classified based on the highest proportion of distinct crack type pixels present within that entire crack **(Figure 4.11 i).** Furthermore, the traced cracks with the image in the background are then used as input into the algorithm to provide the ground truth (**Figure 4.11j**).

A) original image **B) mask with manually traced cracks**

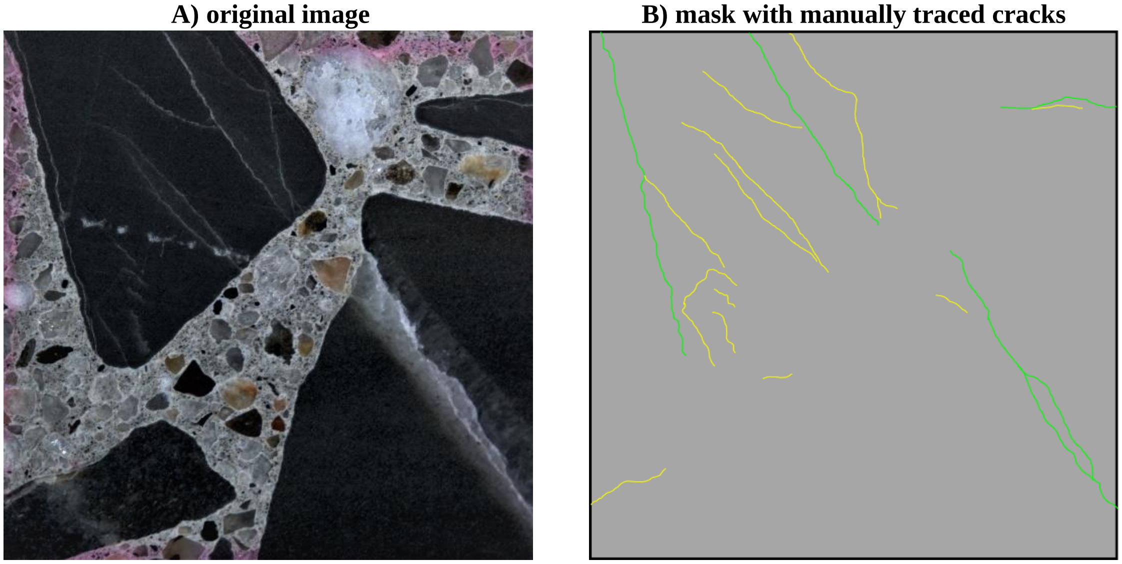

C) crack detection

D) crack type prediction

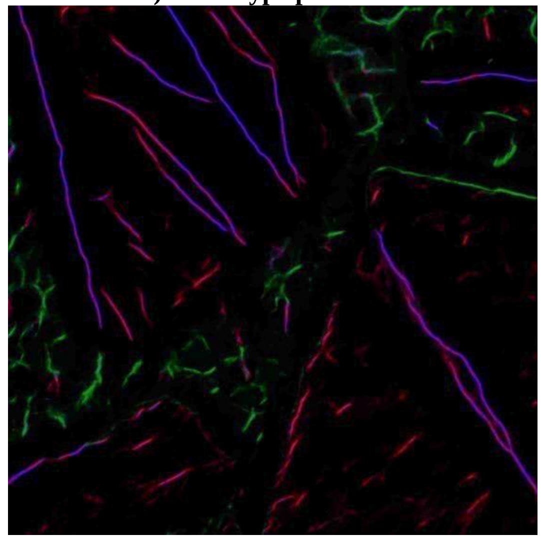

E) output including weak pixels

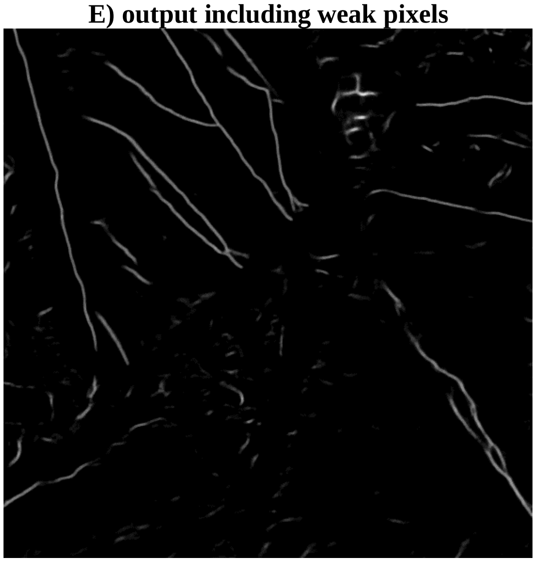

F) weak pixels removed

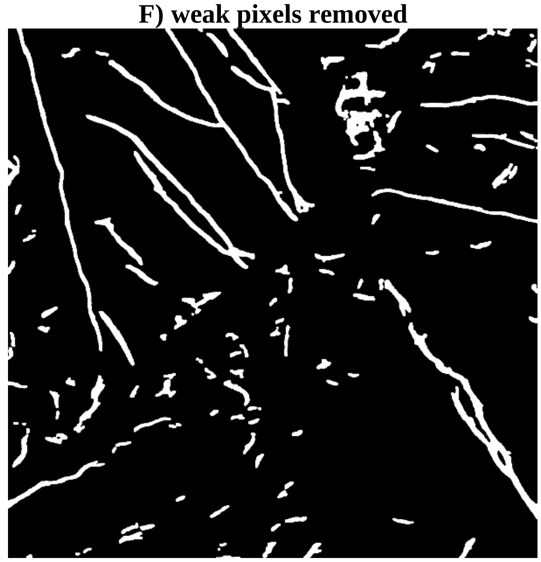

G) crack length measurement

H) cracks smaller than 1mm removed

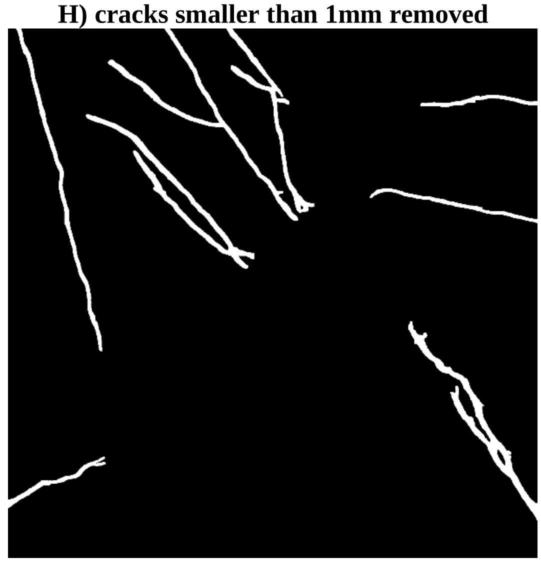

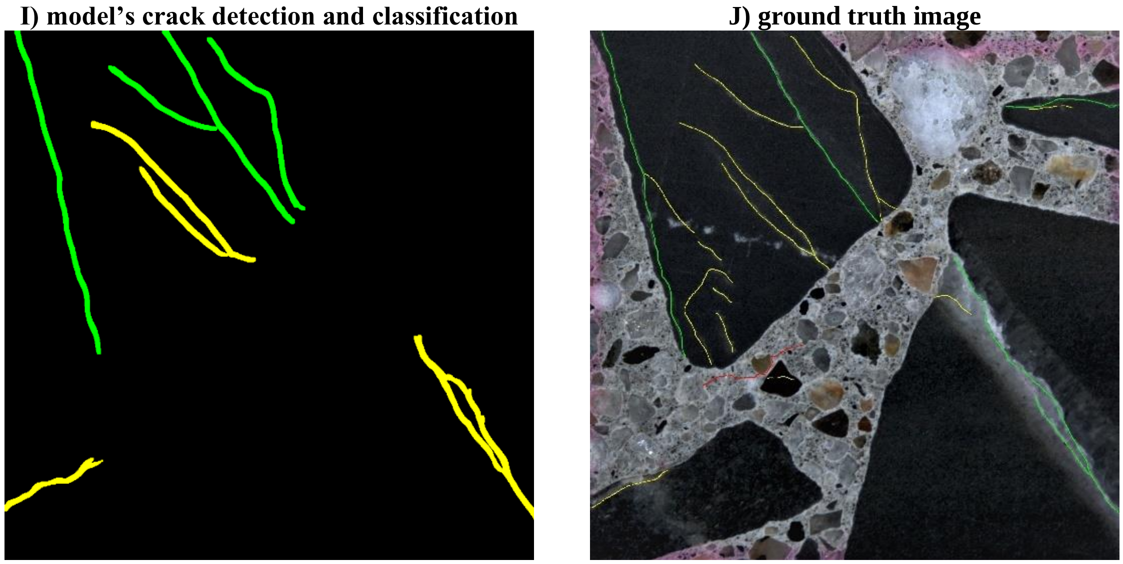

Figure 4.11: Sequence of the algorithm's operations.

The amount of data (i.e., cracks/distress features) provided to the algorithm for the training phase is influenced by each type of distress feature, which occurs in different frequencies, generally increasing with the expansion level. Thus, the OCA and OCAG features were grouped to reduce this impact since both present the same DRI weighting factor and do not alter the final DRI number. Moreover, the CCP+CCPG crack type in the Springhill aggregate specimens presents a very distinctive pixel feature compared to the other two categories of cracks, therefore influencing the algorithm's performance. As such, from **Table 4.5,** it is possible to observe the model's change in behaviour when other specimens containing different aggregates are introduced to the database, reducing bias created by just one source (i.e., aggregate type) and increasing the precision. If the model only considers the Springhill coarse aggregate specimens, the algorithm's accuracy is 74% for all distress features combined due to the number of false-positive results when the CCA is erroneously classified as OCA+OCAG. However, if the model considers other coarse aggregate types, the accuracy increases to 88% on average.

Table 4.5: Model's Precision

Feature Type	Quantity of features	Precision	
		Springhill	Overall Data
CCA	27,679	72%	84%
OCA+OCAG	23,539	76%	91%
CCP+CCPG	3,837	81%	83%

4.5.3. Automated DRI Estimation

Once the model's accuracy was achieved, the individual 1 cm by 1 cm images were uploaded into the algorithm and analyzed one by one. The outcome from this analysis is not only the crack count and classification but also the DRI estimation of those single images (**Figure 12).** illustrates the algorithm's process to achieve the DRI estimation following the guidelines developed to perform the conventional DRI.

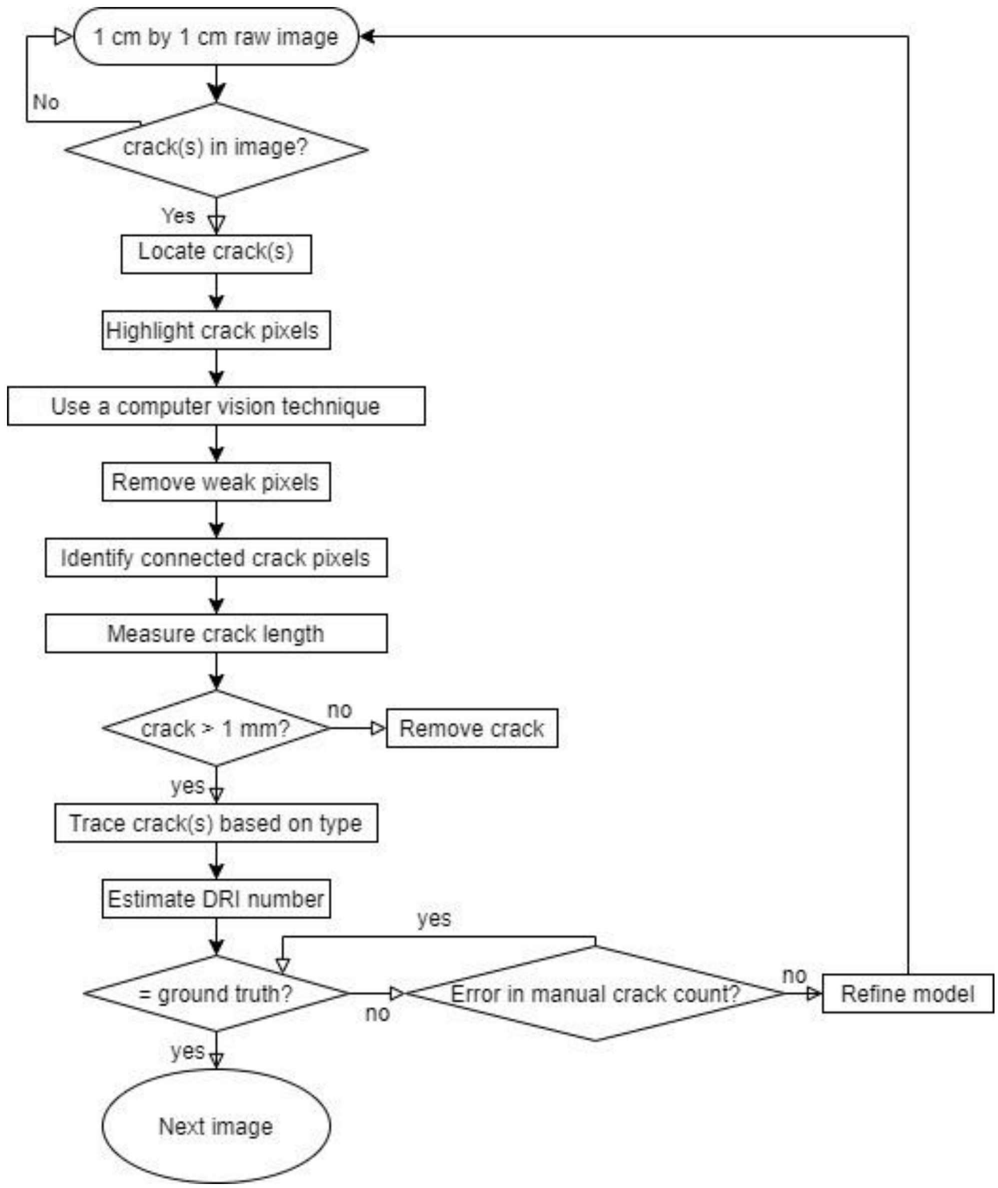

Figure 4.12: Automated DRI estimation process.

The charts presented in **Figure 4.13** demonstrate the DRI results obtained from individual 1 cm by 1 cm squares and the trend they should follow to achieve 100% accuracy highlighted in red; the linear correlation between the ground truth (x-axis) and the algorithm's estimation (y-axis) where x is equal to y. In this project, the Ground Truth (GT) are the DRI values provided by the petrographer, and the CNN estimated, are the values assembled from the algorithm. From **Figure 4.13 a**, the 0.05% expansion accumulates more results along the y-axis, indicating that the estimated results are higher than the DRI provided as ground truth (performed by the petrographer). A high variation is observed in the data when the model is used to assess low expansion levels (i.e. 0.05%); however, for higher expansion levels, the majority of the results are more equally dispersed on both sides the red line. The accuracy of the model's DRI estimation increases with increasing expansion where more data points are observed on the red line.

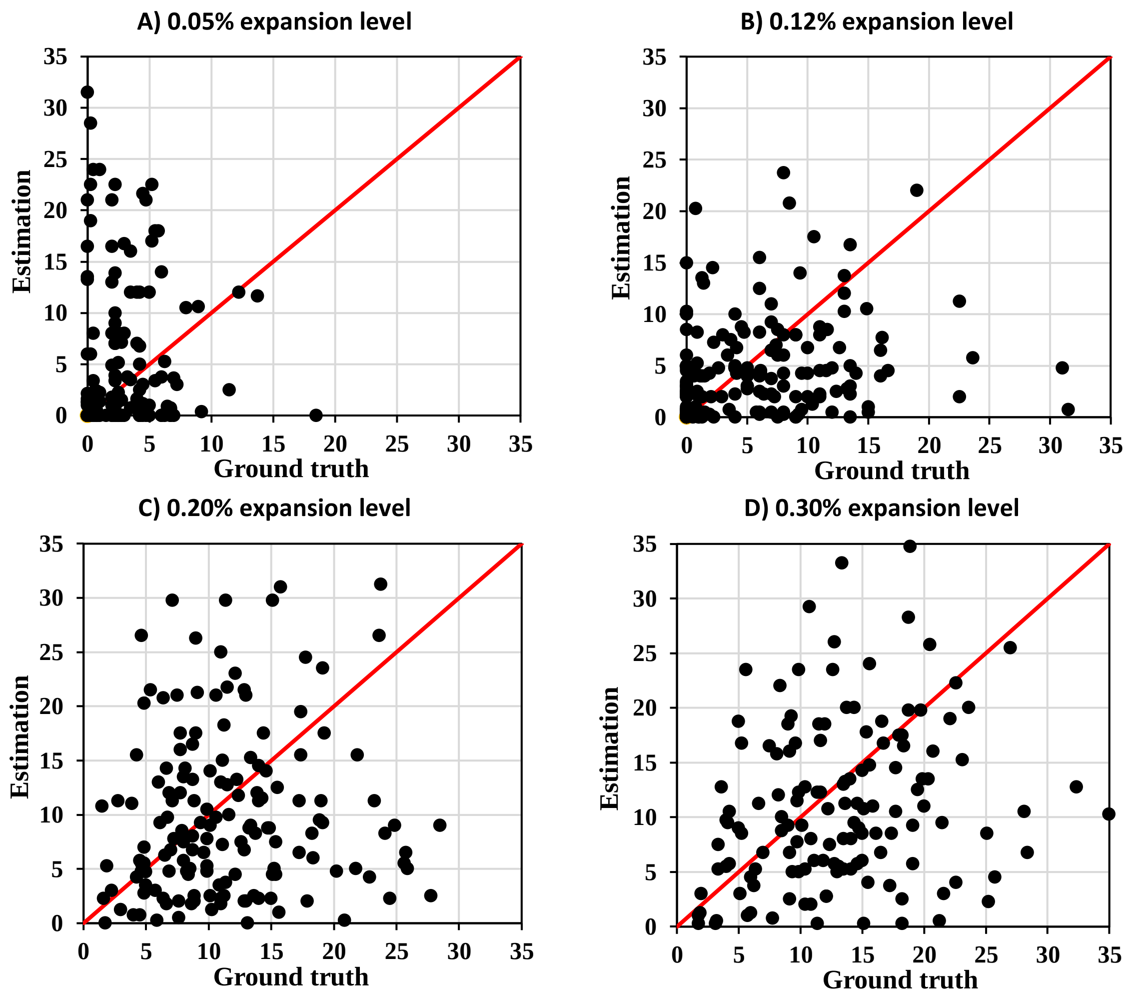

Figure 4.13: DRI results – Algorithm Estimation versus Ground Truth

The overall estimated DRI numbers (i.e., for the entire specimens and normalized to 100 cm^2) using the DL/CNN algorithm compared to the DRI numbers obtained using the conventional method are quite similar yet, the DL/CNN overestimates the DRI number (**Figure 4.14**).

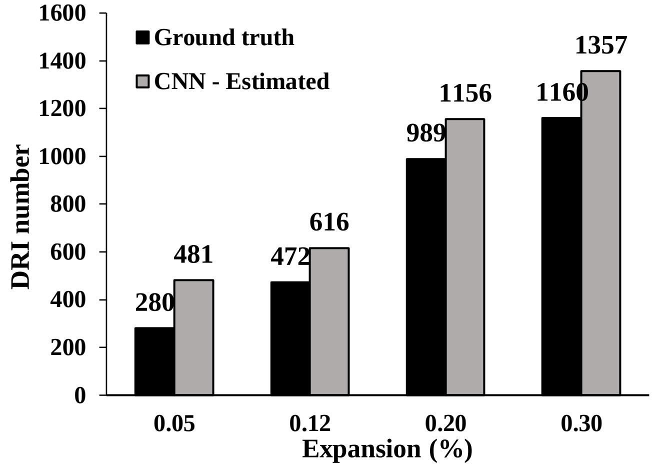

Figure 4.14: Calculated and estimated DRI numbers per expansion level.

4.6. Discussion

4.6.1. Identification of distinct ASR distress features

The DL/CNN model first performs the crack detection without classification or weighting factors as per the DRI. The total counts per square centimeter are therefore presented in **Figure 4.15** for both the ground truth (i.e. manually counted) and through the DL/CNN algorithm in order to understand the DRI over estimation. Similar to the DRI numbers achieved in **Figure 4.14**, the algorithm overcounts the number of cracks present within each 1 cm by 1 cm square. However, the difference between the results is minor since the total counts range from 296 to 963 for the ground truth and the algorithm counted 351 and 1079 features in total. Noticeably, the algorithm is able to capture the increase in distress features as the expansion increases.

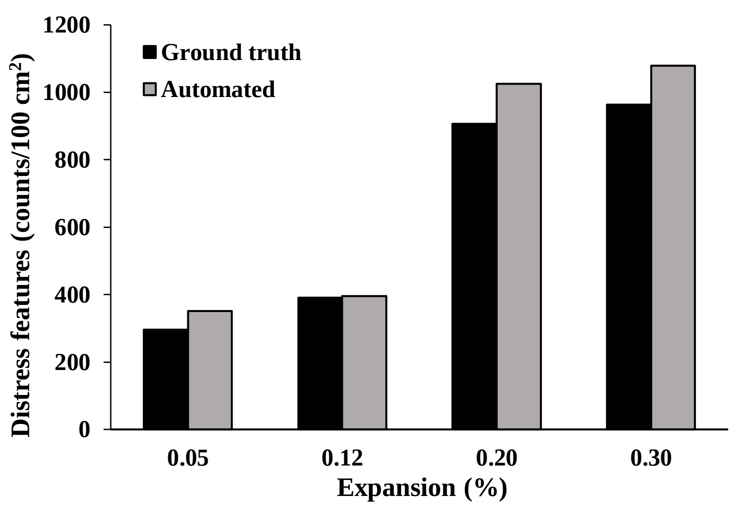

Figure 4.15: Total counts of distress features per expansion level.

As previously discussed, the algorithm was trained in two different perspectives: 1) using a large database of ASR-affected concrete containing 6 different mixtures presenting distinct strengths and incorporating a wide range of aggregates and, 2) only utilizing the Springhill aggregate. Both natural (i.e., gravel) and manufactured (i.e., crushed) reactive aggregates were first used to train the algorithm to identify ASR distress features; aggregates presenting different features such as colours, textures, shapes, sizes, etc., were used. Moreover, fine, and coarse reactive aggregates were also selected to be part of the database of training.

Among the particularities of the training phase, the use of natural aggregates was quite challenging. This type of material displays a rounded shape, most susceptible to onion-type cracks, and contains natural veins in its formation, resembling cracks to an untrained petrographer. Evidently, this can lead to a misidentification of these features and classify them as a distress instead of natural features; thus, increasing the total number of cracks and consequently influencing the calculated damage degree. **Figure 4.16a** presents the aggregate samples composed of natural features, which faintly change in colour when compared to the distress feature; in some cases, even for a petrographer, the proper classification could be challenging. Likewise, certain aggregates present a certain level of transparent, crystallized quartz structure (**Figure 4.16b**), which may resemble distress for untrained petrographers but is part of the mineralogical structure of the aggregate.

It is essential to notice that all the aggregates used in this database present petrographic characteristics similar to the material assessed in the study proposed by Sanchez et al. [4], allowing to correlate between DRI numbers and damage degrees. The ranges presented in that work were generated from different sources, coarse and fine aggregates, natural and manufactured thus, highlighting that those thresholds do not strictly represent the material but enlighten the critical patterns, enabling a broad comparison with lower bias.

a) Natural aggregate presenting natural veins and ASR-damage features **b) Natural quartz aggregate feature versus AS-damage features**

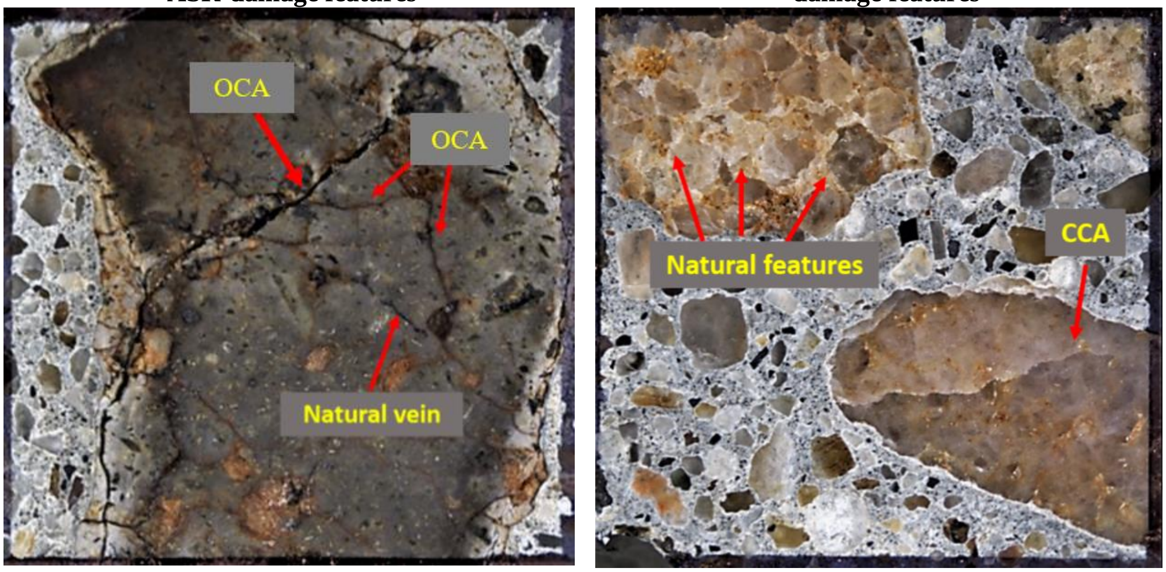

Figure 4.16: Natural features from gravel misclassified as damage features.

4.6.2. Classification of ASR features based on the DRI

Following the crack identification, the DL/CNN model begins to classify the detected cracks based on their types as per the DRI (i.e., CCA, OCA+OCAG and CCP+CCPG). **Figure 4.17** shows the automated counts of distress features as counts per 100 cm2 and proportions according to the extended version of the DRI proposed by Sanchez et al [2], which are fairly similar to those presented in **Figure 4.5**. Noticeably, the automated counts of the cracks in the cement paste (i.e., CCP+CCPG) are higher than the ground truth (**Figure 4.7a**) for all expansion levels. This overcounting, however, may be associated to the model considering the ITZ and porous areas with a significant width, recognizing them as cracks in the cement paste since they somehow present similar characteristics (e.g., change in colour when compared to the bulk cement paste). Likewise, although the counts of the cracks in the aggregates (i.e., CCA and OCA+OCAG) are very similar, a higher count of closed cracks in the aggregates is observed through the automated counts for expansion levels of 0.20% and 0.30% (i.e., 612 and 570, respectively) compared to the ground truth (i.e., 501 and 498, respectively) while the open cracks in the aggregates present a lower automated count (i.e., 236 and 313, respectively) compared to 355 and 356, respectively, obtained by the ground truth. Therefore, the DL-CNN algorithm tends to overestimate CCA whereas the OCA+OCAG are underestimated.

Evidently, the difference between cracks in the aggregates and cracks in the cement paste are more easily distinguished by a petrographer than the DL-CNN model; yet, the model faces a challenge when encountering cracks in the aggregates and their distinction. Consequently, the model's filters cannot accurately differentiate the main differences between CCA and OCA+OCAG, which significantly influences the DRI number since their weighting factors are considerably different (i.e. 0.25 and 2, respectively). Moreover, the aforementioned could be explained from two perspectives: 1) the most optimistic where the model can recognize more features than humans, presenting a better assessment than humans; or 2) the less optimistic, where the model misclassifies ITZ and porous areas as cracks in the cement paste and open cracks in the aggregates as closed.

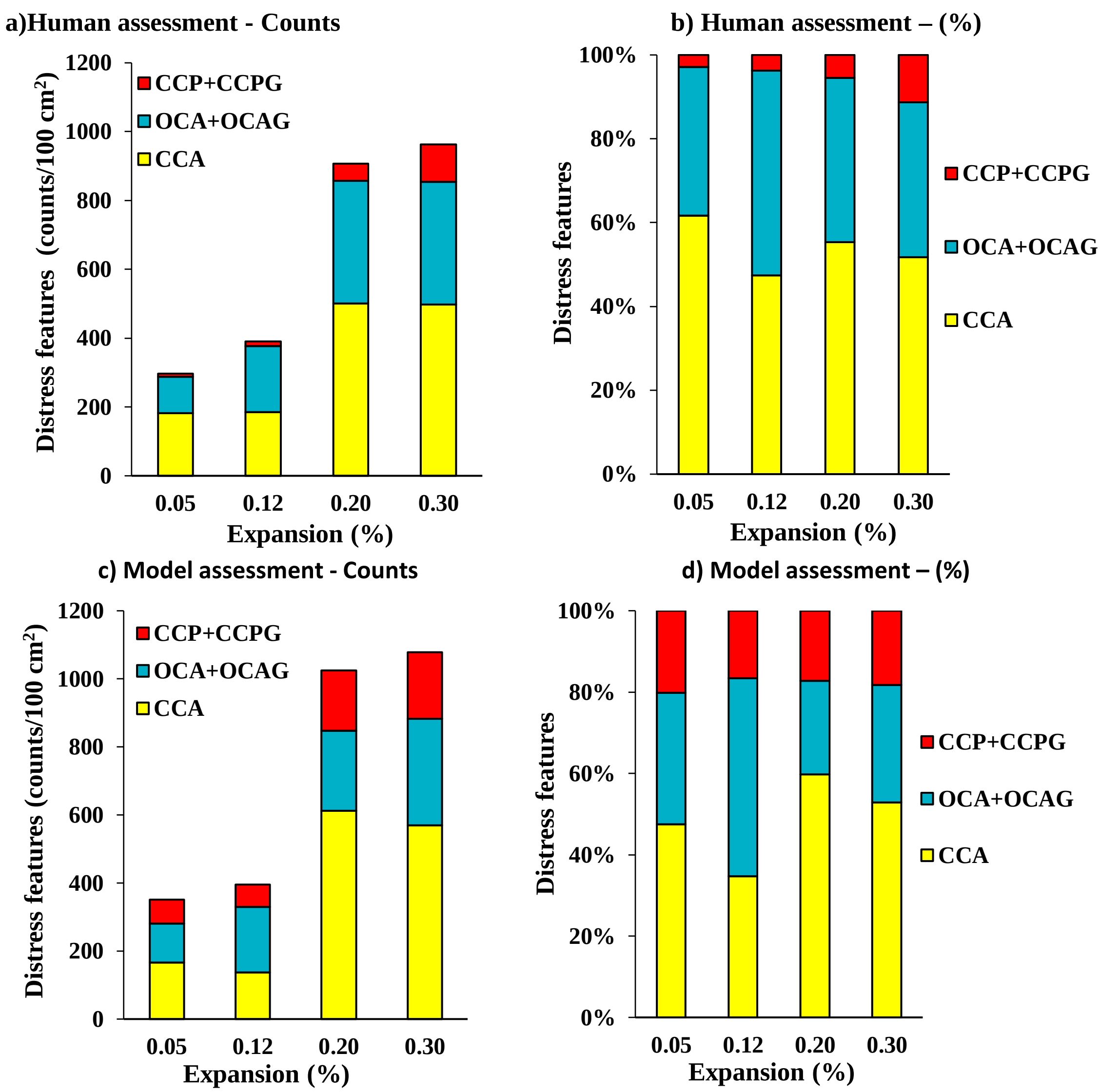

Figure 4.17: Distress Features**:** Humans and Automated counts (a,c) and proportions (%) (b,d).

Aiming to understand these crack classification discrepancies, the number of distress features per type (i.e., CCA, OCA+OCAG and CCP+CCPG) pertaining to the individual 1 cm by 1 cm squares was plotted as displayed in **Figure 4.18**. Noticeably, the CCP is overcounted by the algorithm at an 0.05% expansion level, which significantly increases the DRI number as these types of cracks are infrequently observed at low damage degrees (**Figure 4.9**).

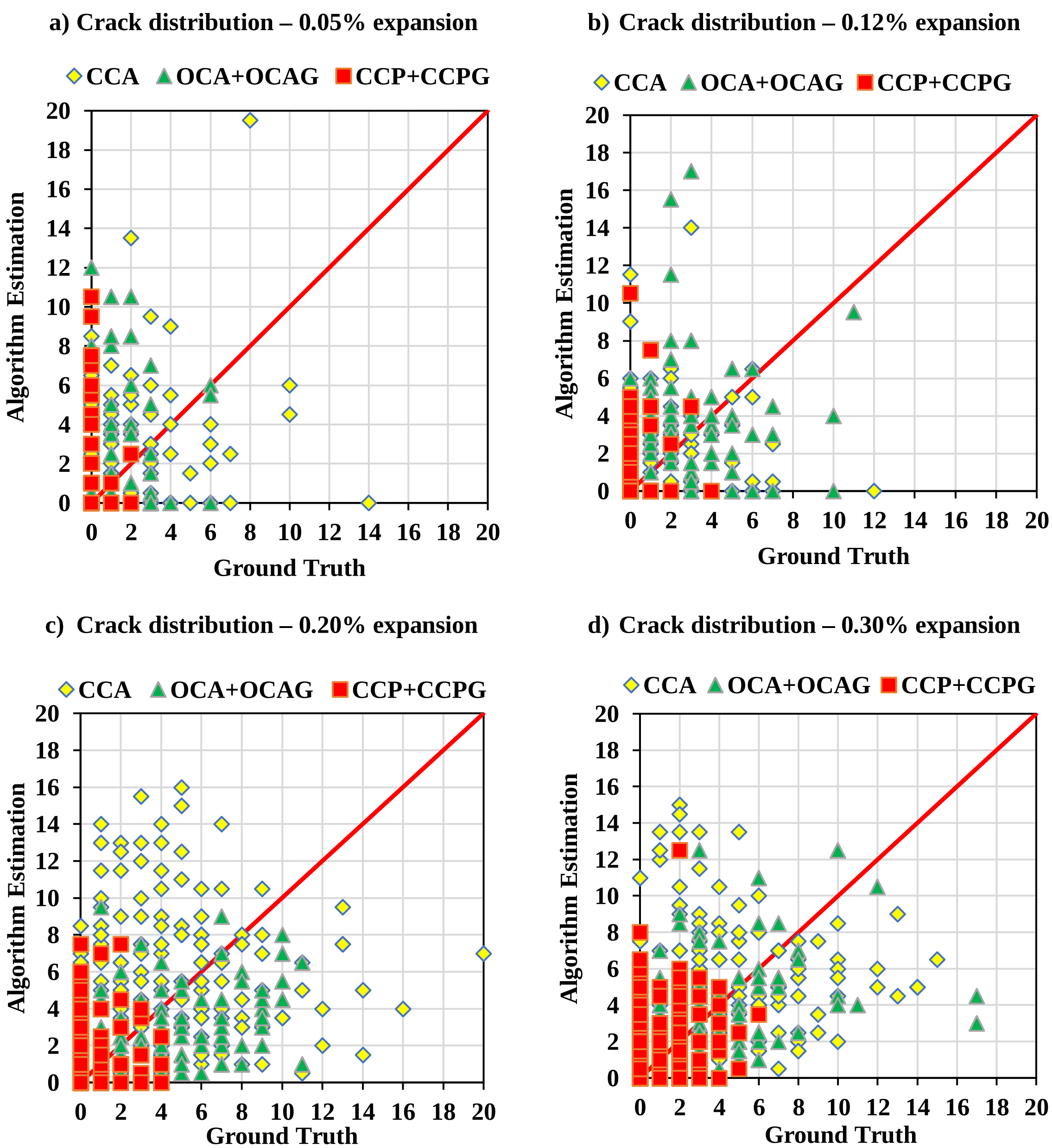

Figure 4.18: Crack counts and classification: ground truth versus algorithm counts.

Analogous challenges were faced in the classification of the ASR features. At high expansion levels, the model can predict with plausible precision the crack location and type (i.e., identification and classification). However, when it comes to lower expansion levels, the filters less accurately distinguish the main differences between CCA and OCA+OCAG, which significantly influences the DRI number since their weighting factors are significantly different (i.e., 0.25 and 2, respectively). Moreover, the aforementioned could be explained from two perspectives: 1) the most optimistic where the model can recognize more features than humans, presenting a better assessment than humans; or 2) the less optimistic, where the model misclassifies CCAs as being part of OCA+OCAG and considers scratches as cracks.

4.6.3. DRI estimation - Machine vs human

The obtained DRI number is associated to a degree of damage where a higher DRI number represents a higher degree of damage. **Table 4.6** displays the specific DRI number ranges for ASR-affected concrete per expansion level and compares the results from the machine and petrographer(s). Moreover, the DRI numbers obtained by the petrographers in this study at 0.20% and 0.30% of expansion are slightly above range, although the crack propagation at these expansion levels follows that of the model proposed by Sanchez et al. (2015) [2] and shown in **Figure 4.3**. The aggregate selected for this study is a highly reactive aggregate presenting a significantly high number of distress features within the aggregate hence, the slightly higher DRI number. This aggregate was selected due to this increased number of features per 1 cm by 1 cm image to train the DL/CNN algorithm. Nevertheless, the model could capture those distress features. Although the estimated DRI numbers obtained are higher than those obtained by the petrographer, they increase with expansion which shows that the machine properly captures the increase in damage and, therefore, the damage degree. Nevertheless, some minor divergences in the estimated DRI number results can be acceptable given that the time required to perform the automated version of the DRI from scanning the sample to obtaining the final DRI number is accomplished in minutes as opposed to hours when using the traditional procedure. It is evident that the crack counting, and the classification influence the DRI estimation therefore, their improvements will improve the DRI estimation.

Table 4.6: Comparison between DRI calculation and estimation performed

Damage degree	Expansion level (%)	DRI number		
		Typical range [4]	**Petrographer**	**Machine**
Negligible	0.00	100-155	-	-
Marginal	0.05	210-400	280	481
Moderate	0.12	330-500	472	616
High	0.20	500-765	989	1156
Very high	0.30	600-925	1160	1357

The DRI is an extremely useful tool accompanied with a time-consuming procedure. Although the DRI produces a quantitative value that can be used to assess damage in ASR affected concrete, the process of performing the DRI gives the petrographer an indication of the condition of the affected concrete through the cause and extent of the damage; hence the DRI being a tool and not merely an output. Several different outputs can be obtained while performing the DRI such as its extended version as aforementioned and thoroughly used throughout this research to compare the machine and human assessment. Among these outputs, the crack density (i.e., counts/cm2) presents interesting results since cracks most associated to ASR (i.e., OCA+OCAG and CCP+CCPG) are summed and evaluated**. Figure 4.19** displays the crack density for both the ground truth and the automation through the DL/CNN model as a function of expansion. The crack densities seem to become more similar after 0.05% of expansion, being almost identical at 0.20% of expansion (i.e., 4 counts/cm^2). The largest difference is observed at 0.05% of expansion with 1 count/cm^2 as the ground truth and 2 counts/cm^2 through the automation. This discrepancy may be associated to the training phase of the model since specimens containing many different types of distress features were required; hence the use of specimens as higher expansion levels to include all three types of cracks in the images provided. As such, the DL/CNN model was not familiar with a significantly lower number of distress features at low expansion levels (i.e., 0.05%). Moreover, the model may even be forecasting the crack propagation at such expansion levels.

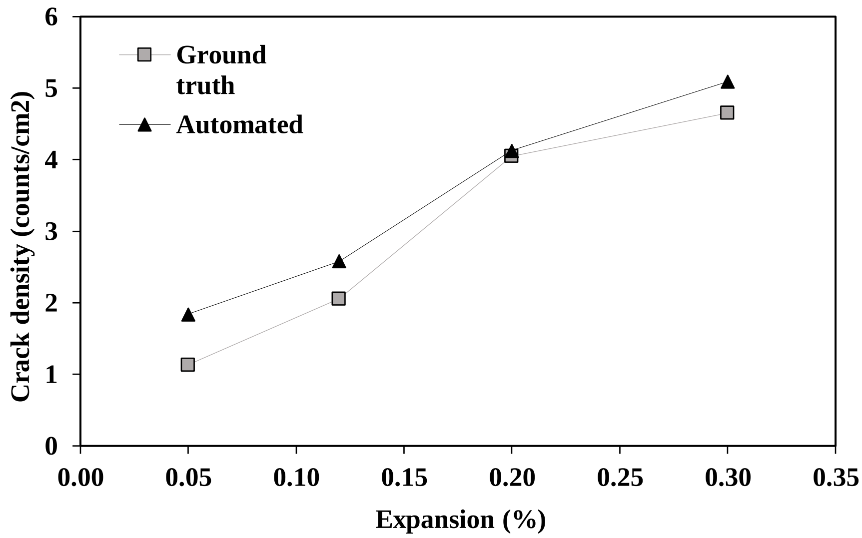

Figure 4.19: Crack density as a function of expansion.

Despite the unprecedented method presented in this work, future works will be necessary to improve the distinction between cracks in the cement paste and the porosity areas, ITZ and cracks in the aggregate. Additionally, the algorithm classifies a crack based on the most significant number of pixels belonging to a particular type of crack present within that crack. Therefore, a crack that extends into the cement paste from the aggregate and contains more pixels inside of the aggregate or the cement paste will be counted as one crack in the aggregate or the cement paste, respectively, as opposed to one crack in the aggregate and one crack in the cement paste for a total of two cracks. Although this underestimates the DRI number, an established distinction between the different phases along the crack in the concrete is required.

4.7. Conclusion

The purpose of this project is to automate the DRI test protocol to evaluate ASR-affected concrete thoroughly, regardless of the deterioration level or material's constituents, predicting not only types, amounts, and features of cracks but also the overall DRI evaluation. The main breakthroughs of this project are presented henceforth.

- The image preparation and acquisition parameters play an essential part in the outcomes of pixel segmentation models and machine learning techniques, enhancing the tridimensional (e.g., the depth) notion in images, even if they are displayed in 2D;

- The image acquisition should be performed excluding the grid interface from the image, so the misclassification associated with it can be eliminated from the system.

- The Machine Learning (ML) algorithm was trained based on the number, location and nature of the cracks identified while performing the Damage Rating Index (DRI). The samples used to train the model were derived from various aggregates. When compared the precision attained by the model using the Overall Data and only the Springhill, the variation encountered between the results was 14% for Closed Crack Aggregates (CCA), 16% for Open Crack Aggregates with and without Gel (OCA+OCAG) and only 2% for the crack in the Cement Paste with and without Gel (CCP+CCPG), being the overall data more precise. So, it is possible to conclude that the database requires variability in its constituents to reduce the bias created during the learning process. It should be analyzed more carefully to reduce as much as possible the bias in the system;

- The results gathered in this research indicate that the automated DRI presents a better performance at high expansion levels. At 0.20% expansion the DRI shows a precision of 83% and 82% at 0.30%. Conversely, the most notable differences in the DRI automated and DRI performed by humans were noticed at lower expansion levels, being the 0.05% the most inconsistent result, presenting a precision of 30%. Though, at 0.12% of expansion, the model shows 70% of precision, between the estimated and ground truth results. Overall, the automated DRI presents an average accuracy of 74.4%, with a precision of 76.5%.

- The overcounting experienced at the lower expansion levels is partially because the model recognizes the Interfacial Transition Zone (ITZ) and porous areas with a significant width and classifying them as CCP+CCPG since they present similar characteristics. Likewise, the grid used to delimitate the area 1cm x 1cm is misclassified as a crack in some cases.

- The DRI overestimation at low expansion levels is explained by the overcounting of CCP+CCPG that possesses the highest weighting factor, impacting more the DRI results when compared with the other two groups. Therefore, further training is required at low expansion levels.

- Overall, the model works appropriately at moderate and high expansion levels, and the Automated DRI procedure only takes minutes to estimate the damage, besides providing all the individual counting and images with the cracks traced.

- Future investigation is necessary to evaluate if the model might be dividing one crack into multiple sections when there is a mineral variation in the aggregate, which could interfere in the pixel consolidation, working as the so-called “noise” in the data.

- Implementation of the crack length and width measurements as an output of the model are also features of interest to be implemented in the future. The algorithm can measure the crack’s length using the diagonals of the bounding boxes; yet, it is currently only used to remove cracks smaller than 300 pixels.

- Finally, additional research is recommended to use the sophisticated DL/CNN system to evaluate ASR-affected concrete triggered by a reactive fine aggregate, along with other damage mechanisms such as external and internal sulphate attack, freeze-thaw, etc. damage. The proposed approach has the potential to become a comprehensive protocol for evaluating damage in concrete.

4.8. References

[1] L.F.M. Sanchez, B. Fournier, M. Jolin, M.A.B. Bedoya, J. Bastien, J. Duchesne, Use of Damage Rating Index to quantify alkali-silica reaction damage in concrete: Fine versus coarse aggregate, ACI Mater. J. 113 (2016) 395–407. https://doi.org/10.14359/51688983.

[2] L.F.M. Sanchez, B. Fournier, M. Jolin, J. Duchesne, Reliable quantification of AAR damage through assessment of the Damage Rating Index (DRI), Cem. Concr. Res. 67 (2015) 74–92. https://doi.org/10.1016/j.cemconres.2014.08.002.

[3] M.T. Benoit Fournier, Marc-André Bérubé, Kevin J. Folliard, Report on ASR Mitigation, Fed. Highw. Adm. Publ. FHWA-HRT-04-113 Techbr. FHWA-HRT-06-071. (2010).

[4] L.F.M. Sanchez, T. Drimalas, B. Fournier, D. Mitchell, J. Bastien, Comprehensive damage assessment in concrete affected by different internal swelling reaction (ISR) mechanisms, Cem. Concr. Res. 107 (2018) 284–303. https://doi.org/10.1016/j.cemconres.2018.02.017.

[5] D.J. De Souza, L.F.M. Sanchez, M.T. De Grazia, Evaluation of a direct shear test setup to quantify AAR-induced expansion and damage in concrete, Constr. Build. Mater. 229 (2019) 116806. https://doi.org/10.1016/j.conbuildmat.2019.116806.

[6] C. Trottier, A. Zahedi, R. Ziapour, L. Sanchez, F. Locati, Microscopic assessment of recycled concrete aggregate (RCA) mixtures affected by alkali-silica reaction (ASR), Constr. Build. Mater. 269 (2021) 121250. https://doi.org/10.1016/j.conbuildmat.2020.121250.

[7] N. Smaoui, B. Bissonnette, M.A. Bérubé, B. Fournier, B. Durand, Mechanical properties of ASR-affected concrete containing fine or coarse reactive aggregates, J. ASTM Int. 3 (2006) 1–16. https://doi.org/10.1520/jai12010.

[8] R.B. Figueira, R. Sousa, L. Coelho, M. Azenha, J.M. de Almeida, P.A.S. Jorge, C.J.R. Silva, Alkali-silica reaction in concrete: Mechanisms, mitigation and test methods, Constr. Build. Mater. 222 (2019) 903–931. https://doi.org/10.1016/j.conbuildmat.2019.07.230.

[9] I. Yurtdas, D. Chen, D.W. Hu, J.F. Shao, Influence of alkali silica reaction (ASR) on mechanical properties of mortar, Constr. Build. Mater. 47 (2013) 165–174. https://doi.org/10.1016/j.conbuildmat.2013.04.046.

[10] T. Chappex, K. Scrivener, Alkali fixation of C-S-H in blended cement pastes and its relation to alkali silica reaction, Cem. Concr. Res. 42 (2012) 1049–1054. https://doi.org/10.1016/j.cemconres.2012.03.010.

[11] Y. Khajehnouri, M. Chouteau, P. Rivard, C.L. Bérubé, Non-destructive non-invasive assessment of the development of alkali-silica reaction in concrete by spectral induced polarization: Evaluation of the complex electrical properties, Constr. Build. Mater. 238 (2020) 117719. https://doi.org/10.1016/j.conbuildmat.2019.117719.

[12] L.F.M. Sanchez, B. Fournier, M. Jolin, D. Mitchell, J. Bastien, Overall assessment of Alkali-Aggregate Reaction (AAR) in concretes presenting different strengths and incorporating a wide range of reactive aggregate types and natures, Cem. Concr. Res. 93 (2017) 17–31. https://doi.org/10.1016/j.cemconres.2016.12.001.

[13] V. Villenneuve, B. Fournier, J. Duchesne, Determination of the damage in concrete affected by ASR – The damage rating index (DRI)., in: 14th Int. Conf. Alkali-Aggregate React. (ICAAR)., Austin, USA., 2012.

[14] A. Zahedi, C. Trottier, L.F.M. Sanchez, M. Noël, Microscopic assessment of ASR-affected concrete under confinement conditions, Cem. Concr. Res. 145 (2021). https://doi.org/10.1016/j.cemconres.2021.106456.

[15] L.F.M. Sanchez, B. Fournier, D. Mitchell, J. Bastien, Condition assessment of an ASR-affected overpass after nearly 50 years in service, Constr. Build. Mater. 236 (2020) 117554. https://doi.org/10.1016/j.conbuildmat.2019.117554.

[16] B. Fournier, M.A. Bérubé, K.J. Folliard, M. Thomas, ASR Testing and Evaluation Protocols Prepared for the Federal Highway Administration by :, (2008).

[17] S. Bilodeau, A. Allard, J. Bastien, F. Pissot, B. Fournier, B. Bissonnette, Performance Evaluation of Thick Concrete Slabs Affected by Alkali-Silica Reaction (ASR) - Part II: Structural Aspects, Conf. Proc. 15th ICAAR. (2016) 1–9.

[18] E.R. Giannini, L.F.M. Sanchez, A. Tuinukuafe, K.J. Folliard, Characterization of concrete affected by delayed ettringite formation using the stiffness damage test, Constr. Build. Mater. 162 (2018) 253–264. https://doi.org/10.1016/j.conbuildmat.2017.12.012.

[19] AASHTO T 380, Standard Method of Test for Potential Alkali Reactivity of Aggregates and Effectiveness of ASR Mitigation Measures (Miniature Concrete Prism Test, MCPT), (2019) 1–10.

[20] P.A. Dunbar, P.E. Grattan-Bellew, Results of damage rating evaluation of condition of concrete from a number of structures affected by AAR, in: Proc. CANMET/ACI Int. Work. Alkali-Aggregate React. Concr., National Resources Canada, Dartmouth, 1995: pp. 257–265.

[21] Grattan-Bellew, E., D. Mitchell, J. Margeson, D. Min, Is alkali-carbonate reaction just a variant of alkali-silica reaction ACR = ASR?, Cem. Concr. Res. 40 (2010) 556–562. https://doi.org/10.1016/j.cemconres.2009.09.002.

[22] P. Rivard, B. Fournier, G. Ballivy, Quantitative petrographic technique for concrete damage due to ASR: Experimental and application, Cem. Concr. Aggregates. 22 (2000) 63–72. https://doi.org/10.1520/cca10465j.

[23] P. Rivard, B. Fournier, G. Ballivy, The damage rating index method for ASR affected concrete - A critical review of petrographic features of deterioration and evaluation criteria, Cem. Concr. Aggregates. 24 (2002) 81–91. https://doi.org/10.1520/cca10531j.

[24] and D.V. Alexis Courtois, Eric R. Giannini, Alexandre Boule, Jean-Marie Hénault, Laurence Jacobs, Benoit Masson, Patrice Rivard, Jerǒme Sausse, Diagnosis & Prognosis of AAR Affected Structures, in: Diagnosis Progn. AAR Affect. Struct., RILEM - Springer, 2020: pp. 41–93.

[25] L.F.M. Sanchez, B. Fournier, M. Jolin, D. Mitchell, M. Noel, Thorough Characterization of Concrete Damage Caused By Aar Through the Use of a Multi-Level Approach, 15th Int. Conf. Alkali-Aggregate React. (2016).

[26] N. Castro, B.J. Wigum, Assessment of the potential alkali-reactivity of aggregates for concrete by image analysis petrography, Cem. Concr. Res. 42 (2012) 1635–1644. https://doi.org/10.1016/j.cemconres.2012.08.009.

[27] S. Multon, F. Toutlemonde, Effect of applied stresses on alkali-silica reaction-induced expansions, Cem. Concr. Res. 36 (2006) 912–920. https://doi.org/10.1016/j.cemconres.2005.11.012.

[28] M.D.A. n Fournier, B., Bérubé, M.A., Folliard, K.J. and Thomas, Report on the diagnosis, prognosis and mitigation of alkali-silica reaction (ASR) in transportation structures. FHWAHIF-09-004, 2010.

[29] ACI 228.1R-19, Report on Methods for Estimating In-Place Concrete Strength, Sustain. 11 (2019) 1–14. http://scioteca.caf.com/bitstream/handle/123456789/1091/RED2017-Eng-8ene.pdf?sequence=12&isAllowed=y%0Ahttp://dx.doi.org/10.1016/j.regsciurbeco.2008.06.005%0Ahttps://www.researchgate.net/publication/305320484_SISTEM_PEMBETUNGAN_TERPUSAT_STRATEGI_MELESTARI.

[30] P.E. Grattan-Bellew, L.D. Mitchell, Quantitative Petrographic Analysis of Concrete – The Damage Rating Index (DRI) Method , A Review, 8th CANMET/ACI Int. Conf. Recent Adv. Concr. Technol. (2006) 14.

[31] L.F.M. Sanchez, B. Fournier, M. Jolin, J. Bastien, Evaluation of the Stiffness Damage Test (SDT) as a tool for assessing damage in concrete due to alkali-silica reaction (ASR): Input parameters and variability of the test responses, Constr. Build. Mater. 77 (2015) 20–32. https://doi.org/10.1016/j.conbuildmat.2014.11.071.

[32] P. Fecteau, B. Fournier, G. Engineering, USE OF SCMs ON ACR-AFFECTED CONCRETE : EXPANSION AND DAMAGE EVALUATION THROUGH THE DAMAGE RATING INDEX, 15th Int. Conf. Alkali-Aggregate React. (2016).

[33] L.F.M. Sanchez, B. Fournier, T. Drimalas, J. Bastien, L.D. Mitchell, M. Noel, Semi-Quantitative Condition Assessment of Concrete Distress Through the Damage Rating Index, Int. Conf. Alkali Aggragete React. (2016) 10.

[34] L.F.M. Sanchez, B. Fournier, M. Jolin, J. Bastien, D. Mitchell, M. Noel, The Use of the Damage Rating Index (DRI) for the Condition Assessment of Aging Distressed Concrete, 15th Int. Conf. Alkali-Aggregate React. (2016) 10.

[35] V. Jensen, S. Sujjavanich, Alkali Silica Reaction in Concrete Foundations in Thailand, 15th ICAAR - Intenational Conf. Alkali Aggreg. React. Concr. (2016).

[36] V. Jensen, Diagnosis of Alkali Silica Reaction, 15th Int. Conf. Alkali-Aggregate React. (2016).

[37] T. Sugiyama, M.A.B. Promentilla, T. Hitomi, N. Takeda, Application of synchrotron microtomography for pore structure characterization of deteriorated cementitious materials due to leaching, Cem. Concr. Res. 40 (2010) 1265–1270. https://doi.org/10.1016/j.cemconres.2009.10.009.

[38] Unsupervised learning foundations of neural computation, MIT Press, Cambridge, Mass, 1999.

[39] N. Li, X. Hou, X. Yang, Y. Dong, Automation Recognition of Pavement Surface Distress Based on Support Vector Machine, in: 2009 Second Int. Conf. Intell. Networks Intell. Syst., 2009: pp. 346–349. https://doi.org/10.1109/ICINIS.2009.95.

[40] M. Gavilán, D. Balcones, O. Marcos, D. Llorca, M. Sotelo, I. Parra, M. Ocaña, P. Aliseda, A. Amírola, A. Yarza, Adaptive Road Crack Detection System by Pavement Classification, Sensors. 11 (2011) 9628–9657.

[41] S. Wang, S. Qiu, W. Wang, D. Xiao, K.C.P. Wang, Cracking classification using minimum rectangular cover-based support vector machine, J. Comput. Civ. Eng. 31 (2017).

[42] N.-D. Hoang, An Artificial Intelligence Method for Asphalt Pavement Pothole Detection Using Least Squares Support Vector Machine and Neural Network with Steerable Filter-Based Feature Extraction, Adv. Civ. Eng. 2018 (2018) 1–12.

[43] H.D. Cheng, J. Wang, Y.G. Hu, C. Glazier, X.J. Shi, X.W. Chen, Novel approach to pavement cracking detection based on neural network, Transp. Res. Rec. 1764 (2001) 119–127.

[44] Y.-A. Hsieh, Y.J. Tsai, Machine Learning for Crack Detection: Review and Model Performance Comparison, J. Comput. Civ. Eng. 34 (2020).

[45] M.H. Ke Ma, D. Samaras, Large-scale Continual Road Inspection: Visual Infrastructure Assessment in the Wild, in: Proc. Br. Mach. Vis. Conf., 2017.

[46] K. Gopalakrishnan, H. Gholami, A. Vidyadharan, A. Choudhary, A. Agrawal, CRACK DAMAGE DETECTION IN UNMANNED AERIAL VEHICLE IMAGES OF CIVIL INFRASTRUCTURE USING PRE-TRAINED DEEP LEARNING MODEL, Int. J. Traffic Transp. Eng. 8 (2018) 1–14.

[47] M. Eisenbach, R. Stricker, D. Seichter, K. Amende, K. Debes, M. Sesselmann, D. Ebersbach, U. Stoeckert, H. Gross, How to get pavement distress detection ready for deep learning? A systematic approach, in: 2017 Int. Jt. Conf. Neural Networks, 2017: pp. 2039–2047. https://doi.org/10.1109/IJCNN.2017.7966101.

[48] F.-C. Chen, M.R. Jahanshahi, NB-CNN: Deep Learning-Based Crack Detection Using Convolutional Neural Network and Naïve Bayes Data Fusion, IEEE Trans. Ind. Electron. 65 (2018) 4392–4400.

[49] H. Maeda, Y. Sekimoto, T. Seto, T. Kashiyama, H. Omata, Road Damage Detection and Classification Using Deep Neural Networks with Smartphone Images: Road damage detection and classification, Comput. Civ. Infrastruct. Eng. 33 (2018) 1127–1141.

[50] V. Mandal, L. Uong, Y. Adu-Gyamfi, Automated Road Crack Detection Using Deep Convolutional Neural Networks, in: 2018 IEEE Int. Conf. Big Data (Big Data), 2018: pp. 5212–5215. https://doi.org/10.1109/BigData.2018.8622327.

[51] Y. Xue, Y. Li, A Fast Detection Method via Region-Based Fully Convolutional Neural Networks for Shield Tunnel Lining Defects, Comput. Civ. Infrastruct. Eng. 33 (2018) 638–654. https://doi.org/10.1111/mice.12367.

[52] K. Simonyan, A. Zisserman, Very deep convolutional networks for large-scale image recognition, ArXiv Prepr. ArXiv1409.1556. (2014).

[53] S. Ren, K. He, R. Girshick, J. Sun, Faster R-CNN: Towards Real-Time Object Detection with Region Proposal Networks, IEEE Trans. Pattern Anal. Mach. Intell. 39 (2017) 1137–1149. https://doi.org/10.1109/TPAMI.2016.2577031.

[54] K. He, X. Zhang, S. Ren, J. Sun, Deep Residual Learning for Image Recognition, in: 2016 IEEE Conf. Comput. Vis. Pattern Recognit., 2016: pp. 770–778. https://doi.org/10.1109/CVPR.2016.90.

[55] F. Yang, L. Zhang, S. Yu, D. Prokhorov, X. Mei, H. Ling, Feature Pyramid and Hierarchical Boosting Network for Pavement Crack Detection, IEEE Trans. Intell. Transp. Syst. 21 (2020) 1525–1535. https://doi.org/10.1109/TITS.2019.2910595.

[56] Q. Zou, Y. Cao, Q. Li, Q. Mao, S. Wang, CrackTree: Automatic crack detection from pavement images, Pattern Recognit. Lett. 33 (2012) 227–238.

[57] S. Bang, S. Park, H. Kim, H. Kim, Encoder-decoder network for pixel-level road crack detection in black-box images, Comput. Civ. Infrastruct. Eng. 34 (2019) 713–727.

[58] M.A. Hariri-Ardebili, F. Pourkamali-Anaraki, Simplified reliability analysis of multi hazard risk in gravity dams via machine learning techniques, Arch. Civ. Mech. Eng. 18 (2018) 592–610. https://doi.org/10.1016/j.acme.2017.09.003.

[59] M.A. Hariri-Ardebili, B. Sudret, Polynomial chaos expansion for uncertainty quantification of dam engineering problems, Eng. Struct. 203 (2020) 109631. https://doi.org/10.1016/j.engstruct.2019.109631.

[60] V. Ranković, N. Grujović, D. Divac, N. Milivojević, Development of support vector regression identification model for prediction of dam structural behaviour, Struct. Saf. 48 (2014) 33–39. https://doi.org/10.1016/j.strusafe.2014.02.004.

[61] G.H. Beckman, D. Polyzois, Y.J. Cha, Deep learning-based automatic volumetric damage quantification using depth camera, Autom. Constr. 99 (2019) 114–124. https://doi.org/10.1016/j.autcon.2018.12.006.

[62] C.V. Dung, L.D. Anh, Autonomous concrete crack detection using deep fully convolutional neural network, Autom. Constr. 99 (2019) 52–58. https://doi.org/10.1016/j.autcon.2018.11.028.

[63] J. Kim, S. Shim, Y. Cha, G.C. Cho, Lightweight pixel-wise segmentation for efficient concrete crack detection using hierarchical convolutional neural network, Smart Mater. Struct. 30 (2021). https://doi.org/10.1088/1361-665X/abea1e.

[64] J. Deng, Y. Lu, V.C.S. Lee, Concrete crack detection with handwriting script interferences using faster region-based convolutional neural network, Comput. Civ. Infrastruct. Eng. 35 (2020) 373–388. https://doi.org/10.1111/mice.12497.

[65] Sauvik Acharjee, A Comprehensive Guide to Convolutional Neural Networks(2021), JiSAW Acad. (2021). https://www.jigsawacademy.com/blogs/ai-ml/convolutional-neural-network/#Pooling-Layer (accessed May 13, 2021).

[66] Z. Wang, G. Xu, Y. Ding, B. Wu, G. Lu, A vision-based active learning convolutional neural network model for concrete surface crack detection, Adv. Struct. Eng. 23 (2020) 2952–2964. https://doi.org/10.1177/1369433220924792.

[67] H. Nhat-Duc, Q.L. Nguyen, V.D. Tran, Automatic recognition of asphalt pavement cracks using metaheuristic optimized edge detection algorithms and convolution neural network, Autom. Constr. 94 (2018) 203–213. https://doi.org/10.1016/j.autcon.2018.07.008.

[68] W. Song, G. Jia, H. Zhu, D. Jia, L. Gao, Automated pavement crack damage detection using deep multiscale convolutional features, J. Adv. Transp. 2020 (2020). https://doi.org/10.1155/2020/6412562.

[69] A. Sellier, É. Grimal, S. Multon, É. Bourdarot, eds., Swelling Concrete in Dams and Hydraulic Structures, Wiey, 2017. https://doi.org/10.1002/9781119437703.

[70] T.B.J. Coenen, A. Golroo, A review on automated pavement distress detection methods, Cogent Eng. 4 (2017). https://doi.org/10.1080/23311916.2017.1374822.

[71] Y.J. Cha, W. Choi, O. Büyüköztürk, Deep Learning-Based Crack Damage Detection Using Convolutional Neural Networks, Comput. Civ. Infrastruct. Eng. 32 (2017) 361–378. https://doi.org/10.1111/mice.12263.

[72] S. Li, X. Zhao, Image-Based Concrete Crack Detection Using Convolutional Neural Network and Exhaustive Search Technique, Adv. Civ. Eng. 2019 (2019). https://doi.org/10.1155/2019/6520620.

[73] X. Weng, Y. Huang, W. Wang, Segment-based pavement crack quantification, Autom. Constr. 105 (2019). https://doi.org/10.1016/j.autcon.2019.04.014.

[74] H. Klee, Briefing: The cement sustainability initiative, 2004. https://doi.org/10.1680/ensu.2004.157.1.9.

[75] A. Dehghan, P. Zhang, E. Ossetchkina, D. Sloan, K. Peterson, Digital microscopy applied to damage rating index for Alkali-Silica reaction in concrete, ASTM Spec. Tech. Publ. STP 1613 (2018) 105–125. https://doi.org/10.1520/STP161320180003.

[76] L.F.M. Sanchez, M. Terra, Using Machine Learning for Condition Assessment of Concrete Infrastructure: A review of the associated challenges and potential benefits, Am. Concr. Inst. (2019) 35–39.

[77] ASTM C490/C490M, Standard practice for use of apparatus for the determination of length change of hardened cement paste , mortar , and concrete, ASTM Int. (2017) 1–5. https://doi.org/10.1520/C0490.

[78] British Cement Association, The Diagnosis of Alkali-Silica Reaction, in: Wexham Springs, Slough, UK, 1992.

CHAPTER FIVE: CONCLUSION AND FUTURE RECOMMENDATIONS

The purpose of this study was to use artificial intelligence techniques, specifically Convolutional Neural Networks (CNN), to automate the Damage Rating Index (DRI), so the concrete affected by Alkali-silica Reaction (ASR) could be assessed without the drawbacks encountered in the DRI, as the excessively time required to train an operator, which could vary from 3 to 6 months, besides the time to perform the method itself, usually three hours. Additionally, the operator-sensitivity issue will be resolved. The evolution of the techniques and the estate of the art in the use of artificial intelligence to assess ASR-affected concrete are presented by this project hereafter:

- The first method used to automate the DRI procedure was a Machine Learning (ML) technique, the so-called Convolutional Neural Network (CNN). This method enables to model to learn based on what is taught to it, using several layers, also called filters, with the information necessary to assess the input and give the desired output. Additionally, the model was trained using traced cracks to teach him how to identify and classify them. The method used to identify cracks was the sliding window, which generates heatmaps with low quality, thus impacting crack recognition in the aggregate particles, whereas in the cement paste the results where promising.

- To address those limitations aforementioned, the new model now works on pixel-level detection problems, which are usually referred to as image segmentation, which requires the algorithm to predict, for each pixel, whether it belongs to a crack or not. This method can predict the crack location, length, shapes and direction. To achieve those results, the algorithm architecture was built using 50 layers with the core information regarding the different classifications to be performed. Furthermore, to achieve the pixel-level prediction, the models preserve the spatial information during the inference so that a one-to-one correspondence relationship can be constructed between the pixels of the input image and the output prediction.

- The image preparation and acquisition parameters play an essential part in the outcomes of pixel segmentation models and CNN techniques, enhancing the tridimensional (e.g., the depth) notion in images, even if they are exhibited in 2D. Additionally, the image acquisition should be performed excluding the grid interface from the image, so the misclassification associated with it can be eliminated from the system.

- The Machine Learning (ML) algorithm was trained based on the number, location and nature of the cracks identified while performing the Damage Rating Index (DRI). The samples used to train the model were derived from various aggregates, including the Springhill (Greywacke). When compared the precision attained by the model using the Overall Data and only the Springhill, the variation encountered between the results was 14% for Closed Crack Aggregates (CCA), 16% for Open Crack Aggregates with and without Gel (OCA+OCAG) and only 2% for the crack in the Cement Paste with and without Gel (CCP+CCPG), being the overall data more precise. So, it is possible to conclude that the database requires variability in its constituents to reduce the bias created during the learning process. It should be analyzed more carefully to reduce as much as possible the bias in the system;

- The results collected in this research indicate that the automated DRI presents a better performance at high expansion levels. At 0.20% expansion the DRI shows a precision of 83% and 82% at 0.30%. On The Other Hand, the most notable differences in the DRI automated and DRI performed by humans were noticed at lower expansion levels, being the 0.05% the most inconsistent result, presenting a precision of 30%. However, at 0.12% of expansion, the model shows 70% of precision, between the estimated and ground-truth results;

- Overall, the automated DRI presents an Average accuracy of 88% for all features, different types of aggregates, and 74% for Springhill aggregate, with a precision of 76.5%. At moderate, high and ultra high expansion levels, the models demonstrates

- The overcounting noticed at the lower expansion lever is somewhat because the model recognizes the Interfacial Transition Zone (ITZ) and prominent porous areas with a significant width and classifying them as CCP+CCPG since they present analogous characteristics.

- The DRI overestimation at low expansion levels is explained by the overcounting of CCP+CCPG that possess the higher weighting faction, impacting more in the DRI results when compared with the other two groups.

- The higher estimated DRI number does not signify that the algorithm does not perform well; it might also indicate that the computer is able to identify the cracks in the cement paste better than humans. Some individual squares were verified under the microscope to check whether the CCP pointed by the model was true, and a considerable amount was there, but humans could not see.

- Overall, the model works fittingly at moderate and high expansion levels, and the Automated DRI procedure only takes minutes to estimate the damage, besides providing all the individual counting and images with the cracks traced by it. By doing this, months of training can be saved, and a reliable method could become more accessible.

Yet, there is some supplementary research suggestions to improve this formidable tool to assess damaged concrete affected by ASR; further work is suggested in this project:

- When the algorithm at low expansion levels reaches accuracy similar to that achieved by high levels, new types of reactive aggregates of different mineralogic compositions and different sizes (coarse and fine) should be introduced into the training database, then the model can be used more thoroughly.
- Future investigation is necessary to evaluate if the model might be dividing one crack into multiple sections when there is a mineral variation in the aggregate, which could interfere in the pixel consolidation, working as the so-called "noise" in the data.
- Additional research is recommended to use the sophisticated CNN system to evaluate other damage mechanisms such as external and internal sulphate attack, F/T damage, and steel corrosion. The proposed approach can become a comprehensive protocol for evaluating critical ageing infrastructure.